References

Al-Noaman A., Rawlinson S.C.F., Hill R.G., "Bioactive glass-stoichiometric wollastonite glass alloys to reduce TEC of bioactive glass coatings for dental implants," *Material Letters*, **94** (2013) 69-71.

Al-Sanabani F.A., Ahmed A. Madfa1, Nasr H. Al-Qudaimi2 "Alumina ceramic for dental applications: A review article," *American Journal of Material Research*, **1** (2014) 26-34.

Andou Y., Kawahara A., "The refinement of the structure of synthetic kalsilite," Mineralogical Journal, **12** (1984) 153-161.

Anusavice K.J., Gray A.E., "Influence of framework design, contraction mismatch, and thermal history on porcelain checking in fixed partial dentures," *Dental Materials*, **5 (**1989) 58-63.

Anusavice, K.J., Dental Ceramics, Phillips' Science of Dental Materials,11th Edition, Sauder, St. Louis, MO, 2003.

Balaz P. Achimovicova M., Balaz M. Billik P., Zara Cherkezova-Zheleva, Jose Manuel Criado, Francesco Delogu, Erika Dutkova, Eric Gaffet Francisco Jose Gotor Rakesh Kumar,h Ivan Mitov, Tadej Rojac, Mamoru Senna, Andrey Streletskiikl and Krystyna Wieczorek-Ciurowam, "Hallmarks of mechanochemistry: from nanoparticles to technology," *Chemical Society Reviews*, **42** (2013) 7571-7637.

Barghi N., Lorenzana R.E., "Optimum thicknesses of opaque and body porcelains," *Journal of Prosthetic Dentistry*, **48** (1982) 429-431.

Barreto M.T., Goldberg A.J., Nitkin D.A., G. Mumford, "Effect of investment on casting high-fusing alloys," *Journal of Prosthetic Dentistry,* **44** (1980) 504-507.

Becerro A.I. (a), Escudero A., Mantovani M. "The hydrothermal conversion of kaolinite to kalsilite: Influence of time, temperature, and pH," *Am Mineral*, **94** (2009) 1672–1678.

Becerro A.I. (b), Mantovani M., Escudero A., "M. Hydrothermal synthesis of kalsilite: a simple and economical method," *The Journal of the American Ceramic Society,* **92** (2009) 2204–2206.

Bergenholtz G., Cox C.F., Loesche W.J., Syed S.A., "Bacterial leakage around dental restorations: its effect on the dental pulp," *Journal of Oral Pathology & Medicine*, **11** (1982) 439-450.

Bogdanoviciene I., Jankeviciute A., Pinkas J., Beganskiene A., Kareiva A., "Sol-gel Synthesis and Characterization of Kalsilite-type Alumosilicates," *Materials Science*, **13** (2007) 3-6.

Bogdanoviciene I., Jankeviciute A.,, Pinkas J., Beganskiene A., Kareiva A., "Study of Aluminosilicate Porcelain: Sol–Gel preparation, characterization and Erosion evaluated by gravimetric method," *Material Research Bulletin*," **43 (**2008) 2998-3007.

Brodkin D., Panzera C., U.S. Patent 6090194, 2000.

Brodkin D., Panzera C., W.O. Patent No. 1891099, 1999.

Cattell M.J., Chadwick T.C., Knowles J.C., Clarke R.L., "The crystallization of an aluminosilicate glass in the K_2O–Al_2O_3–SiO_2 system," *Dental Materials,* **21** (2005) 811-822.

Chatzistavrou X., Esteve D., Hatzistavrou E., Kontonasaki E., Paraskevopoulos K.M., Boccaccini A.R., "Sol–gel based fabrication of novel glass-ceramics and composites for dental applications," *Materials Science and Engineering: C*, **30** (2010) 730-739.

Chatzistavrou X., Tsigkou O., Harsh D.A., Paraskevopoulos M.K., Salih V., Boccaccini A.R., "Sol–gel based fabrication and characterization of new bioactive glass–ceramic composites for dental applications," *Journal of European Ceramic Society*, **32** (2012) 3051-3061.

Chen G., Niu D., Liu X., "Preparation of $SrAl_2O_4$ from an oxide mixture via a high-energy ball milling," *Journal of Alloys and Compounds*, **399** (2005) 280-283.

Chen X., Chadwick T.C., Wilson R.M., Hill R.G., Cattell M.J. "Crystallization and flexural strength optimization of fine-grained leucite glass-ceramics for dentistry," *Dental Materials*, **27** (2011) 1153-1161.

Cheung K.C., Darvell B.W., "Sintering of dental porcelain: effect of time and temperature on appearance and porosity," *Dental Materials*, **18** (2002) 163-173.

Christensen G.J., "Porcelain-Fused-to-Metal versus Zirconia-Based Ceramic Restorations," *The Journal of the American Dental Association*, **140** (2009): 1036-1039.

Christensen G.J., "The use of porcelain-fused-to-metal restorations in current dental practice: a survey," *Journal of Prosthetic Dentistry*, **56** (1986) 1-3.

Coornaert J., Adriaens P., Boever J.D., "Long-term clinical study of porcelain-fused-to-gold restorations," *Journal of Prosthetic Dentistry*, **51** (1984) 338-346.

Craig R.G., LeGeros R.Z., "Early events associated with periodontal connective tissue attachment formation on titanium and hydroxyapatite surfaces," *Journal of Biomedical Material Research*, **47** (1999) 585-594.

Davis B.K., Aquilino S.A., Lund P.S., Diaz-Arnold A.M., Denehy G.E., "Subjective evaluation of the effect of porcelain opacity on the resultant color of porcelain veneers," *International Journal of Prosthodontics*, **3** (1990) 567-72.

Denry I., Kelly J.R., "State of the art of zirconia for dental applications." *Dental Materials*, **24** (2008) 299-307.

Denry I.L. (a), "Recent advances in ceramics for dentistry," *Critical Reviews in Oral Biology & Medicine*, **7** (1996) 134-143.

Denry I.L. (b), Mackert J.R., Holloway J.A., Rosenstiel S.F., "Effect of cubic leucite stabilization on the flexural strength of Feldspathic dental ceramics," *Journal of Dental Research*, **75** (1996) 1928-1935.

Denry I.L. (c) , Mackert J.R., Holloway J.A., Rosenstiel S.F., "Cubic Leucite stabilization in feldspathic dental porcelain Bioceramics," *Material and Applications II*: **1** (1996) 115-121.

Denry I.L., “Contemporary Fixed Prosthodontics, third ed., Mosby Inc., St. Louis, 2001.

Derand P., Peter V., “Wear of low fusing dental porcelains,” *Journal of Prosthetic Dentistry*, **81** (1999) 460-63.

Dimitrijevic R., Dondur V., “Synthesis and characterization of $KAlSiO_4$ Polymorphs on the SiO_2-$KAlO_2$ Join,” *Journal Solid State Chemistry*, **115 (**1995) 214–24.

Ding J., Tsuzuki T., McCormick P.G., “Ultrafine alumina particles prepared by mechanochemical/thermal processing,” *Journal of the American Ceramic Society*, **79** (1996) 2956-2958.

El-Meliegy E.A.M., “Low fusion fluorophlogopite–leucite containing porcelain,” *British Ceramic Transactions*, **103** (2004) 231-234.

Erpenstein H., Borchard R., Kerschbaum T., “Long-term clinical results of galvano-ceramic and glass-ceramic individual crowns,” *Journal of Prosthetic Dentistry*, **83** (2000) 530-534.

Estafan D., David A., David S., Calamia J., “A new approach to restorative dentistry: fabricating ceramic restorations using CEREC CAD/CAM,” *Compendium*, **20** (1999) 555-560.

Felton D.A., Kanoy B.E., Bayne S.C., Wirthman G.P., “Effect of in vivo crown margin discrepancies on periodontal health,” *Journal of Prosthetic Dentistry*, **65** (1991) 357-364.

Fetner A.E., Hartigan M.S., Low S.B., “Periodontal repair using PerioGlas® in non-human primates: Clinical and historical obceravation*,”Compendium*, **15** (1994) 932-938.

Fischer J., Zbaren C., Stawarczyk B., Hammerle C.H.F., “The effect of thermal cycling on metal–ceramic bond strength,” *Journal of dentistry*, **37** (2009) 549-553.

Fredericci C., Yoshimura H.N., Molisani A.L., Pinto M.M., “Effect of temperature and heating rate on the sintering of leucite-based dental porcelains,” *Ceramics International*, **37** (2011) 1073-1078.

Ghaffari M., “How bone marrow-derived human mesenchymal stem cells respond to poorly crystalline apatite coated orthopedic and dental titanium implants,” *Ceramic International*, **39** (2013) 7793-7802.

Giordano R., A comparison of all-ceramic restorative systems: part 2,” *General Dentistry*, **48** (2000) 43–45.

Goudouri O.M., Kontonasaki E., Kantiranis N., Chatzistavrou X., Papadopoulou L., Koidis P. Paraskevopoulos K. M., “A bioactive glass/dental porcelain system by the sol gel route: fabrication and characterization,” *Key Engineering Material*, **396-398** (2009) 95-98.

Goudouri O.M., Kontonasaki E., Papadopoulou L., Kantiranis N., Lazaridis N.K., Chrissafis K., Chatzistavrou X., Koidis P., Paraskevopoulos K.M., “Towards the synthesis of an experimental bioactive dental ceramic. Part I: Crystallinity

characterization and bioactive behavior evaluation," *Materials Chemistry & Physics* **145** (2014) 125-134.

Goudouri O.M., Kontonasaki E., Theocharidou A., Papadopoulou L., Kantiranis N., Chatzistavrou X., Koidis P., Paraskevopoulos K.M., "Modifying a dental ceramic by bioactive glass via the sol–gel route: Characterization and bioactivity investigation," *Materials Chemistry & Physics,* **125** (2011) 309-313.

Guazzato M., Albakry M, Ringer SP, Swain MV., "Strength, fracture toughness and microstructure of a selection of all-ceramic materials. Part I. pressable and alumina glass infiltrated ceramics," *Dental Materials,* **20** (2004) 441-448.

Hamzawy E.M.A., El-Meliegy E.A.M., "Preparation of nepheline glass–ceramics for dental applications," *Materials Chemistry and Physics*, **112** (2008) 432-435.

Hashimoto S., Yamaguchi A., Fukuda K., Zhang S. "Low-temperature synthesis of leucite crystals using kaolin," *Materials Research Bulletin,* **40** (2005) 1577-1583.

Heintze S.D., Cavalleri A., Zellweger G., Buchler A., Zappini G., "Fracture frequency of all-ceramic crowns during dynamic loading in a chewing simulator using different loading and luting protocols," *Dental Materials,* 24 (2008) 1352-1361.

Hench L.L., "Bioactive materials: The potential for tissue regeneration," *Journal of Biomedical Material Research,* **41** (1998) 511-518.

Hench L.L., Paschall H.A., "Direct chemical bond of bioactive glass ceramic materials to bone and muscle," *Journal of Biomed Material Research,* **7** (1973) 25-42.

Heuer A.H., Hobbs L.W., "Science and Technology of Zirconia," *Journal of the American Ceramic Society*: Vol 3, Westerville, Ohio, 1981.

Holland W., Schweiger M., Frank M., Rheinberger V., "A comparison of the microstructure and properties of the IPS Empress 2 and the IPS Empress glass-ceramics," *Journal Biomed Materials Research*, **53** (2000) 297-303.

Holland W., Schweiger M., Rheinberger V.M., Kappert H., "Bioceramics and their application for dental restoration," *Advances in Applied Ceramics*, **108** (2009) 373-380.

http// www.vbceramics.com

http//www.fei.com/products/sem/fei-sem

http//www.google.utm

http//www.kaplasscientificsupplier

http//www.nobledental.com.au

http//www.wikipedia.com

http//www.wikiwand.com

http//www4.nau.edu

Hussam M., Festy F., Watson T.F., Thompson I., Banerjee A., "Enamel white spot lesions can remineralise using bio-active glass and polyacrylic acid modified bio-active glass powders," *Journal of dentistry* **42** (2014) 158-166.

Jaeggi T., Lussi A., "Prevalence, incidence and distribution of erosion," *Monographs Oral Science*, **20** (2006) 44-65.

Jankeviciute A., Kareiva A., "Synthesis and characterization of leucite ceramics using sol-gel derived molecular precursors," *Mendeleev Communications*, **21** (2011) 287-288.

Kallai L.H., Lapides I., "Thermal Reactions of Kaolinite with Potassium Carbonate," *Journal of Thermal Analysis and Calorimetry*, **71 (**2003) 689-98.

Kawahara A., Andou Y., Marumo F., Okuno M., "The crystal structure of high temperature form of kalsilite (KAlS104) at 950 °C," *Minerological Journal*, **13** (1987) 260-270.

Kelly J.R. Giordano R., Pober R., Cima M.J., "Fracture surface analysis of dental ceramics: clinically failed restorations." *International Journal Prosthodontics*, **3** (1990) 430-440.

Kelly J.R., "Dental ceramics: current thinking and trends," *The Dental Clilnic North America*, **48** (2004) 513-530.

Kelly J.R., Campbell S.D., Bowen H.K., "Fracture-surface analysis of dental ceramics," Journal of Prosthetic Dentistry, **62** (1989) 536-541.

Kelly J.R., Luthy H., Gougoulakis A., Pober. R, Mormann W.H., "Machining effects on feldspathic porcelain and glass ceramic: fractographic analysis," *Proc Int Symp Computer Restorations*, 1991, 253-273.

Kelly J.R., Nishimura I, Campbell S.D., "Ceramics in dentistry historical roots and current perspectives," *Journal of Prosthetic Dentistry,* **75** (1996) 18-32.

Khater G.A., Hamzawy E.M.A., Metwally H.I., El-Meliegy E., "Spodumene nepheline- anorthite glass ceramics for dental applications," *Journal of Applied Sciences Research*, **9** (2013) 821-825.

Klein C.A., "Flexural strength of sapphire: Weibull statistical analysis of stressed area, surface coating, and polishing procedure effects," *Journal of Applied Physics*, **96** (2004) 3172-3179.

Kokoti M., Sivropoulou A., Koidis P., Garefis P., "Comparison of cell proliferation on modified dental ceramics," *Journal of Oral Rehabil,* **28** (2001) 880-887.

Kokubo T., Ito S., Sakka S., Yamamuro T., "Formation of a High-Strength Bioactive Glass-Ceramic in the System MgO-CaO-SiO_2-P_2O_5," *Journal of Material Science*, **21** (1986) 536-540.

Kokubo T., Takadama H., "How useful is SBF in predicting in vivo bone bioactivity," *Biomaterials*, **27** (2006) 2907-2915.

Kong L.B., Ma J., Huang H., Zhang R.F., Que W.X., "Barium titanate derived from mechanochemically activated powders," *Journal of Alloys Compounds*, **337** (2002) 226-230.

Kontonasaki E., Kantiranis N., Papadopoulou L., Chatzistavrou X., Kavouras P., Zorba T., Sivropoulou A., Chrissafis K., "Microstructural characterization and comparative evaluation of physical, mechanical and biological properties of three ceramics for metal-ceramic restorations," *Dental materials*, **24** (2008) 1362-1373.

Kontonasaki E., Papadopoulou L., Zorba T., Pavlidou E., Paraskevopoulos K., Koidis P., "Apatite formation on dental ceramics modified by a bioactive glass," *Journal of Oral Rehabilitation*, **30** (2003) 893-902.

Kontonasaki E., Sivropoulou A., Papadopoulou L., Garefis P., Paraskevopoulos K., Koidis P., "Attachment and proliferation of human periodontal ligament fibroblasts on bioactive glass modified ceramics," *Journal of Oral Rehabilitation* **34 (**2007) 57–67.

Kopp O.C., Harris A., Clark G.W., "The Hydrothermal Conversion of Muscovite to Kalsilite and an Iron-Rich Mica," *American Mineralogist*, **46 (**1961) 719-727.

Kurklu D., Azer S.S., Yilmaz B., Johnston W.M., "Porcelain thickness and cement shade effects on the color and translucency of porcelain veneering materials," *Journal of dentistry*, **41** (2013) 1043-1050.

Levin E.M., Robin C.R., McMurdie H.F. "Phase Diagrams for Ceramists," *Journal of the American Ceramic Society*, (1964) 156-407.

Lianshui S., Weifan C., Xuezhen Z., Fujian Z., Yongxiu L., "Pr-doped 3Y–TZP nano powders for colored dental restorations: mechanochemical processing, chromaticity and cytotoxicity", Ceramics International, **40** (2014) 8569–8574.

Lopez-Esteban S., Saiz E., Fujino S., Oku T., Suganuma K., Tomsia A.P., "Bioactive glass coatings for orthopedic metallic implants," *Journal of European Ceramic Society*, **23** (2003) 2921-2930.

MacCulloch W.T., "Advances in dental ceramics," *British Dental Journal*, **124** (1968) 361-365.

Mackert J.R. (a), Butts M.B., Fairhurst C.W., "The effect of the leucite transformation on dental porcelain expansion," *Dental Materials*, **2** (1986) 32-36.

Mackert J.R. (b), Butts M.B., Morena R., Fairhurst C.W., "Phase changes in leucite containing dental porcelain frit," *Journal of American Ceramic Society*, **69** (1986) 60-69.

Mackert J.R., Evans A.L., "Effect of cooling rate on leucite volume fraction in dental porcelains," *Journal of Dental Research*, **70** (1991) 137-139.

Mackert J.R., Ringle R.D., Parry E.E., Evans A.L., Fairhurst C.W., "The relationship between oxide adherence and porcelain metal bonding," *Journal of Dental Research*, **67** (1988) 474-478.

Mackert J.R., Rodway J., Russell C.M., "Leucite crystallization during processing of a heat pressed dental ceramic," *International Journal of Prosthodontics*, **9** (1996) 261-265.

Mackert J.R., Twiggs S.W., Evans-Williams A.L., "Isothermal anneal effect on leucite content in dental porcelains," *Journal of Dental Research*, **74** (1995), 1259-1265.

Mackert J.R., Twiggs S.W., Russell C.M., Williams A.L., "Evidence of a Critical Leucite Particle Size for Micro cracking in Dental Porcelains," *Journal of Dental Research*, **80** (2001) 1574-1579.

Malhotra M.L., "Dental porcelain in alloys: a review," *Trends & techniques in the contemporary dental laboratory*, **62** (1989) 42-44.

Manna P.P., Hira S.K., Das A.A., Bandyopadhyay S., Gupta K.K., "IL-15 activated human peripheral blood dendritic cell kill allogeneic and xenogeneic endothelial cells via apoptosis," *Cytokine*, **61** (2013) 118-126.

Masayuki K., Kawano F., Asaoka K., Matsumoto N., "Effect of leucite crystals on the strength of glassy porcelain," *Journal of Dental Materials*, **13** (1994) 138-147.

McCabe F. J., "Ceramics and Porcelain Fused to Metal, Applied Dental Materials, Oxford OX4 2DQ, UK, 2008.

McLean J.W., Hughes T.H., "The reinforcement of dental porcelain with ceramic oxides," *Journal of British Dental*, 119 (6) (1965) 251-267.

Meijering A.C., Creugers N.H.J, Roeters F.J.M, Mulder J. "Survival of three types of veneer restorations in a clinical trial a 2.5-year interim evaluation," Journal of Dentistry, **26** (1998) 563-568.

Meliegy E.E., Glasses and Glass Ceramics for Medical Applications, Chapter-10 Leucite Glass Ceramics, Springer science & business media, LLC 2012.

Meriani S., Zirconia 88 Advances in Zirconia Science and Technology, Springer Verlag, Berlin, Germany, 1989.

Milleding P, Wennerberg A, Aladdin S, Karlsson S, Simon E., "Surface corrosion of dental ceramics in vitro,"Biomaterials **20** (1999) 733-746.

Milly H., Festy F., Watson T.F., Thompson I., Banerjee A., "Enamel white spot lesions can remineralise using bio-active glass and polyacrylic acid modified bio-active glass powders," *Journal of dentistry* **42** (2014) 158-166.

Mrazova A.. Klouzkova A., "Leucite porcelain fused to metals for dental restoration," *Ceramic Silikaty,* 53 (2009) 225-230

Munck J. D., Vargas M., Landuyt K. V., Hikita K., Lambrechts P., Van B. Meerbeek, "Bonding of an auto-adhesive luting material to enamel and dentin," *Dental Materials,* **20** (2004) 963-971.

Nakamura T., Yamamuro T., Higashi S., Kokubo T., Itoo S., "A new glass-ceramic for bone replacement: Evaluation of its bonding to bone tissue," *Journal of Biomedical Material Research,* **19** (1985) 685-698.

Nan-Chung W., Min-Hsiung H., "Preparation of nepheline glass-ceramics dental porcelain," *Materials Chemistry and Physics,* **37** (1994) 370-375.

Napankangas R., Raustia A., "Twenty-year follow-up of metal ceramic single crown: a retrospective study," *International Journal of Prosthodontics,* **21** (2008) 307-311.

Narayan R., Biomedical Materials, Biomaterials for Dental application, New York, NY, USA, 2009.

Noni A. D, Hotza D., Soler V.C., Vilches E.S., "Effect of quartz particle size on the mechanical behavior of porcelain tile subjected to different cooling rates," *Journal of the European Ceramic Society,* **29** (2009) 1039-1046.

Novotna M., Satava V., Kostka P., Lezal D., Maixner D., Klouzkova A. “Synthesis of leucite for application in dentistry,” *Glass Technology,* **45** (2004) 105-107.

Oishi S., Miyata T., Suzuki T. “Growth of Leucite Crystals from a K2Mo2O7 Flux,” *Journal of Material Science Letters,* **22** (2003) 927-929.

Ota T., Takahashi M., Yamai I., Suzuki H., “High-Thermal-Expansion Polycrystalline Leucite Ceramic,” *Journal of the American Ceramic Society*, **76** (1993) 2379-2389.

Ota T., Takebayashi T., Takahashi M., Hikichi Y., Suzuki H. “High thermal expansion $KAISiO_4$ ceramic. *Journal of Materials Science,* **31 (**1996) 1431-1433.

Ozcan M., Niedermeier W., “Clinical study on the reasons for and location of failures of metal-ceramic restorations and survival of repairs,” *International Journal of Prosthodontics*, **15 (**2002) 299-302.

Ozcelik T.B., Yilmaz B., Ozcan I., Kircelli C., “Colorimetric analysis of opaque porcelain fired to different base metal alloys used in metal ceramic restorations,” Journal of Prosthetic Dentistry, 99 (2008) 193-202.

Papadopoulou L., Kontonasaki E., Zorba T., Chatzistavrou X., Pavlidou E., Paraskevopoulos K, Sklavounos S., Koidis P., “Dental ceramics coated with bioactive glass: Surface changes after exposure in a simulated body fluid under static and dynamic conditions,” *Physical Status Solidi A*, **198** (2003) 65-75.

Perrotta A.J., Smith J.V., “The crystal structure of kalsilite, $KAlSiO_4$,” *Mineralogical Magazine,* **35** (1965) 588-595.

Pitaru S., Tal H., Soldinger M., Grosskop A., Noff M., "Partial regeneration of periodontal tissues using collagen barriers. Initial observations in the canine," *Journal of Periodontics,* **59** (1988) 380-386

Pospiech P., "All-ceramic crowns: bonding or cementing," *Clinical Oral Invest,* **6** (2002) 189-197.

Rahaman M.N. II Edison, Ceramic processing and sintering, Synthesis of Powders, Madison Avenue, New York, 2003.

Ravarian R., Moztarzadeh F., Hashjin M.S., Rabiee S.M., Khoshakhlagh P., Tahriria M., "Synthesis characterization and bioactivity investigation of bioglass hydroxyapatite composite," *Ceramic International,* **36** (2010) 291-297.

Rouf M.A., "Crystallization of glasses in the primary plan field of leucite in the K_2O–Al_2O_3 –SiO_2 system," *Transactions of The British Ceramic Society,* **77** (1978) 36-39.

Saito F., Zhang Q., Kano J., "Mechanochemical approach for preparing nano structural materials," *Journal of Material Science,* **39** (2004) 5051-5055.

Sheu T.S., Obrien W.J., Rasmussen S.T., Tien T., "Mechanical properties and thermal expansion behavior in leucite containing materials," *Journal of Materials Science,* **29** (1994) 125-128.

Siriphannon P., Hayashi S., Yasumori A., Okada K., "Preparation and sintering of $CaSiO_3$ from co precipitated powder using NaOH as a precipitant and its apatite formation in simulated body fluid solution," *Journal of Material Research,* **14** (1999) 529-536.

Sohmura T., Takahashi J., "Use of CAD/CAM System to Fabricate Dental Prostheses: Part 1. CAD for a Clinical Crown Restoration," *International Journal of Prosthodontics*, **8** (1995) 252-258.

Stacey G.D., "A shear stress analysis of the bonding of porcelain veneers to enamel," *The Journal of Prosthetic Dentistry*, **70** (1993) 395-402.

Stanley H.R., Hall M.B., Clark A.E., King C.J., Hench L.L., Berte J.J., "Using 45S5 Bioglass Cones as Endosseous Ridge Maintenance Implants to Prevent Alveolar Ridge Resorption: A 5-Year Evaluation," *Journal of Oral Maxillofac Implants*, **12** (1997) 1-19.

Steyern V.V.P., "All-ceramic fixed partial dentures. Studies on aluminum oxideand zirconium dioxide-based ceramic systems," *Swedish Dental Journal of Supplement, **173*** (2005) 1– 69.

Takuya T., Paul G.M., "Mechanochemical synthesis of nanoparticles", *J. of Mater. Sci*. **39** (2004) 5143-5146.

Tsetsekou A., Papadopoulos T., Adamopoulos O., "Microstructure effect on the properties of commercial low-fusing dental porcelain," *Journal of Material Science Material Medicine*, 13 (2002) 407-416.

Tsuzuki T., McCormic P.G., "Mechanochemical synthesis of nanoparticles", *Journal Of Materials Science*, **39** (2004) 5143-5146

Waerhaug J., "Tissue reaction around artificial crowns," *Journal of Periodontalogy*, **24** (1953) 172-185.

Walton J.N., Michael Gardner F., Agar J.R., "A survey of crown and fixed partial denture failures: length of service and reasons for replacement," *Journal of Prosthetic Dentistry,* **56** (1986) 416-421.

Wolfram H., Frank M., Rheinberger V., "Surface crystallization of leucite in glasses," *Journal of Non-Crystalline Solids,* **180** (1995) 292-307.

Xue Junmin, Wan Dongmei, See-Ee Lee, Wang John, "Mechanochemical Synthesis of Lead Zirconate Titanate from Mixed Oxides", *Journal of the American Ceramic Society,* **82**, (1999) 1687–1692.

Yao L., Peng C., Wu J., "Fabrication of Superfine Leucite-Reinforced Dental Material by Hydrothermal Precursor and Low-Temperature Frit", *Journal of the American Ceramic Society,* **94**, (2011) 3694–3697.

Yilmaz B., Ozcelik T.B., Johnston W.M., Yilmaz S.K. "Effect of alloy recasting on the color of opaque porcelain applied on different dental alloy systems," *Journal of Prosthetic Dentistry,* **108** (2012) 362-369.

Yilmaz H., Dincer C., "Comparison of the bond compatibility of titanium and an NiCr alloy to dental porcelain," *Journal of Dentistry,* **27** (1999) 215–222.

Zhang Y. (a), Qu C., Rao P., Ming Lv, Wu J., "Nano crystalline Seeding Effect on the crystallization of two leucite precursors," *Journal of the American Ceramic Society,* **90** (2007) 2390-2398.

Zhang Y. (b), Ming Lv., Dongdan C. Wu J., "Leucite crystallization kinetics with kalsilite as a transition phase," *Material Letters,* **61 (**2007) 2978-2981.

Zhang Y., Wu J., Rao P., Lv M., "Low temperature synthesis of high purity leucite," *Material Letters,* **60 (**2006) 2819–2823.

Zhang Yi., Rao P., Ming Lu, Jianqing. Wu, "Mechanical properties of dental ceramics with different leucite particle sizes," *Journal of the American Ceramic Society,* **91** (2008) 527-534.

List of Publications

1. **Pattem Hemanth Kumar**, Abhinav Srivastava, Vijay Kumar, Nandini Jaiswal and Vinay Kumar Singh, "Role of MgF_2 addition on high energy ball milled kalsilite: Implementation as dental porcelain with low temperature frit" ***Journal of Advanced Ceramics***, **3**(4), 332–338 (2014). DOI: 10.1007/s40145-014-0125-x

2. **P. H. Kumar**, A. Srivastava, V. Kumar, H. Singh, S. Sharma, P. Kumar and V. K. Singh, "Role of CaF_2 on mechanochemically synthesized leucite as dental veneering glass ceramics" ***Advances in Applied Ceramics***, **114**, 107-117 (2015). DOI: 10.1179/1743676114Y.0000000208

3. **Pattem Kumar,** Vinay Kumar Singh*, Sumit Kumar Hira, Pradeep Kumar, Partha Pratim Manna, "In-vitro cytotoxicity, apoptotic and hemolysis assay of kalsilite based glass-ceramics for dental veneering application" ***International Journal of Applied Ceramic Technology***, 1–10 (2015). DOI:10.1111/ijac.12433

4. **Pattem Hemanth Kumar**, Vinay Kumar Singh, Sumit Kumar Hira, Pradeep Kumar, Partha Pratim Manna, "Mechanochemically synthesized leucite based bioactive glass ceramic composite for dental veneering" ***Ceramics international***, **41**, 11161– 11168 (2015). DOI: 10.1016/j.ceramint.2015.05.065

5. **Pattem Hemanth Kumar,** Vinay Kumar Singh*, Pradeep Kumar, "Mechanochemically synthesized kalsilite based bioactive glass-ceramic composite for dental vaneering" (**Accepted in *Journal of Applied Nanoscie*nce**, 2015). DOI: 10.1007/s13204-015-0491-x.

6. **Pattem Hemanth Kumar**, Vinay Kumar Singh, Sumit Kumar Hira, Pradeep Kumar, Partha Pratim Manna, "Effect of Al_2O_3 on leucite based bioactive glass ceramic composite for dental veneering" ***Ceramics international*, 42**, 3591–3597 (2016). DOI: 10.1016/j.ceramint.2015.11.022

Journal of Advanced Ceramics
2014, 3(4): 332–338
DOI: 10.1007/s40145-014-0125-x

ISSN 2226-4108
CN 10-1154/TQ

Research Article

Role of MgF_2 addition on high energy ball milled kalsilite: Implementation as dental porcelain with low temperature frit

Pattem Hemanth KUMAR[a,*], Abhinav SRIVASTAVA[a], Vijay KUMAR[a], Nandini JAISWAL[a], Pradeep KUMAR[b], Vinay Kumar SINGH[a]

[a]*Department of Ceramic Engineering*, *Indian Institute of Technology* (*BHU*), *Varanasi*, *India*
[b]*Department of Chemical Engineering*, *Indian Institute of Technology* (*BHU*), *Varanasi*, *India*

Received: June 17, 2014; Revised: August 11, 2014; Accepted: August 18, 2014

Abstract: Porcelain fused to metal (PFM) has received great attention over the last few years due to its importance in the dentistry. Kalsilite ($K_2O{\cdot}Al_2O_3{\cdot}SiO_2$) is a high thermal expansion porcelain, suitable for bonding to metals. However, kalsilite is a metastable phase which gets converted into crystalline leucite upon heating. In the current work feasibility of developing stable kalsilite phase, dispersion of MgF_2 in it as an additive and using mechanochemical synthesis are studied. Micro fine dental material has been formulated by mixing prepared kalsilite with low temperature frit (LTF) in different ratio. The crystalline phases evolved in fired powders are characterized by powder X-ray diffraction (XRD) technique. Kalsilite with different ratio of LTF has been cold pressed and heat treated to examine its coefficient of thermal expansion (CTE), flexural strength, apparent porosity (AP), bulk density (BD) and microstructure. Results indicate that MgF_2 addition and high milling duration help in kalsilite stabilization. Temperature also plays an important role in this stabilization, and at 1100 ℃ single phase kalsilite formation is observed. Present outcomes demonstrate that it is easily possible to synthesize a stable single phase kalsilite with desirable properties.

Keywords: kalsilite; porcelain fused to metal (PFM); dental ceramic; mechanochemical synthesis; thermal expansion; X-ray diffraction (XRD)

1 Introduction

Ceramic materials have been widely used in porcelain fused to metal (PFM) and all ceramic restoration systems over the last decade. They typically have high coefficient of thermal expansion (CTE) and high flexural strength. Kalsilite ($KAlSiO_4$) mineral has a network of tetrahedral Si and Al elements with charge balancing alkali metal ions [1]. CTE of kalsilite is $16\times10^{-6}\,(℃)^{-1}$ [2]. Kalsilite is a significant constituent in PFM and ceramic restoration systems [3]. It is used as the precursor of leucite [4]. Becerro *et al*. [4] have previously reported that kalsilite being a high thermal expansion ceramic, is suitable for bonding to metals. Kalsilite however crystallizes as a metastable phase when synthesizing leucite [5,6].

Kalsilite has been synthesized previously by various techniques such as hydrothermal method [7], sol–gel method [8,9] and solid-state method [10,11]. Accompanying with other synthesis methods, mechanochemical process is economical and suitable to prepare pure materials with a micro fine particle size [12–14]. This synthesis involves chemical reactions of solids under the action of mechanical forces. Driving

* Corresponding author.
E-mail: phemanth111@gmail.com

force for mechanochemical synthesis is the strain energy stored in the fine powders. The mechanical energy produces structural imperfections in the powder particles during grinding and increases the reactivity of ground materials.

There is lack of research in the stabilization and implementation of this material as PFM. So in order to produce fine stoichiometric kalsilite, mechanochemical synthesis was employed. The aim to improve the stability of kalsilite phase using 2 wt% MgF_2 as an additive has been studied in the present investigation. The ground powders were heat treated at different temperatures and characterized via powder X-ray diffraction (XRD) technique. Optimised kalsilite powders were then mixed with different weight ratio of low temperature frit (LTF) and characterized for CTE, flexural strength, apparent porosity, bulk density and morphology.

2 Experimental procedure

2.1 Materials

Analytical reagent (AR) grade aluminium oxide (Al_2O_3), potassium carbonate (K_2CO_3) and silica (SiO_2) were used as raw materials for kalsilite formulation. Sodium carbonate (Na_2CO_3), potassium nitrate (KNO_3), silica (SiO_2), potassium carbonate (K_2CO_3), borax ($Na_2H_3BO_4{\cdot}10H_2O$), feldspar ($K_2O{\cdot}Al_2O_3{\cdot}6SiO_2$) and magnesium fluoride (MgF_2) were used for preparation of LTF. All materials were AR grade and procured from Loba Chemie Pvt. Ltd (Mumbai, India)

2.2 Preparation of kalsilite and LTF

Potassium carbonate, alumina and silica were weighed in stoichiometric ratio of kalsilite 1:1:1. Weighed mixtures of materials with and without the incorporation of 2 wt% MgF_2 were prepared in the same manner. These mixtures were then pulverized in a high energy planetary ball mill (supplied by V.B. Ceramics, Chennai, India) for 3 h and 6 h with the rate of 250 rpm. Milling was done in a 250 ml zirconia cylindrical jar. The grinding balls made of zirconia having diameter 10 mm were used as a hard grinding medium. Ball to powder weight ratio was kept 4:1. The milling operation of mixtures was carried out continuously at room temperature for 3 h and 6 h. The milled powders were heat treated in an electric furnace at 900–1100 ℃ at a heating rate of 6 ℃/min and soaked for 1 h. The furnace was equipped with SiC heating element and a program PID528 manufactured by Selectron Process Controls Pvt Ltd., India. This program has the temperature control accuracy of ±1 ℃. To prepare LTF, starting components were mixed in an agate mortar. The mixture was melt in an alumina crucible at 1350 ℃ for 60 min. The molten frit was quenched in deionized water, air dried and then ball milled to pass a 350 mesh BSS.

2.3 Preparation of samples

The samples prepared for characterization contained different weight percentage of kalsilite. Optimization in choosing the prepared kalsilite was based on its maximum phase formation. Different formulations are presented in Table 1. Rectangular test bars were prepared using a uniaxial hydraulic press under 200 MPa. These bars were heated in a VITA VACUMAT 40T according to a standard dental veneering firing cycle pre-programmed by VITA. It consists of five steps from room temperature to 800 ℃. These five steps of firing cycle are: pre-heating at 500 ℃ for 2 min, heating from 500 ℃ to 800 ℃ for 6 min, 1 min soaking at 800 ℃ followed by cooling to 600 ℃ in 1 min.

2.4 Characterizations

The crystalline phases were identified by powder XRD technique. XRD patterns were observed using a portable XRD machine (Rigaku, Japan) using Cu Kα radiation employing Ni filter operating at 30 mA and 40 kV. Phase identification was carried out by comparing the respective powder XRD patterns with the standard database stated by JCPDS (PDF-2 Database 2003).

The thermal expansion of the material was

Table 1 Batch composition of different weight percentage of kalsilite and LTF samples

Sample coding	Firing temperature (℃)	Kalsilite (wt%)	LTF (wt%)
$K_{1000\text{-}20/80}$	1000	20	80
$K_{1000\text{-}25/75}$	1000	25	75
$K_{1000\text{-}30/70}$	1000	30	70
$K_{M1000\text{-}20/80}$	1000	20	80
$K_{M1000\text{-}25/75}$	1000	25	75
$K_{M1000\text{-}30/70}$	1000	30	70

determined by dilatometer (supplied by VB Ceramic Consultants, India) in the temperature range 20–550 ℃ at 6 ℃/min. The dilatometer was equipped with SiC heating element with a control accuracy of ±1 ℃. It had Nippon PID programmable digital temperature indicator cum controller. The samples for CTE measurement were cut and polished uniformly to the size of 45 mm × 15 mm × 10 mm.

Flexural strength measurements were done according to ASTM C78/C78M using universal testing machine Instron, 3344 (Germany). The specimens were bent in a three-point crossways fit with 20 mm span between the two supports (three-point bending). The load and the corresponding deflections were recorded. The flexural strength was calculated using the following equation:

$$F = \frac{3PL}{2bd^2} \quad (1)$$

where F is the flexural strength (kg/cm^2); P is the maximum applied load; L is the span length; b is the width of specimen; and d is the depth of specimen.

Apparent porosity (AP) and bulk density (BD) of all the kalsilite and LTF samples were determined according to ASTM C20-00. All specimens were polished using emery papers of grades 1/0, 2/0, 3/0 and 4/0 (Sia, Switzerland) followed by polishing on a velvet cloth using diamond paste of grade 1/4-OS-475 (HIFIN). These polished specimens were chemically etched with 40% hydrofluoric acid for 10 s and then washed with distilled water. Finally they were dried and gold sputtered. Micrographs were recorded with the help of a scanning electron microscope (INSPECT 50 FEI).

3 Results and discussion

3.1 Phase analysis of the ground kalsilite at different temperatures

Figure 1 shows the XRD patterns of the sample milled for 3 h at different firing temperatures. Diffraction peaks are well matched to JCPDS Card No. 87-1707. It can be seen that XRD pattern of precursor fired at 900 ℃ contains hexagonal kalsilite as a major phase alike to JCPDS Card No. 87-1707. As temperature increases from 1000 ℃ to 1100 ℃, kalsilite is present as a major phase in addition to small amount of leucite phase. Unit-cell parameters are $a = b = 5.157$ Å and $c = 8.706$ Å and more similar to those given by Becerro *et al*. [4] ($a = 5.166$ Å and $c = 8.7123$ Å). Presence of broad peaks in XRD patterns shows the small crystallite size of the kalsilite.

Figure 2 shows the XRD patterns of the sample containing 2 wt% of MgF_2 milled for 3 h. It can be noted that XRD patterns of precursor fired at 900 ℃ and 1000 ℃ contains kalsilite as a major phase with hexagonal crystal structure. Furthermore when heat treatment is increased to 1100 ℃, kalsilite occurs as a major phase with some peaks of leucite crystalline phase. It can be noted that formation of leucite crystalline phase occurs at high temperature. Formation of leucite phase is less in the sample containing MgF_2 in comparison to that of the sample without MgF_2. It is probable that the presence of MgF_2 additive suppresses the crystallization of leucite.

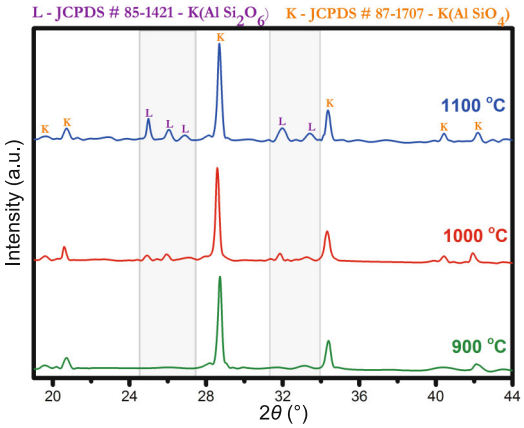

Fig. 1 XRD patterns of the sample milled for 3 h at different firing temperatures.

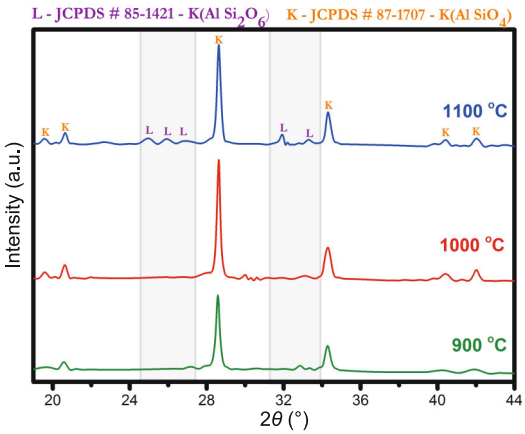

Fig. 2 XRD patterns of the sample containing 2 wt% of MgF_2 milled for 3 h at different firing temperatures.

Figure 3 shows the XRD patterns of the sample milled for 6 h. X-ray lines of the sample fired at 900 ℃ contain kalsilite as a major phase with small peaks of leucite phase. At temperatures 1000 ℃ and 1100 ℃, leucite is present as a main phase with small peaks of kalsilite crystalline phase. It might be due to high surface energy of ground sample. The smaller the particle size is, the larger the surface area and hence the higher the surface energy will be. Therefore, it can be concluded that the heat for formation of leucite is higher than that of kalsilite. It has also been previously reported by Zhang *et al*. [5] that activation energy for formation of leucite is higher than that of kalsilite. Kalsilite, therefore, crystallizes first as a metastable phase and then reacts with SiO_2 tetrahedra, which leads to formation of leucite phase. In the present work, the sample milled for 6 h has very fine particles in comparison to sample milled for 3 h. In former case therefore, most of the kalsilite coverts into leucite at higher temperatures.

Figure 4 shows the XRD patterns of the sample containing 2 wt% of MgF_2 milled for 6 h. It shows hexagonal kalsilite as a major phase with small peaks of leucite at 900 ℃, 1000 ℃ and 1100 ℃. Diffraction peaks are well matched to JCPDS Card Nos. 87-1707 and 85-1421. It can be concluded that MgF_2 promotes the formation of kalsilite. Zhang *et al*. [6] studied the effect of addition of CaF_2 on the crystallization of leucite. They found that CaF_2 decreases the crystallization temperature of leucite. Ionic radius of F^- ion (1.33 Å) is very close to radius of O^{2-} ion (1.4 Å); therefore, it replaces the O^{2-} ion and forms the Si–F or Al–F bonds [6]. Due to strong electrostatic attraction between Ca^{2+} and O^{2-} ions, network becomes loose. It

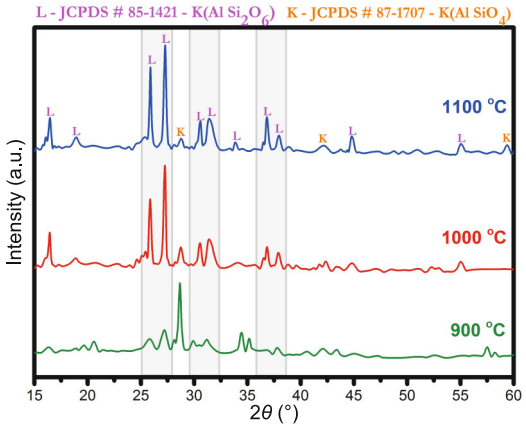

Fig. 3 XRD patterns of the sample milled for 6 h at different firing temperatures.

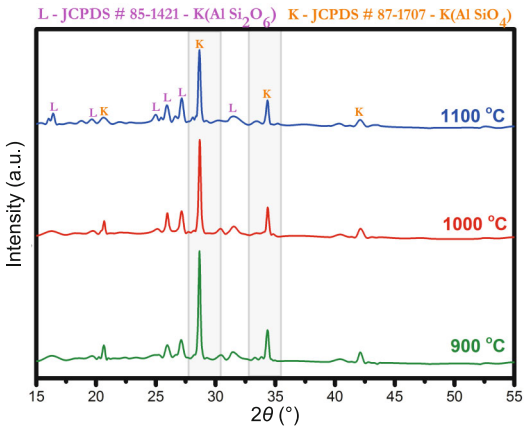

Fig. 4 XRD patterns of the sample containing 2 wt% of MgF_2 milled for 6 h at different firing temperatures.

helps the conversion of metastable kalsilite phase into stable leucite phase at low temperature.

In the present work, whereas, MgF_2 inhibits the formation of leucite phase and stabilizes the kalsilite metastable phase. It may be due to small amount of free silica present in the matrix. When F^- ion replaces O^{2-} ion in K^+, free Mg^{2+} reacts with free silica forming low temperature eutectic phase, enstatite ($MgO{\cdot}SiO_2$). It decreases any silica present around grain boundary around the kalsilite and hence supresses the formation of leucite.

3.2 Coefficient of thermal expansion

Thermal compatibility of PFM from room temperature to the glass transition temperature can be assessed by measuring the average expansion coefficient of metal and porcelain in the range of 20–550 ℃. Its thermal expansion is essential to assure good bonding of the ceramic to metal. Figure 5 shows the CTE curves of kalsilite with different weight percentage of LTF, $K_{1000\text{-}20/80}$, $K_{1000\text{-}25/75}$ and $K_{1000\text{-}30/60}$. It is found that the addition of kalsilite to LTF increases the CTE of the whole matrix. It may be due to formation of leucite crystalline phase which has high CTE. Glass transition temperatures (T_g) of $K_{1000\text{-}20/80}$, $K_{1000\text{-}25/75}$ and $K_{1000\text{-}30/70}$, are determined to be 415 ℃, 425 ℃ and 440 ℃, respectively.

Figure 6 shows the CTE curves of kalsilite–2 wt% MgF_2 with different weight percentage of LTF, $K_{M1000\text{-}20/80}$, $K_{M1000\text{-}25/75}$ and $K_{M1000\text{-}30/70}$. It is found that the addition of MgF_2 to kalsilite decreases the CTE of final mixture. These CTE values are about 40% less than that of samples without MgF_2. This may be due to

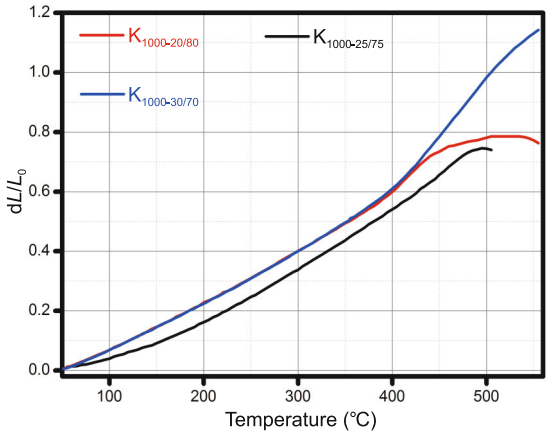

Fig. 5 CTE curves of the samples with different weight percentage of kalsilite and LTF.

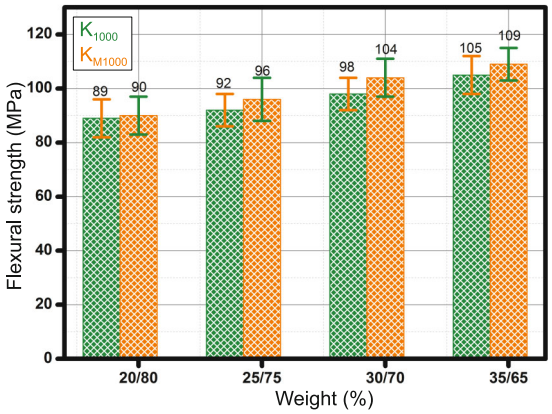

Fig. 7 Flexural strength of K_{1000} and K_{M1000} with different weight percentage of kalsilite and LTF.

the formation of low CTE major kalsilite phase. These results are in conformity with the results of XRD where the sample with MgF_2 has kalsilite as a major phase, i.e., MgF_2 suppresses the formation of leucite. The glass transition temperatures (T_g) of $K_{M1000\text{-}20/80}$, $K_{M1000\text{-}25/75}$ and $K_{M1000\text{-}30/70}$ are determined to be 415 ℃, 425 ℃ and 430 ℃, respectively. These prepared materials are suitable for PFM, as their CTE values of 14.0×10^{-6}–14.8×10^{-6} $(℃)^{-1}$ are close to standard CTE of nickel–chrome alloy (13.9×10^{-6} $(℃)^{-1}$).

3.3 Flexural strength

Figure 7 shows the flexural strength of K_{1000} and K_{M1000} with different weight percentage of kalsilite in LTF. Flexural strength increases with increasing the micro fine kalsilite in matrix. Homogenous dispersion of micro fine kalsilite grains within the glassy matrix leads to enhance the mechanical strength. K_{M1000} has higher flexural strength than K_{1000}. Subsequently the synthesised samples show better sinterability, low porosity and high flexural strength. The flexural strength is more or less similar for all samples. However, the mixed samples with 20 wt%, 25 wt%, 30 wt% and 35 wt% kalsilite expressively result in higher flexural strength. This is due to presence of micro fine particles, i.e., larger surface area and hence less porosity.

3.4 Bulk density and apparent porosity

Figure 8 shows the variation of BD and AP with different weight percentage of kalsilite and LTF. It can be noted from Fig. 8 that BD increases with increasing the content of kalsilite followed by a continuous decrease of AP. Micro fine kalsilite particles dispersed throughout the glassy matrix help in improvement of packing density of the samples.

3.5 Microstructure evaluation through SEM

The microstructures of kalsilite with (K_{M1000}) and without (K_{1000}) MgF_2 with different weight percentage

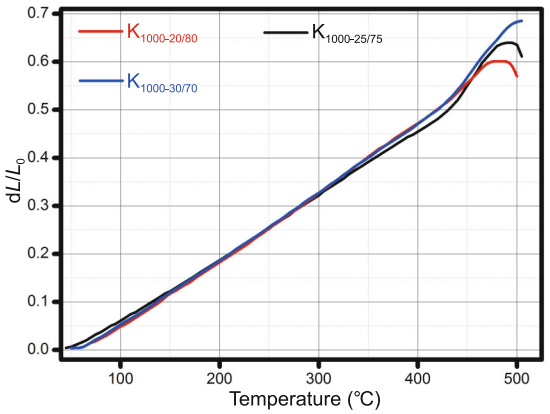

Fig. 6 CTE curves of the samples with different weight percentage of kalsilite–2 wt% MgF_2 and LTF.

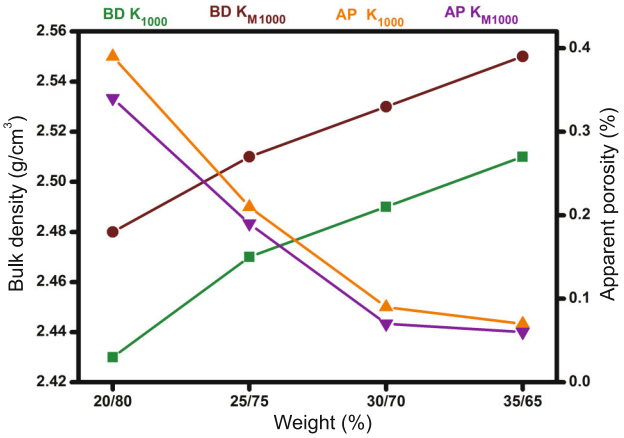

Fig. 8 BD and AP of the samples with different weight percentage of kalsilite and LTF.

of LTF are shown in Fig. 9. There is no visible micro-crack appearance due to phase transformation. Micrographs show a very dense structure which is also in conformity with the AP and BD plots. This also results in the high flexural strength.

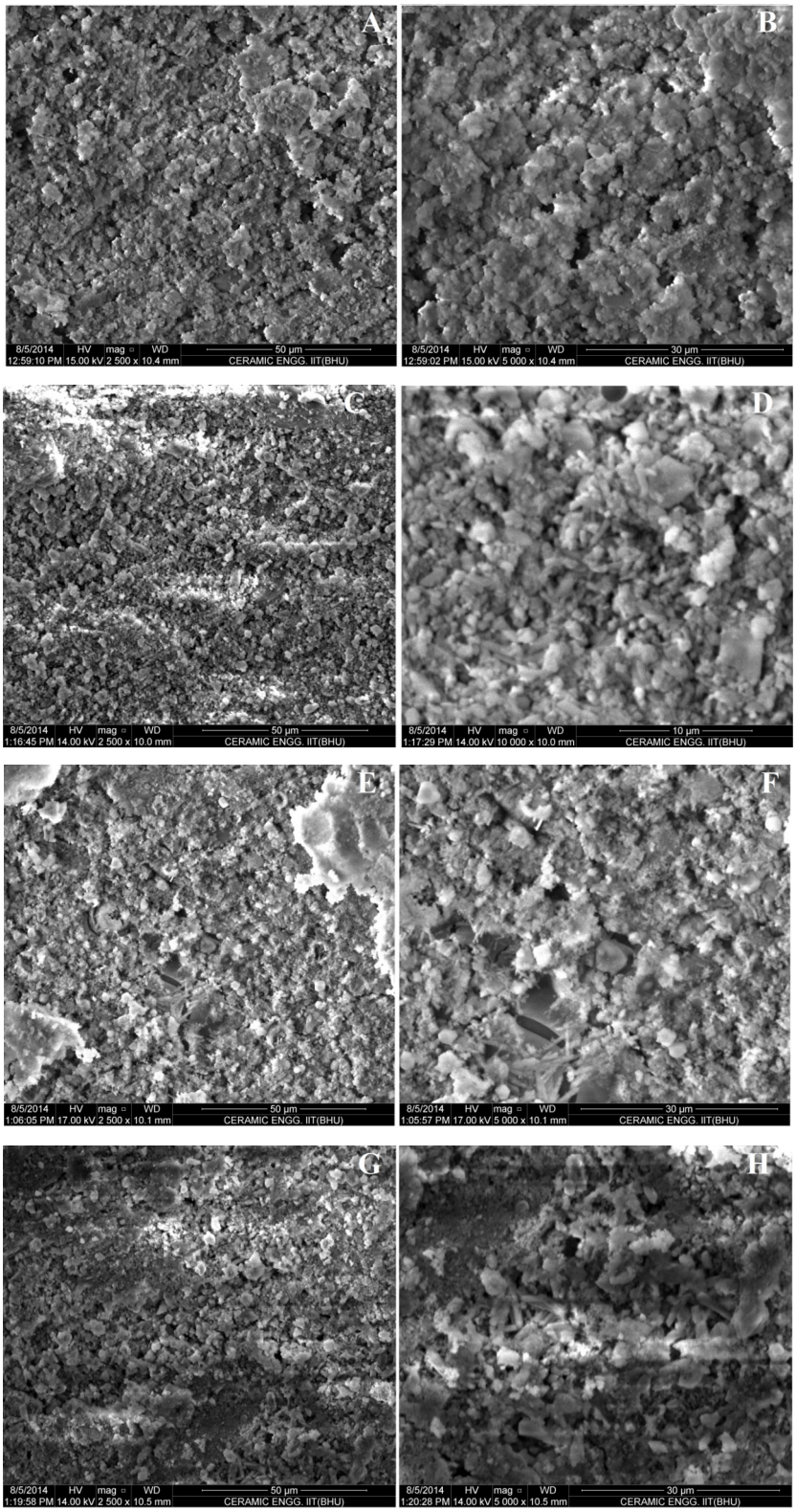

Fig. 9 Scanning electron micrographs of kalsilite with (K_{M1000}) and without (K_{1000}) MgF_2 with different weight percentage of LTF in different magnification: (a, b) $K_{M1000\text{-}25/75}$; (c, d) $K_{M1000\text{-}30/70}$; (e, f) $K_{1000\text{-}25/75}$; (g, h) $K_{1000\text{-}30/70}$.

4 Conclusions

Micro fine kalsilite has been successfully synthesised by high energy ball milling. Addition of MgF_2 supresses the formation of leucite phase and stabilizes the kalsilite phase. Kalsilite–2 wt% MgF_2 with different weight percentage of LTF, shows the CTE value of 14.0×10^{-6} $(℃)^{-1}$ to 14.8×10^{-6} $(℃)^{-1}$. This value is close to standard CTE of nickel–chrome alloy (13.9×10^{-6} $(℃)^{-1}$). Samples with 20 wt%, 25 wt% and 30 wt% kalsilite have higher flexural strength due to presence of micro fine kalsilite particles in the matrix. Micrographs show very dense structure with no visible cracks. This makes present material suitable for application in porcelain fused to metal.

Acknowledgements

The authors gratefully acknowledge the financial support of DST (TDT division, reference No. DST/SSTP/UP/197 (G) 2012), Ministry of Science & Technology, New Delhi, India.

References

[1] Andou Y, Kawahara A. The renfinement of the structure of synthetic kalsilite. *Mineral J* 1984, **12**: 153–161.

[2] Ota T, Takebayashi T, Takahashi M, *et al.* High thermal expansion $KAlSiO_4$ ceramic. *J Mater Sci* 1996, **31**: 1431–1433.

[3] Becerro AI, Escudero A, Mantovani M. The hydrothermal conversion of kaolinite to kalsilite: Influence of time, temperature, and pH. *Am Mineral* 2009, **94**: 1672–1678.

[4] Becerro AI, Mantovani M, Escudero A. Hydrothermal synthesis of kalsilite: A simple and economical method. *J Am Ceram Soc* 2009, **92**: 2204–2206.

[5] Zhang Y, Lv M, Chen D, *et al.* Leucite crystallization kinetics with kalsilite as a transition phase. *Mater Lett* 2007, **61**: 2978–2981.

[6] Zhang Y, Wu J, Rao P, *et al.* Low temperature synthesis of high purity leucite. *Mater Lett* 2006, **60**: 2819–2823.

[7] Kopp OC, Harris LA, Clark GW. The hydrothermal conversion of muscovite to kalsilite and an iron-rich mica. *Am Mineral* 1961, **46**: 719–727.

[8] Bogdanoviciene I, Jankeviciute A, Pinkas J, *et al.* Study of alumposilicate porcelain: Sol–gel preparation, characterization and erosion evaluated by gravimetric method. *Mater Res Bull* 2008, **43**: 2998–3007.

[9] Bogdanoviciene I, Jankeviciute A, Pinkas J, *et al.* Sol–gel synthesis and characterization of kalsilite-type alumosilicates. *Mater Sci* 2007, **13**: 214–218.

[10] Dimitrijevic R, Dondur V. Synthesis and characterization of $KAlSiO_4$ polymorphs on the SiO_2–$KAlO_2$ join. *J Solid State Chem* 1995, **115**: 214–224.

[11] Heller-Kallai L, Lapides I. Thermal reactions of kaolinite with potassium carbonate. *J Therm Anal Calorim* 2003, **71**: 689–698.

[12] Baláž P, Achimovičová M, Baláž M, *et al*. Hallmarks of mechanochemistry: From nanoparticles to technology. *Chem Soc Rev* 2013, **42**: 7571–7637.

[13] Kumar PH, Srivastava A, Kumar V, *et al*. Effect of high-energy ball milling and silica fume addition in $BaCO_3$–Al_2O_3. Part I: Formation of cementing phases. *J Am Ceram Soc* 2014, DOI: 10.1111/jace.13173.

[14] Srivastava A, Singh VK, Kumar V, *et al*. Low cement castable based on auto combustion processed high alumina cement and mechanochemically synthesized cordierite: Formulation and properties. *Ceram Int* 2014, **40**: 14061–14072.

Role of CaF_2 on mechanochemically synthesized leucite as dental veneering glass ceramics

P. H. Kumar*[1], A. Srivastava[1], V. Kumar[1], H. Singh[1], S. Sharma[1], P. Kumar[2] and V. K. Singh[1]

Leucite based glass ceramic is widely used in dental ceramics as porcelain fused to metals for veneering applications. Main properties considered here are high coefficient of thermal expansion and good mechanical properties. Owing to these requirements, high expansion phase such as leucite is incorporated in these glass ceramics. The present work was aimed to synthesise leucite using its stoichiometric batch compositions and subsequent high energy ball milling. CaF_2 was also added in another mix to study its role on leucite formation. Further prepared, leucite phase was added in separately prepared low temperature glass frit powders to control amount of glass and leucite content. X-ray diffraction results displayed that high energy ball milling and additive promoted the formation of leucite as a major crystalline phase. Furthermore, CaF_2 also suppressed the subsidiary crystallisation of kalsilite phase. Evaluated average coefficient of thermal expansion in the temperature range of 20–500°C was very close to the theoretical value of pure leucite.

Keywords: Mechanochemical synthesis, Thermal expansion, Leucite, Dental glass ceramic, Microstructure, Porcelain fused to metal, X-ray diffraction

Introduction

Metal–ceramic systems for making dental crowns and bridges are being marketed since 1960s. Employed for more than half a century, Porcelain fused to metal (PFM) is still the most significant dental restorative due to its lower cost than all ceramic systems such as zirconia, spinel and alumina.[1] Success of PFM depends on the proper applications of different layers of glass ceramics and subsequent firing in vacuum onto a metal substructure to produce an aesthetical acceptable restoration. Veneering ceramics for metal ceramic restorations are commonly named as feldspathic porcelains based on leucite phase.[2] Feldspar derived glass ceramics exhibits a low coefficient of thermal expansion (CTE), $\sim 8{\cdot}6 \times 10^{-6}\ K^{-1}$ if leucite is not crystallised during manufacturing process. Therefore, leucite should be present in high amount in these glass ceramics for a successful veneering.[3] Leucite glass ceramic is the widely used ceramic for all type of metal alloys used as coping. It provides high CTE ($20–27 \times 10^{-6\circ}C$), high strength, colour appeal, suitable refractive index and excellent biocompatibility.[4–6] Leucite enhances the CTE of glass ceramic to make it thermally suitable with metal.[7] Pure leucite phase has a high melting point of 1693°C.[8] This phase is partially obtained, when potash feldspar melts incongruently in temperature range of 1120–1150°C. The main drawback with feldspar is natural impurities, present in it. These impurities may discolour glass ceramics or undesirable colour may be produced. Traditional method for manufacturing feldspathic dental glass ceramic is to make glass frits and subsequent heat treatments for crystal growth. In another approach, this material has also been synthesised by various wet chemical routes such as sol–gel, coprecipitation and hydrothermal process. Formation of leucite by conventional method is always accompanied by a glassy phase and a common intergrowth of kalsilite. The synthesis of pure leucite is difficult at low temperatures. It also undergoes phase transformation from tetragonal to cubic during heating leucite based glass ceramics.[9,10] The tetragonal leucite possesses a high CTE $27{\cdot}2 \times 10^{-6\circ}C$, whereas its cubic form exhibit lower CTE value $15{\cdot}9 \times 10^{-6\circ}C$.[11] The presence of tetragonal leucite phase in the matrix of a low temperature frit (LTF) is helpful to increase its CTE and proficient bonding can be obtained with metals. Tetragonal leucite volume fraction in commercially available dental porcelain typically ranges between 17 and 45 wt-% in a LTF matrix.[12,13]

Natural inventory of leucite is very rare. Synthesis of leucite glass ceramic powders has been a challenging subject till now. Previous literatures suggest that glass ceramic preparation with high content of leucite is possible by solid state sintering,[14,15] salt bath,[16] coprecipitation,[17] sol–gel[18] and hydrothermal[19,20] processes.

[1]Department of Ceramic Engineering, IIT (BHU), Varanasi, India
[2]Department of Chemical Engineering, IIT (BHU), Varanasi, India

*Corresponding author, email phemanth111@gmail.com

Published by Maney on behalf of the Institute
Received 9 June 2014; accepted 14 September 2014
DOI 10.1179/1743676114Y.0000000208

Although leucite glass ceramic has been synthesised by several methods, the synthesis of complete crystalline leucite has never been reported, as it is always accompanied by a glassy phase. Erbe and Sapieszko reported the formation of leucite with some impurity of kalsilite at 1000°C.[21] Jankeviciute and Kareiva[22] synthesised leucite at 950°C via sol–gel derived molecular precursor. Zhang *et al.*[23] synthesised pure leucite at 850°C by sol–gel method. Other than solid state, all approaches increase the cost of the product. Mechanochemical process is a chemical reaction induced by a self-propagating process, resulting in lowering of calcination and sintering temperature.[24] The source of energy for reaction is the increased thermal reactivity of very fine powder particles. When a small portion of starting mixes start reacting at relatively low temperatures due to extra fineness, it further promotes thermal reactions in unreacted slightly coarse particles at low temperatures. That is the reason that formation of leucite glass ceramics is possible at lower temperatures. This preparation method is simple, economical and also suitable for large scale production of other nanoparticles ceramic system.[25] This process has been successfully utilised to obtain a number of nanomaterials including Al_2O_3,[26] ZnO,[27] $SrAl_2O_4$,[28] ZrO_2,[29] $BaTiO_3$[30] and $BaAl_2O_4$.[31]

The main idea of the present work is to demonstrate that submicrometre size leucite glass ceramics can be produced at relatively low temperatures using mechanically activated precursors. Two blends in which one containing Al_2O_3, SiO_2 and K_2CO_3 in the stoichiometric ratio of leucite and the other with same stoichiometric ratio with 2 wt-%CaF_2 as additive was prepared. The starting mixes were mechanochemically activated before heat treatment to study phase formations at different temperatures. The role of additive on the phase formation as well as thermal expansion behaviour was observed. The effects of mechanical activation and calcium fluoride addition on microstructure and flexural strength have also been investigated. Further low temperature glass frits based on alumino-alkalis-silica-boric oxide, were prepared. The prepared leucite was mixed in ground frit in different proportions, and their physicothermal properties were studied

Experimental

Materials

Aluminium oxide (Al_2O_3), potassium carbonate (K_2CO_3), calcium fluoride (CaF_2) and silicon dioxide (SiO_2) were used for leucite synthesis. Sodium carbonate (Na_2CO_3), potassium nitrate (KNO_3), silicon dioxide (SiO_2), potassium carbonate (K_2CO_3), borax ($Na_2H_3BO_4.10H_2O$), feldspar ($K_2OAl_2O_36SiO_2$), magnesium oxide (MgO), calcium carbonate ($CaCO_3$), zirconium dioxide (ZrO_2) and calcium fluoride (CaF_2) were used for preparation of LTF. All materials were analytical reagent grade and procured from Loba Chemie Pvt. Ltd (Mumbai, India).

Preparation of leucite glass ceramics

Aluminium oxide, potassium carbonate and silicon dioxide were weighed in leucite stoichiometric ratio of 1 : 1 : 2. Weighed mixes of materials were termed as MCL without CaF_2 and as MCL-C with the incorporation of 2 wt-%CaF_2. The raw materials were first thoroughly mixed in an agate mortar pestle for 30 min. These mixtures were then pulverised in a high energy planetary ball mill. This planetary ball mill was manufactured by V.B. Ceramics, Chennai, India. It consists of a 250 mL zirconia cylindrical jar. The grinding balls made of zirconia having diameter 10 mm were used as a hard grinding medium. Grinding media and the material weight ratio were kept 3 : 1, and mill was set to rotate at a constant speed of 300 rev min^{-1} during the study. The milling operation of mixes was carried out continuously at room temperature for 6 h. The pulverised powders were kept in an alumina crucible and heated in an electric furnace at 900, 1000 and 1100°C respectively at a heating rate of 10°C min^{-1} for a soaking period of 1 h. The furnace was equipped with SiC heating elements and a programmer PID528, manufactured by Selectron Process Controls Pvt Ltd, India. This programmer has the temperature control accuracy of ± 1°C.

Preparation of LTF

The raw materials were taken for making LTF frit to obtain its composition in a weight proportion to meet $59SiO_2$–$13Al_2O_3$–$9K_2O$–$10Na_2O$–$2CaO$–$2CeO_2$–$1{\cdot}5Li_2O$–$1CaF_2$–$1MgO$–$1BaO$–$0{\cdot}5ZrO_2$ after firing. This composition was selected because its thermal expansion value was near to dental metal alloys in our experiments. To prepare LTF, starting components were mixed in an agate mortar pestle. The mixture was melt in a platinum crucible at 1350°C for 1 h. The melted frit was quenched in deionised water then pulverised to pass a 350 mesh.

Sample preparation and sintering

The rectangular bar shaped samples were formulated with 25 wt-% leucite (as prepared in the section on 'Preparation of leucite glass ceramics') and 75 wt-%LTF (as prepared in the section on 'Preparation of LTF'). These bars were formed using a uniaxial hydraulic pressure at 200 MPa. These samples were heated in a dental furnace (Model: VITA VACUMAT 40T by Vita International, Germany). This furnace comes with preprogramed firing schedules for firing wash opaque, opaque, dentin, incisor, glazer and margin according to marketed products. Our selected programme had five steps, from room temperature to 800°C. These five steps of firing cycle were preheating at 500°C for 2 min, heating from 500 to 800°C in 6 min in vacuum, 1 min soaking at 800°C followed by cooling to 600°C in 1 min.

Characterisations

X-ray diffraction

The crystalline phases were identified by XRD for investigation of phases present. X-ray diffraction patterns were observed using a portable XRD machine (Rigaku, Japan) using Ni filtered Cu K_α radiation operating at 30 mA and 40 kV. Phase identification analysis was carried out by comparing the powder XRD patterns with the standard database stated by Joint Committee on Powder Diffraction Standards (PDF-2 database 2003). The crystallite size is determined from the Scherrer's formula given as

$$D = 0{\cdot}9\lambda/\beta\cos\theta \quad (1)$$

where D is the apparent size of crystal, λ is the wavelength of the X-rays, β is the full width at half maximum of the corresponding line and θ is angle of diffraction of the peak.

Coefficient of thermal expansion

The thermal expansion of samples was determined by a dilatometer (supplied by VB Ceramic Consultants, India) from 20 to 500°C at 6°C min^{-1}. The dilatometer was equipped with SiC heating element with a control accuracy of ±1°C. It had a Nippon PID programmable digital temperature indicator cum controller. The samples for CTE measurements were cut and polished uniformly to the size of 45 × 15 × 10 mm.

Flexural strength testing

Flexural strength measurements were performed according to ASTM C78/C78M. The specimens were tested in a three-point bending fixture with 20 mm span length between the two supports. The universal testing machine Instron, 3344 (Germany) was used for this measurement. The load and the corresponding deflection were recorded. The flexural strength was calculated using the following equation

$$R = \frac{3\,PL}{2\,bd^2} \tag{2}$$

where R is the flexural strength (kg cm^{-2}), P is the maximum applied load, L is the span length, b is the width of specimen and d is the depth of specimen. The standard deviation S of the flexural strength values was calculated using the following formula

$$S = \left[\frac{1}{N-1}\sum_{i=1}^{N}(x_i - \bar{x})^2\right]^{1/2} \tag{3}$$

where N is the number of samples, x_i is the value of one sample and $\bar{x}$ is the mean value.

Statistical analysis

Weibull statistical analysis of the results of fracture strengths was carried out. Weibull statistical analysis is a common tool to interpret the strength data on the basis of a semi empirical expression derived from Weibull's statistical theory of fracture as given below[32]

$$P(\sigma) = 1 - \exp\left[-\left(\frac{\sigma}{\sigma_N}\right)^m\right] \tag{4}$$

It describes the cumulative failure probability P as a function of the applied tensile stress σ. The σ_N and m are the nominal strength and Weibull modulus respectively. These parameters can be determined from a set of experimental data by fitting the estimated failure probability to equation (4). In the logarithm form equation (4) can be written as

$$\ln[-\ln(1-P)] = m\log\sigma - m\log\sigma_N \tag{5}$$

which gives Weibull modulus from the slope and nominal strength from the ln $[-\ln(1-P)]=0$ intercept. Evidently, the strength σ_N does not take into account the potential impact of the test method (loading geometry and specimen size) and does not relate to the intrinsic strength in an obvious manner.[32] The failure probability P_i was calculated in following steps:

(i) rank by ascending order (i=1…5) the observed stresses at fracture and assign cumulative probabilities of failure according to $P_i=(i-0{\cdot}5)/n$, where i is the rank, and n is the number of broken samples[33]

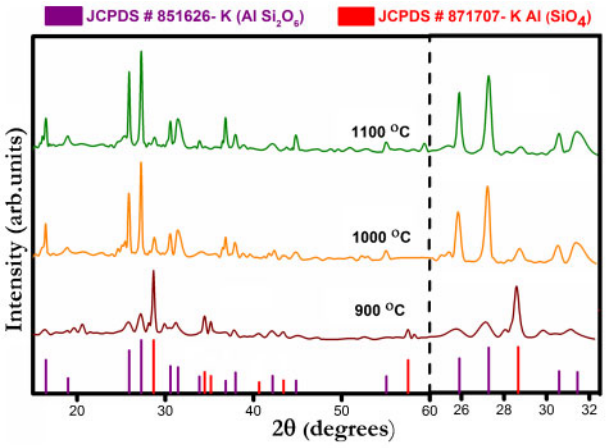

1 X-ray diffraction patterns of 6 h milled MCL heat treated at different temperatures

(ii) fit the ln$[-\ln(1-P)]$ versus ln σ data points to a straight line using linear fit programme.

Microstructure

The leucite glass ceramics samples synthesised at 1100°C were polished using emery papers of grade 1/0, 2/0, 3/0, and 4/0 (Sia, Switzerland) followed by polishing on a velvet cloth using diamond paste of grade 1/4-OS-475 (HIFIN). All specimens were cleaned with ethanol and finally gold sputtered. Micrographs were recorded with the help of a SEM (INSPECT 50 FEI).

A bright field transmission electron microscope (FEI, Eindhoven, the Netherlands) equipped with SIS Mega View III CCD camera at 120 kV employing Analysis software (SIS, Muenster, Germany) was used for TEM investigations. Powder samples for TEM were first dispersed in double distilled water by ultrasonication and then dropped on a conventional carbon coated copper grid.

Results and discussion

Phase analysis through XRD

Figure 1 is the XRD patterns of milled MCL powders heat treated at varying temperatures. It can be noted that XRD pattern of mixes fired at 900°C for 1 h had kalsilite as a major phase with small peaks of crystalline leucite. Furthermore, heat treatment was increased to 1000°C, where leucite occurred as a major phase and peaks of metastable kalsilite diminished. At 1100°C, complete leucite phase formation occurred. Thus, it was concluded that increasing temperature plays an important role in complete phase formation of leucite crystalline phase. The existence of broad peaks indicates formation of small crystallite size leucite and coexistence of glassy matrix. It may be interpreted that metastable kalsilite reacted with residual vitreous SiO_2, converting into leucite phase. The above explanation is also supported by studies of Zhang *et al.*,[7] who reported disappearance of kalsilite at high temperatures and or with increase in soaking period.

Figure 2 shows the ground MCL-C fired at 900, 1000 and 1100°C for 2 h. Leucite crystalline phase is formed in all samples, with a very small amount of kalsilite crystalline phase at 900°C. No secondary crystalline phases were identified in samples fired at 1000 and

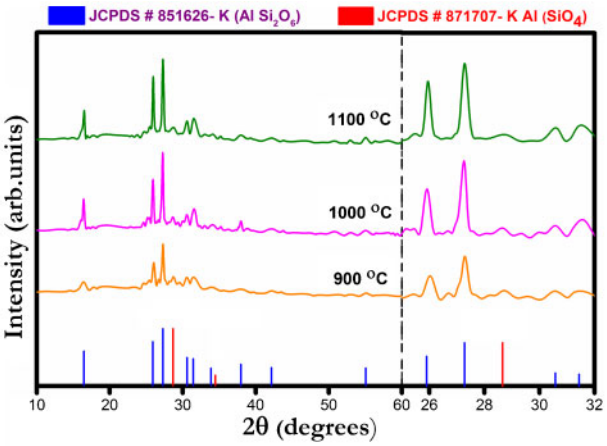

2 X-ray diffraction patterns of 6 h milled MCL-C heat treated at different temperatures

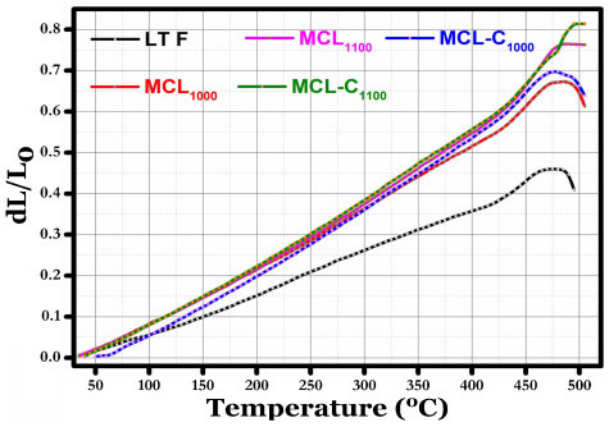

4 Coefficient of thermal expansion curves of LTF, MCL1000, MCL1100, MCL-C1000 and MCL-C1100

1100°C. It is anticipated that presence of CaF_2 additive suppressed the crystallisation of kalsilite. This phase transformation is previously reported by Zhang *et al.*[23] The eutectoid formed after CaF_2 addition also assists the phase transformation from kalsilite to leucite in a relative short heat preservation. A small amount of CaO (up to 2 wt-%) is therefore essential for good crystallisation of tetragonal leucite.[32] Leucite phase formation at 900°C indicates that high energy ball milling promotes its crystallisation at low temperature. Nanocrystalline powder is formed as a result of high energy ball milling. This statement was confirmed by crystallite size determination through the Scherrer's formula.

Figure 3 demonstrates the crystallite size of the samples as a function of firing temperature. From this plot, it can be observed that crystallite size increases with the firing temperature. The respective crystallite sizes are 46, 47 and 48 nm for samples fired at 900, 1000 and 1100°C. The crystallite size of sample MCL-C was much larger than sample MCL, which suggests grain growth due to additive.

Coefficient of thermal expansion

The CTE is the most significant characteristic for a reliable porcelain fused to metal restoration. Thermal compatibility of ceramic fused to metal from room temperature to the glass transition temperature can be assessed by measuring the average expansion coefficient of metal and porcelain in the range of 20–550°C. If a dental ceramic is to be used as a veneer on a metal base, then in order to avoid detrimental cracks, its thermal expansion must be controlled to assure good bonding of the ceramic to metal. Surface crystallisation indicated that glass powder with uniform leucite by tribochemical activation of the grain surfaces of glass granules, in particular results in controlled uniform formation and growth processes. Leucite crystals form around the nucleation centres of glass grain-like petals around a flower in a dendritic growth process. This enables optimal properties, such as a high CTE to be achieved.[33,34]

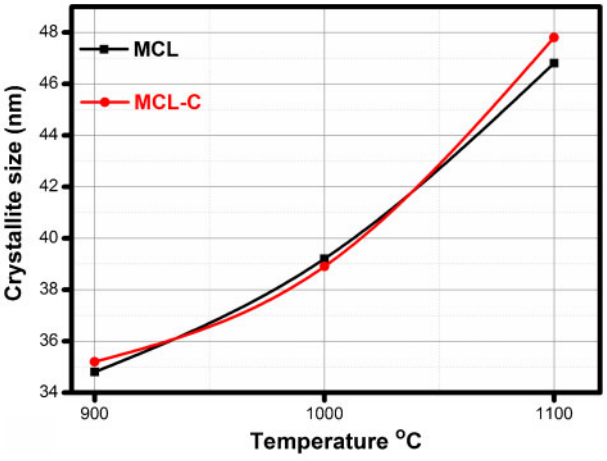

3 Variation of crystallite size of MCL and MCL-C with temperature

Figure 4 illustrates the CTE curves of LTF, MCL_{1000}, MCL_{1100}, MCL-C_{1000}, and MCL-C_{1100} samples. It is observed that the addition of leucite weight fraction to LTF has a close linear relation with the CTE of the final mixture.[28] The glass transition temperatures T_g of the LTF, MCL_{1000}, MCL_{1100}, MCL-C_{1000} and MCL-C_{1100} were determined to be 405, 415, 425 and 430°C respectively. The CTE of the samples before T_g is $10{\cdot}1 \times 10^{-6}{}^{\circ}C^{-1}$, $14{\cdot}2 \times 10^{-6}{}^{\circ}C^{-1}$, $15{\cdot}3 \times 10^{-6}{}^{\circ}C^{-1}$ and $15{\cdot}7 \times 10^{-6}{}^{\circ}C^{-1}$. The CTE of is sufficient enough to make it a PFM material for dental prosthesis. The calculated CTE (20–500°C) of the leucite glass ceramic synthesised with and without CaF_2 is given in Table 1. These prepared materials are suitable for PFM as its CTE value of $14{\cdot}2 \times 10^{-6}{}^{\circ}C^{-1}$ is close to standard CTE of nickel–chrome alloy ($13{\cdot}9 \times 10^{-6}{}^{\circ}C$).[31]

Table 1 Coefficient of thermal expansion of MCL and MCL-C fired at different temperatures*

Sample coding	Firing temperature/°C	CTE/°C^{-1}	T_g/°C	SP/°C
MCL_{900}	900	$14{\cdot}5 \times 10^{-6}$	400	465
MCL_{1000}	1000	$16{\cdot}1 \times 10^{-6}$	405	475
MCL_{1100}	1100	$16{\cdot}8 \times 10^{-6}$	415	480
MCL-C_{900}	900	$15{\cdot}4 \times 10^{-6}$	420	480
MCL-C_{1000}	1000	$16{\cdot}6 \times 10^{-6}$	425	485
MCL-C_{1100}	1100	$17{\cdot}6 \times 10^{-6}$	430	495

*CTE: coefficient of thermal expansion; T_g: glass transition temperature; SP: softening point.

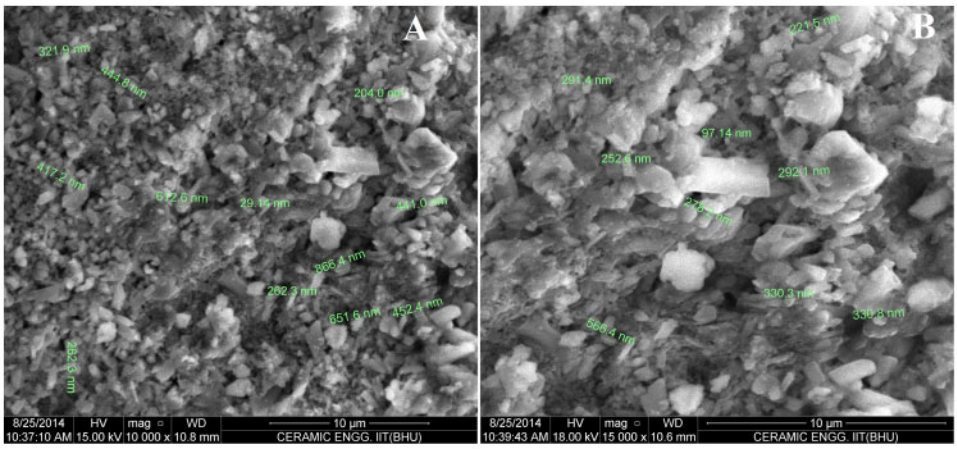

5 Scanning electron micrographs of leucite–LTF composite of MCL samples

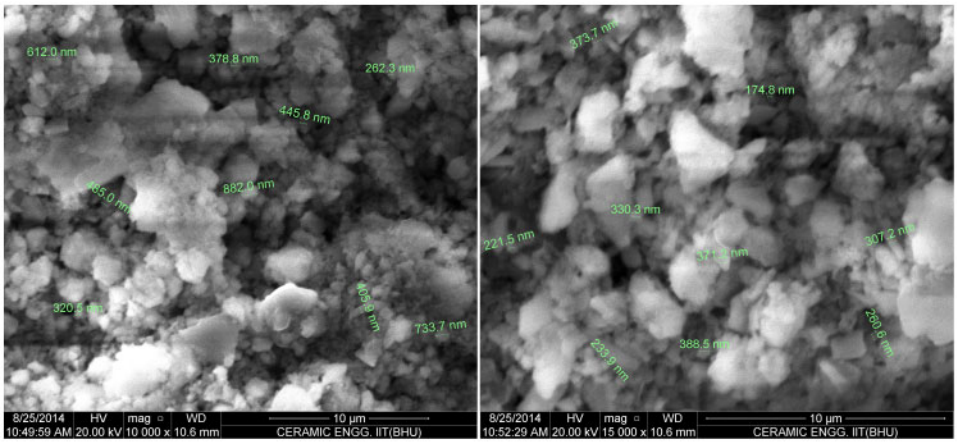

6 Scanning electron micrographs of leucite–LTF composite of MCL-C samples

Microstructure evaluation through SEM

The microstructure of leucite–LTF composite of MCL and MCL-C is shown in Figs. 5 and 6 respectively. The images indicate matrix of homogenously distributed tetragonal leucite crystals. There is no visible microcrack appearance due to phase transformation of metastable kalsilite to leucite. The particle size distribution of the leucite crystal is in the range of 0·6–1·0 µm. Some previous studies suggest that fine leucite crystals is beneficial for the enhancement of its mechanical property.[35] Fine grain leucite increases the abrasion resistance.[36,37]

TEM of milled leucite powders

Typical bright field transmission electron micrographs of the powder of 6 h milled samples are shown in Figs. 7 and 8 These images clearly show that the particles are well spherical in shape. Some agglomerated particles are also observed, which may be the result of long milling duration. Particle size distribution obtained from TEM study is displayed as an inset figure. This was estimated through Olympus Soft Image analysis tool, attached to the TEM equipment. The mean particle diameter 39 nm is in good agreement with the results obtained from XRD data.

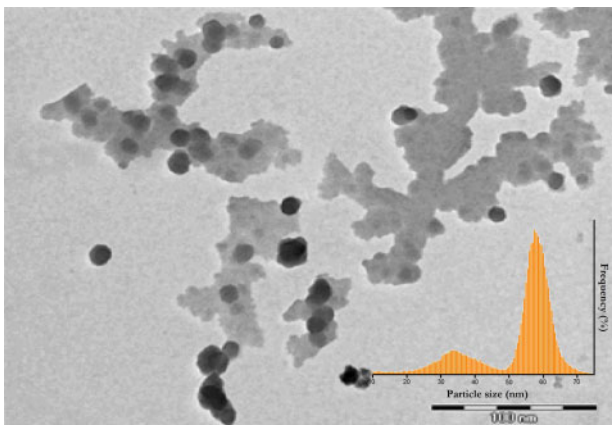

7 TEM of 6 h milled MCL

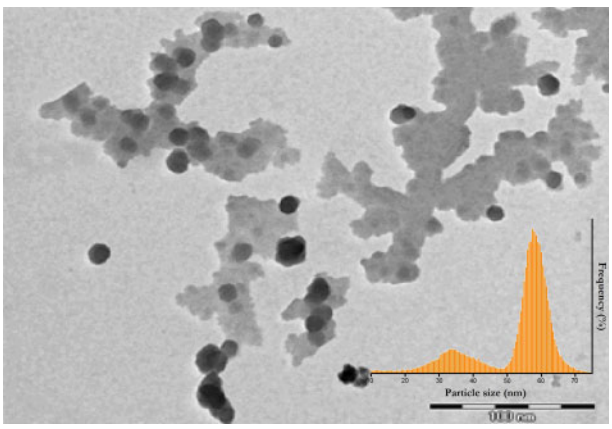

8 TEM of 6 h milled MCL-C

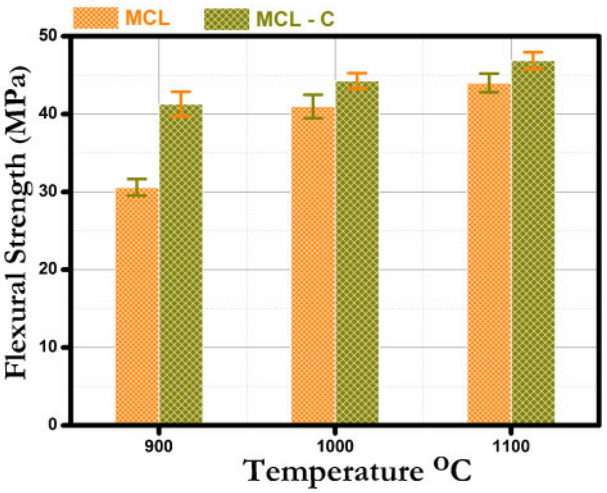

9 Flexural strength of milled MCL and MCL-C at different temperatures

Flexural strength

Figure 9 shows the flexural strength of MCL and MCL-C as a function of firing temperature. Flexural strength of MCL-C is higher than that of MCL. The homogenous dispersion of leucite grains within the glassy matrix leads to its enhanced mechanical strength.[34] Moreover, the synthesised leucite powders has large surface area. Subsequently, the samples produced show better sinterability, low porosity and high flexural strength. The samples MCL_{1100} and $MCL\text{-}C_{1100}$ show improved flexural strength than rest of the batch, due to the formation of uniform glassy matrix surrounding the leucite particles. The flexural strength was similar for all samples, except for the MCL fired at 900°C which has a low strength of 312 kg cm^{-2}. This phenomenon may be correlated to major crystalline phase of metastable kalsilite at 900°C, which has low flexural strength than leucite. The mean and standard deviation values are given in Table. 1.

It can be seen from Table 2 that values of Weibull's modulus '*m*' increases with increasing temperature. This may be due to fine leucite crystal present in the matrix and lack of microcracking in the samples (Figs. 5 and 6). This higher values of '*m*' (m=24·2–38·08) confirms the reliability of these samples.

Conclusions

Leucite glass ceramic was synthesised at 900°C by mechanochemical method after introduction of 2 wt-%CaF_2 as an additive. Complete formation started from 1000°C. Introduction of CaF_2 in leucite raw mixes suppressed kalsilite phase without increasing the leucite synthesis temperature. Coefficient of thermal expansion of prepared bar samples with the mixes of leucite powders and LTF powders nearly matched with coping material (nickel–chrome alloy). The veneering dental glass ceramics prepared by the materials containing nano leucite particles and glass frit can be used in various applications for making PFM crowns or bridges. Composition of these mixes can be adjusted to obtain different value of thermal expansion by varying prepared leucite content. In this new approach, glass ceramic powders for opaque, dentine and glazes for veneering apllications can be prepared, which have different melting temperatures and thermal expansion value. It may be concluded that values of Weibull's modulus increases with increase in synthesis temperature. This may be due to increase in fine leucite crystal content. These higher values confirm the reliability of these samples, which is beneficial for its mechanical properties.

Table 2 Flexural strength and Weibull analysis results*

Sample coding	Mean/MPa	SD/MPa	*m*	σ_N/MPa	r^2
MCL_{900}	30·59	1·047	24·20	31·50	0·978
MCL_{1000}	41·28	1·580	25·00	42·52	0·974
MCL_{1100}	40·99	1·210	33·67	44·25	0·980
$MCL\text{-}C_{900}$	44·27	1·630	27·00	42·09	0·998
$MCL\text{-}C_{1000}$	44·00	1·000	28·68	45·15	0·973
$MCL\text{-}C_{1100}$	46·87	1·036	38·08	46·99	0·966

*SD: standard deviation; *m*: Weibull modulus; σ_N: characteristic strength.

Acknowledgements

The authors gratefully acknowledge the financial support of DST [(TDT Division), reference no. DST/SSTP/UP/197(G) 2012], Ministry of Science & Technology, New Delhi, India.

References

1. J. R. Kelly, I. Nishimural and S. D. Campbell: 'Ceramics in dentistry historical roots and current perspectives', *J. Prosthet. Dent*., 1996, **75**, 18–32.
2. W. M. Weinstein, L. K. Katz and S. A. B. Weinstein: 'Fused porcelain-to-metal teeth', US patent no.3,052,982, 1962.
3. P. J. Vergano, D. C. Hill and D. R. Uhlmann: 'Thermal expansion of feldspar glasses', *J. Am. Ceram. Soc.*, 1967, **50**, 59–60.
4. J. R. Mackert, S. W. Twiggs, C. M. Russell and A. L. Willicims: 'Evidence of a critical leucite particle size for micro cracking in dental porcelains', *J. Dent. Res*., 2001, **80**, 1574–1579.
5. M. Mrazova and A. Klouzkova: 'Leucite porcelain fused to metals for dental restoration', *Ceram. Silik*., 2009, **53**, 225–230.
6. S. Hashimoto, A. Yamaguchi, K. Fukuda and S. Zhang: 'Low-temperature synthesis of leucite crystals using kaolin', *Mater. Res. Bull*., 2005, **40**, 1577–1583.
7. Y. Zhang, M. Lv, D. Chen and J. Wu: 'Leucite crystallization kinetics with kalsilite as a transition phase', *Mater. Lett*., 2007, **61**, 2978–2981.
8. W. Ao, J. Li, H. Yang, X. Zeng and X. Ma: 'Mechanochemical synthesis of zinc oxide nanocrystalline', *Powder Technol*., 2006, **168**, 148–151.
9. J. R. Mackert, M. B. Butts and C. W. Fairhurst: 'The effect of the leucite transformation on dental porcelain expansion', *Dent. Mater*., 1986, **2**, 32–36.
10. J. R. Mackert and A. L. Evans: 'Quantitative x-ray diffraction determination of leucite thermal instability in dental porcelain', *J. Am. Ceram. Soc*., 1991, **74**, 450–453.
11. A. Klouzkova, M. Mrazova and M. Kohoutkova: 'Synthesis of partially stabilized leucite', *J. Phys. Chem. Solids*, 2007, **68**, 1207–1210.
12. H. Yilmaz and C. Dincer: 'Comparison of the bond compatibility of titanium and an NiCr alloy to dental porcelain', *J. Dent.*, 1999, **27**, 215–222.
13. J. R. Mackert and C. M. Russell: 'Leucite crystallization during processing of a heat pressed dental ceramic', *Int. J. Prosthodont.*, 1996, **9**, 261–265.
14. T. Ota, M. Takahashi, I. Yamai and H. Suzuki: 'High-thermal-expansion polycrystalline leucite ceramic', *J. Am. Ceram. Soc.*, 1993, **76**, 2379–2389.
15. H. Wolfram, F. Martin and R. Volker: 'Surface crystallization of leucite in glasses', *J. Non-Cryst. Solids*, 1995, **180**, 292–307.
16. S. Oishi, T. Miyata and T. Suzuki: 'Growth of leucite crystals from $aK_2Mo_2O_7$ flux', *J. Mater. Sci. Lett.*, 2003, **22**, 927–929.

17. T.-S. Sheu, W. J. O'Brien and S. T. Rasmussen: 'Mechanical properties and thermal expansion behavior in leucite containing materials', *J. Mater. Sci.*, 1994, **29**, 125–128.
18. Y. Zhang, C. Qu, P. Rao, L. V. Ming and J. Wuw, 'Nanocrystalline seeding effect on the crystallization of two leucite precursors', *J. Am. Ceram. Soc*., 2007, **90**, 2390–2398.
19. M. Novotna, V. Satava and P. Kostka: 'Synthesis of leucite for application in dentistry', *Glass Technol*., 2004, **45**, 105–107.
20. M. Novotna, V. Satavaa and D. Lezal: 'Preparation and characterization of an alcime powders', *Solid State Phenom*., 2003, **90**, 377.
21. E. M. Erbe and R. S. Sapieszko: 'Chemically derived leucite', US patent no.5,622,551, 1997.
22. A. Jankeviciute and A. Kareiva: 'Synthesis and characterization of leucite ceramics using sol-gel derived molecular precursors', *Mendeleev Commun.*, 2011, **21**, 287–288.
23. Y. Zhang, J. Wu, P. Rao and L. V. Ming: 'Low temperature synthesis of high purity leucite', *Mater. Lett*., 2006, **60**, 2819–2823.
24. F. Saito, Q. Zhang and J. Kano: 'Mechanochemical approach for preparing nano structural materials, *J. Mater. Sci*., 2004, **39**, 5051–5055.
25. J. Ding, T. Tsuzuki, P. G. McCormick: 'Ultrafine alumina particles prepared by mechanochemical/thermal processing', *J. Am. Ceram. Soc*., 1996, **79**, 2956–2958.
26. P. Kathirvel, J. Chandrasekaran, D. Manoharan and S. Kumar: 'Preparation and characterization of alpha alumina nanoparticles by in-flight oxidation of flame syntheses', *J. Alloys Compd*, 2014, **590**, 341–345.
27. T. Tsuzuki and P. G. McCormick: 'ZnO nanoparticles synthesized by mechanochemical processing', *Scr. Mater*., 2001, **44**, 1731–1734.
28. G. Chen, D. Niu and X. Liu: 'Preparation of $SrAl_2O_4$ from an oxide mixture via a high-energy ball milling', *J. Alloys Compd*, 2005, **399**, 280–283.
29. T. D. Isfahani, J. Javadpour, A. Khavandi, R. Dinnebier, H. R. Rezaie and M. Goodarzi: 'Mechanochemical synthesis of zirconia nanoparticles: Formation mechanism and phase transformation', *Int. J. Refract. Met. Hard Mater*., 2012, **31**, 21–27.
30. L. B. Konga, J. Maa, H. Huang, R. F. Zhang and W. X. Que: 'Barium titanate derived from mechanochemically activated powders', *J. Alloys Compd*, 2002, **337**, 226–230.
31. P. H. Kumar, A. Srivastava, V. Kumar, P. Kumar and V. K. Singh: 'Effect of high-energy ball milling and silica fume addition in $BaCO_3Al_2O_3$. Part I: formation of cementing phases', J. Am Ceram. Soc., Early View DOI: 10.1111/jace.13173
32. C. A. Klein: 'Flexural strength of sapphire: Weibull statistical analysis of stressed area, surface coating, and polishing procedure effects', *J. Appl. Phys.*, 2004, **96**, 3172–3179.
33. D. Green: 'An introduction to the mechanical properties of ceramics'; 1998, New York, Cambridge University Press.
34. T. S. Sheu, W. J. Obrien, S. T. Rasmussen and T. Y. Tien: 'Mechanical properties and thermal expansion behavior in leucite containing materials', *J. Mater. Sci*., 1994, **29**, 125–128.
35. X. Chen, C. Thomas, Chadwick, M. R. Wilson, R. G. Hill and M. J. Cattell: 'Crystallization and flexural strength optimization of fine-grained leucite glass-ceramics for dentistry', *Dent. Mater*., 2011, **27**, 1153–1161.
36. W. Holand, V. M. Rheinberger and M. Schweiger: *Adv. Eng. Mater.*, 2001, **3**, 768–774.
37. W. Holand, M. Schweiger, V. M. Rheinberger and H. Kappert: 'Bioceramics and their application for dental restoration', *Adv. Appl. Ceram.*, 2009, **108**, 373–380.

Int. J. Appl. Ceram. Technol., 1–10 (2015)
DOI:10.1111/ijac.12433

In vitro Cytotoxicity, Apoptotic and Hemolysis Assay of Kalsilite-Based Glass Ceramics for Dental Veneering Application

Pattem Kumar and Vinay Singh*

Department of Ceramic Engineering, Indian Institute of Technology (BHU), Varanasi 221005, India

Sumit Hira and Partha Manna

Immunobiology Laboratory, Department of Zoology,Banaras Hindu University, Varanasi 221005, India

Pradeep Kumar

Department of Chemical Engineering, Indian Institute of Technology (BHU), Varanasi 221005, India

Nanocrystalline kalsilite material was synthesized via a gel-trapped coprecipitation for dental veneering applications. The prepared kalsilite powder was further mixed with a separately processed low temperature frit (LTF), in different weight ratio to optimize its coefficient of thermal expansion (CTE). These mixes were analyzed for their flexural strength and surface morphology. The cytocompatibility of mixes was investigated with reference to their effect on human buccal epithelial cells (SCC-25). The flexural strength and CTE values of prepared kalsilite have been found to be comparable to the values obtained for a commercial opaque VMK 95 1M2 (product no. B333250; VITA Zahnfabrik H. Rauter GmbH KG Postfach 1338 D-79704 Bad Sackingen, Germany). This confirmed the feasibility of prepared kalsilite material for dental veneering application. Kalsilite glass-ceramic materials caused moderate levels of apoptosis in SCC-25 cells at higher concentrations and were also tolerable by human RBC as evaluated from hemolytic assay. Human buccal epithelial cells were tolerant to kalsilite glass-ceramic materials at lower concentrations although higher concentration (500 μg/mL) caused moderate damages in proliferative capacity of SCC-25. The improved mechanical and biological properties of the prepared kalsilite confirmed its potential use in dental veneering.

Introduction

Metal–ceramic systems for making dental crowns and bridges are being marketed since the 1960s. Porcelain-fused-to-metal (PFM) is still the most significant dental restorative due to its lower cost than all ceramic systems such as zirconia, spinel, and alumina.[1] Properties of PFM depend on the application of glass-ceramic layers on metal coping and subsequent firing to produce an aesthetically acceptable restoration. This method provides a strong crown or bridge and the marginal fit of the restorations and appearance of natural dentition. Veneering ceramics for metal–ceramic restorations are commonly named feldspathic porcelains,[2] but feldspar-derived glasses only exhibit a low coefficient of thermal expansion (CTE), around 8.6×10^{-6}/°C.[3]

$KAlSiO_4$ is a feldspathoid with a structure of (Si, Al)O_4 tetrahedral framework.[4–6] Kalsilite is a basic silicate mineral which can be used for PFM due to its high CTE[7] and high flexural strength.[8] Becerro *et al.* previously reported that kalsilite has a high CTE for bonding to metals.[5] Irma *et al.* studied the solubility of potassium kalsilite in saliva, beer and Coca-Cola. They concluded that kalsilite is a potential candidate as a porcelain material for dental applications.[7] Kalsilite has a framework of aluminum silicates containing a network of tetrahedral Si and Al elements with alkali metal ions, occupying tetrahedral and octahedral sites to counterbalance the charge valency. Kalsilite has also been studied as the precursor of leucite, which is an important component in porcelain-fused-to-metal (PFM).[9] For the last few years, synthesis of kalsilite has become an attractive subject, especially for veneering applications. Synthesis of kalsilite has been studied using various methods such as mechanochemical,[8] solid-state,[10] and hydrothermal processes.[11,12]

The main aim of this work was to synthesize kalsilite at low temperature using low-cost materials such as microsilica in place of tetraethyl orthosilicate (TEOS), and also this material has not been reported in the literature for the synthesis of kalsilite. Another aim was to match the CTE of kalsilite and increase the bonding to metal crowns of an opaque layer by adding low-tempera-

*vinaycer@gmail.com

ture glass frit (LTF). The prepared kalsilite was mixed with prepared LTF powder in different proportions and was characterized for their mechanical–thermal properties to compare with the existing veneer glass ceramic.

Kalsilite glass-ceramic mixes with LTF were reasonably cytocompatible as demonstrated by their effect on SCC-25 cells. Higher concentrations of the material cause moderate levels of cytotoxicity and retarded the proliferation of SCC-25 cells. Lower concentrations of the materials, however, were well tolerated by the SCC-25 cells. Higher concentrations of the materials only caused low levels of apoptosis in SCC-25 cells. The kalsilite-based veneering glass-ceramic materials were also tolerant to RBC and did not cause hemolysis.

Table I. Coefficient of Thermal Expansion and Glass Transition Temperature of Different wt% of Kalsilite with LTF

Sample coding	Firing temperature (°C)	CTE(per °C)	T_g(°C)
LTF	850	11.0×10^{-16}	410
$K_{1000\ 40/60}$	850	15.9×10^{-6}	415
$K_{1000\ 45/55}$	850	16.6×10^{-6}	425
$K_{100050/50}$	850	17.6×10^{-6}	430
Kalsilite	1000	18.9×10^{-6}	–
VMK 95 A3	950	13.9×10^{-6}	545

CTE, coefficient of thermal expansion; T_g, glass transition temperature; SP, softening point.

Experimental Procedure

Aluminum nitrate nonahydrate [$Al(NO_3)_3\ 9H_2O$], potassium nitrate (KNO_3), and microsilica (SiO_2) were used for kalsilite preparation. Sodium carbonate (Na_2CO_3), potassium nitrate (KNO_3), silicon dioxide (SiO_2), potassium carbonate (K_2CO_3), borax ($Na_2H_3BO_4\ 10H_2O$), feldspar ($K_2O\ Al_2O_3\ 6SiO_2$), magnesium oxide (MgO), calcium carbonate ($CaCO_3$), zirconium dioxide (ZrO_2), and calcium fluoride (CaF_2) were used for the preparation of low-temperature glass frit (LTF). All materials were procured from Loba Chemie Pvt. (Mumbai, India) and of AR grade.

Aluminum nitrate nonahydrate, potassium nitrate, and microsilica were taken as starting materials in a stoichiometric ratio of kalsilite. Microsilica was suspended in 100 mL of distilled water with vigorous stirring at ambient temperature. Potassium nitrate and aluminum nitrate were dissolved separately in distilled water. Both the solutions of metal nitrates were slowly added to the suspended microsilica. Final mixed solution was constantly stirred at room temperature for 1 h to obtain a homogeneous mixing. Ammonia solution of 1 *M* was added drop by drop to the mixed solutions with constant stirring. The mixed solution became a thick gel-like structure, which was further dried at 100°C for 24 h in an electrical oven. The dried gel was ground in an agate mortar using a pestle and separated into three batches. These were calcined at 800, 900, and 1000°C in air for 2 h with a heating rate of 10°C/min. The furnace was equipped with SiC heating elements and a programmer PID 528, manufactured by Selectron Process Controls Pvt., India. This programmer has the temperature control accuracy of ±1°C. To prepare LTF, starting materials were homogeneously mixed in an agate mortar. This mixture was melted in an alumina crucible at 1350°C for 60 min. The molten frit was quenched in deionized water and air-dried. Dried frit was ball-milled to pass a 350-mesh BSS.

The kalsilite powder, calcined at 1000°C, was taken for further characterization because at this temperature, maximum phase formation was found as observed with XRD analysis. Different formulations are presented in Table I. A commercial VMK 95 1M2 opaque, product no. B333250 (VITA Zahnfabrik H. Rauter GmbH KG Postfach 1338 D-79704 Bad Säckingen, Germany), was also characterized for comparison with the developed kalsilite materials. The selection of this product was decided because it is mostly used as opaque material for PFM.

Rectangular test bars were prepared using a uniaxial hydraulic press at a constant pressure of 200 MPa. These bars were heated in a furnace VITA VACUMAT 40T according to a standard dental veneering firing cycle preprogrammed by VITA. It consists of four steps from room temperature to 850°C. These four steps of firing cycle are as follows: preheating at 500°C for 2 min, increase in temperature from 500 to 850°C within 6 min, 1-min soaking at 850°C, and cooling to 600°C in 1 min.

Crystallization temperatures of the precalcined powders were determined by heating at 10°C/min to 1200°C in 100 μL platinum crucibles under synthetic dry air flow of 20 mL/min using a Setaram SETSYS Evolution Simultaneous Differential Thermal Analyzer and Thermal Gravimetric Analyzer (DTA/TGA) (Setaram Instrumentation, Caluire, France). Fused alumina was used as a reference material.

The crystalline phases were identified by powder X-ray diffraction (XRD) technique. X-ray diffraction patterns were observed using a portable XRD machine

(Rigaku, Japan) using Cu Kα radiation employing Ni filter operating at 30 mA and 40 kV. Phase identification was carried out by comparing the respective powder XRD patterns with the standard database stated by JCPDS (PDF-2 database 2003).

Thermal expansion of the material was determined by a dilatometer D50 (supplied by VB Ceramic Consultants, India) in the temperature range 20–550°C at 6°C/min. The dilatometer was equipped with SiC heating element with a control accuracy of ±1°C. It had Nippon PID programmable digital temperature indicator-cum-controller. The samples for CTE measurement were cut and polished uniformly to the size of 45 × 15 × 10 mm.

Flexural strength measurements were taken according to ASTM C78 M using a universal testing machine, Instron 3344 (Germany). The specimens were bent in three-point crossways fit with 20 mm span between the two supports (three-point bending). The load and the corresponding deflections were recorded. The flexural strength was calculated using the following equation:

$$F = \frac{3PL}{2bd^2} \tag{1}$$

where F = flexural strength, kg/cm^2; P = maximum applied load; L = span length; b = width of specimen; and d = depth of specimen.

Weibull statistical analysis of the test samples was conducted. It is a common tool to understand the strength data on the basis of a semi-empirical expression derived from Weibull's statistical theory of fracture as given below:[13]

$$P(\sigma) = 1 - \exp\left[-\left(\frac{\sigma}{\sigma_N}\right)^m\right] \tag{2}$$

It defines the cumulative failure probability P as a function of the applied tensile stress σ. σ_N and m are the nominal strength and Weibull modulus, respectively. These parameters can be determined from a set of experimental data by fitting the estimated failure probability to Eq. (3). In the logarithmic form, Eq. (2) can be written as:

$$\ln[-\ln(1-p)] = m\log\sigma - m\log\sigma_N \tag{3}$$

A plot of ln[-ln(1-p)] versus logσ gives the Weibull modulus from the slope and nominal strength from the intercept ln[-ln(1-p)] = 0. Evidently, the strength σ_N does not take into account the potential impact of the test method (loading geometry and specimen size) and does not relate to the intrinsic strength in an obvious manner.[13] The failure probability P_i was calculated using the following steps:

(1) Ranking by ascending order (i = 1...5) the observed stresses at fracture and assign cumulative probabilities of failure according to $P_i = (i-0.5)/n$, where i is the rank and n is the number of broken samples.[14]
(2) Fitting the ln[-ln(1-p)]. versus lnσ data points to a straight line using a linear fit program.

All specimens were polished using emery papers of grade 400, 500, 600, and 800 grits (Sia, Switzerland) followed by polishing on a velvet cloth using diamond paste of grade 1/4-OS-475 (HIFIN). These polished specimens were chemically etched with 40% hydrofluoric acid for 10 s. Finally, they were dried and gold-sputtered. Micrographs were recorded with the help of a scanning electron microscope (INSPECT 50 FEI).

Human buccal epithelial cell line SCC-25 was originally obtained from American Type Culture Collection (ATCC), Manahass, USA. The cells were maintained in RPMI 1640 (Invitrogen, Carlsbad, CA), supplemented with 10% fetal bovine serum (Hyclone, Logan, UT), 100 U/mL penicillin, and 100 mg/mL streptomycin (Invitrogen, Carlsbad, CA), henceforth called complete medium. The cell line used in this study was free from mycoplasma.

The effect of kalsilite glass-ceramic materials (d < 25 μ) on proliferation of SCC-25 cells was studied by MTT assay, and 5 × 10^3 SCC-25 cells/well were added in a 96-well tissue culture plate and exposed to serial concentrations (5, 10, 25, 50, 100, 250, and 500 μg/mL) of kalsilite glass-ceramic materials. Plates were incubated at 37°C, 5% CO_2, for 48 h. The cell proliferation was measured by CellTiter 96® Non-Radioactive Cell Proliferation Assay (MTT) kit from Promega, USA, according to the manufacturer's protocol. The plates were incubated for 4 h with the MTT reagent, and absorbance was measured at 570 nm using Synergy HT Multi-Mode Microplate Reader (BioTek®, USA). Data are presented as the percentage of inhibition of tumor cells, and it was calculated from the following formula:

$$\%\text{GrowthInhibition} = [1 - \frac{\text{ExperimentalOD570}}{\text{TargetOD570}}] \times 100$$

where Experimental OD value is the reading of tumor cells exposed to various concentrations of kalsilite glass-ceramic materials and Target OD value is the corresponding value of tumor cell cultured in medium only.

The lytic activity of kalsilite glass-ceramic materials against tumor cells was measured by nonradioactive cytotoxicity assay using the CytoTox 96 Non-Radioactive Cytotoxicity Assay kit from Promega, USA (**2**). Buccal

epithelial cells (5×10^3) were added to 96-well tissue culture plates and were exposed to serial concentrations (5, 10, 25, 50, 100, 250, and 500 μg/mL) of kalsilite glass-ceramic materials and incubated for 18 h at 37°C, 5% CO_2. Percent specific lysis was determined using the following formula:

$$\%\text{Cytotoxicity} = \frac{(\text{Experimental} - \text{EffectorSpontaneous} - \text{TargetSpontaneous})}{(\text{TargetMaximum} - \text{TargetSpontaneous})} \times 100$$

Apoptotic cell death in SCC-25 cells by kalsilite glass-ceramic materials (100 μg/mL) was assessed by binding of FITC-conjugated annexin V. After 18 h of incubation, apoptotic cells were analyzed by staining with FITC-conjugated annexin V and propidium iodide (PI) for 20 min in ice-cold PBS. Cells were washed in annexin buffer and were mounted on microscope slides with a drop of mounting medium to reduce fluorescence photobleaching. The FITC-conjugated annexin-V-positive cells were visualized under a fluorescence microscope (Nikon Eclipse 80i; Nikon, Japan).

For time-dependent kinetics, 100 μg/mL kalsilite glass-ceramic materials was incubated with the blood sample. For concentration-dependent kinetics, the blood sample was incubated with varying concentrations (25, 100, and 150 μg/mL) of kalsilite glass-ceramic materials for 4 h. Hemolysis assay was performed according to the standard protocol (**3**). In brief, an aliquot of each blood sample was centrifuged at 600 g for 5 min. A 25-μL plasma aliquot was diluted with 225 μL Drabkin's reagent (Sigma) in a 96-well plate and mixed for 2 min under lateral agitation (300 rpm). After 10 min of equilibration at room temperature, optical density was recorded at 540 nm in Synergy HT Multi-Mode Microplate Reader (BioTek). Blood hemoglobin was determined by measuring the absorbance of 100-fold dilution of the whole blood in Drabkin's reagent at 540 nm. Saponin (2 mg/mL final blood concentration) and PBS were used as positive and negative control, respectively. A sample of plasma without additives was considered basal conditions. Standard calibration curve was obtained with the solutions containing 0.07 to 3.8 mg/mL bovine hemoglobin (Sigma) treated with Drabkin's reagent. The results are presented as percent hemolysis indicating the free plasma hemoglobin (mg/mL), and it was measured as released hemoglobin divided by the total blood hemoglobin (mg/mL) multiplied by 100. All measurements were performed in triplicate.

In this study, n reflects the number of times experiments were performed independently in triplicate. The mean ± SD was calculated for each experimental group ($n = 3$–4). Differences between groups were analyzed by unpaired Student's t-test and one- or two-way ANOVA depending on the requirement. One- or two-way ANOVA followed by Holm–Sidak post hoc multiple comparison tests was used to conduct pairwise comparisons using PRISM statistical analysis software (GraphPad Software, San Diego, CA). Significant differences among groups were calculated at $P < 0.05$ or less ($^*P < 0.05$, $^{**}P < 0.01$, $^{***}P < 0.001$, $^{****}P < 0.0001$ in control versus experimental group).

Results and Discussion

Figure 1 displays the TGA/DTA curve of synthesized kalsilite gel. An examination of the TGA curve shows that the sample weight loss occurs in two steps. The first step, occurring in the temperature range 207–320°C, corresponds to evaporation of moisture and chemically combined water molecules. The weight loss occurring in this step is approximately 50 wt%. The second step, which occurs in the range 329–770°C, consists of decomposition of nitrates resulting in weight loss of 18 wt%. Two broad endothermic peaks are obtained in the DTA curve, corresponding to the weight loss occurring in two distinct steps. A total weight loss of 68 wt% is reported in the range 207–770°C. This is nearly equal to the theoretical weight loss (68.78 wt%) of the sample. The probable calcination reaction is given below:

$$2Al(NO_3)_3 9H_2O + 2KNO_3 + SiO_2 + 2O_2 \rightarrow K_2O.Al_2O_3.SiO_2 + 8NO_3 + 18H_2O \quad (4)$$

Figure 2 shows the XRD of heat-treated sample at different temperatures. Diffraction peaks are well coordinated with JCPDS card No. 87-1707 of kalsilite ($KAlSiO_4$). Two broad peaks are located at 28.86 and 34.37° 2θ values in the XRD pattern. The high K_2O content is important as it increases the stability of the kalsilite phase and also lowers the glass transition temperature.[15,16] The diffraction pattern indicates the formation of impurity-free kalsilite phase. Unit-cell parameters are $a = b = 5.157$ and $c = 8.706$ Å, which are similar to those given by Becerro *et al.* (2009) [$a = 5.166$ and $c = 8.7123$ Å]. As temperature rises from 800 to 1000°C, peak intensity increases. It can be definitely said

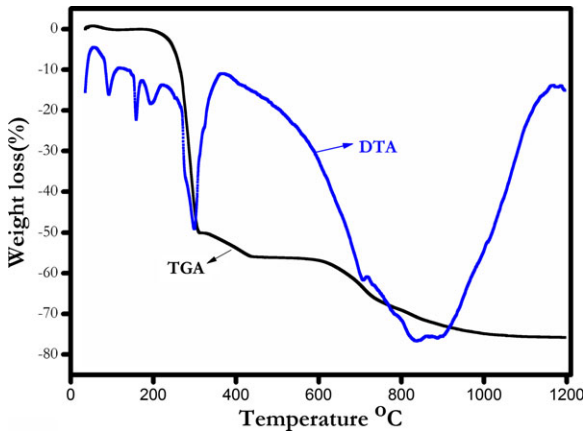

Fig. 1. TGA/DTA curve of synthesized kalsilite gel.

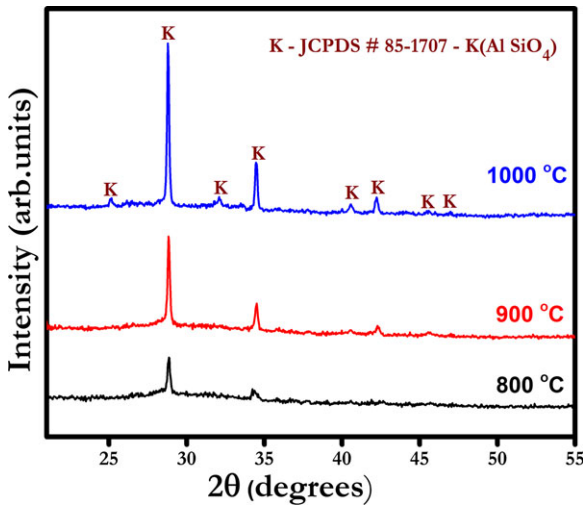

Fig. 2. XRD patterns of the sample heat-treated at different temperatures.

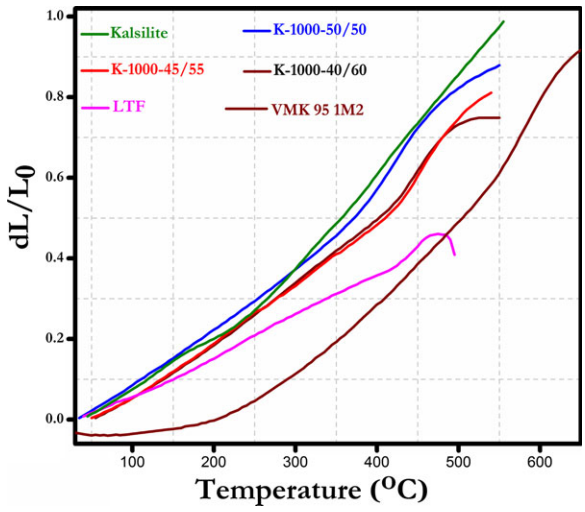

Fig. 3. CTE curves of kalsilite with different wt% of LTF, $K_{1000\ 40/60}$, $K_{1000\ 45/55}$, $K_{1000\ 50/50}$, and VMK 95 1M2.

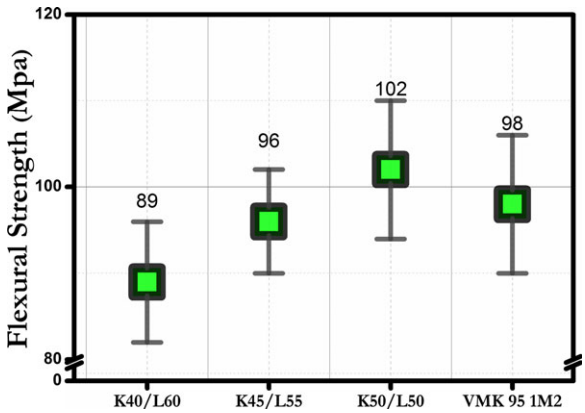

Fig. 4. Flexural strength of K_{1000} with different wt% of kalsilite with LTF and VMK 95 1M2.

that higher temperature supports the crystallization of kalsilite phase.

Thermal expansion is the most significant property for veneering glass-ceramic-fused-to-metal restorations. Thermal compatibility of metal and glass ceramic in the range from ambient temperature to the glass transition temperature can be evaluated by measuring their CTE. CTE control of dental ceramics coated on metal substructures is essential to ensure good bonding of dental prosthesis. Figure 3 shows the thermal expansion of all the compositions along with commercial VMK 95. It is observed that the addition of kalsilite to LTF increases the thermal expansion of the whole matrix. It may be due to the formation of tetragonal kalsilite crystalline phase which has a high CTE (18.9×10^{-6}/°C). Glass transition temperatures (T_g) of the $K_{1000\ 40/60}$, $K_{1000\ 45/55}$, $K_{100050/50}$, and VMK 95 1M2 are determined to be 415, 425, 430, and 545°C, respectively. The presence of LTF in the kalsilite glass-ceramic matrix lowers its glass transition temperature. This is due to the low softening point of the LTF (470°C). The crystallization of kalsilite imparts an increase in the thermal expansion through the dispersion of microfine kalsilite in the glassy matrix. These prepared glass ceramics are useful for PFM owing to their high CTE value of 15.5 to 16.9×10^{-6}/°C in the temperature range 25–550°C. This thermal expansion value is very close to the CTE of alloys ($16.0–17.5 \times 10^{-6}$/°C) used for dental prosthesis,[17] and it is also comparable to the value obtained for VMK 95 A3 opaque 13.9×10^{-6}/°C.

Table II. Flexural Strength and Weibull Analysis Results of Different wt% of Kalsilite with LTF

Sample coding	Mean (MPa)	SD (MPa)	m	σ_0 (MPa)	r^2
$K_{1000\ 40/60}$	89	7.21	13.17	96.24	0.995
$K_{1000\ 45/55}$	96	6.55	10.07	97.89	0.993
$K_{100050/50}$	102	9.16	17.06	106.07	0.983
VMK 95 A3	98	7.96	11.97	98.98	0.989

SD, standard deviation; m, Weibull modulus; σ_0, characteristic strength.

Various testing methods are used for determining the flexural strength of the ceramic materials.[16,18] Among these, three-point bending test is the best and most common for measuring the strength of dental ceramics. Figure 4 shows the flexural strength of K_{1000} with different wt% of kalsilite in LTF along with VMK 95 1M2. Increase in microfine kalsilite content in the matrix increases the flexural strength due to the uniform distribution of large surface area of microfine kalsilite powder.

Composition $K_{100050/50}$ shows the highest value of flexural strength (102 MPa), which is slightly higher than that of VMK 95 1M2 (98 MPa). This may be due to the low porosity and high sinterability of $K_{100050/50}$. Results of flexural strength were analyzed using Weibull statistical analysis. The mean and standard deviation values are given in Table II. It is observed that the value of Weibull modulus, 'm', increases with increasing content of kalsilite in the matrix.[19] This phenomenon can be attributed to the presence of fine kalsilite crystal in the matrix and the absence of microcracks in the samples (Figs 6 and 7). The high values of 'm' (m = 10.07 to 17.06) confirm the reliability of these samples.

A commonly used technique for making a dental prosthesis is the ceramic-fused-to-metal restoration.[17,20] Metal substructure provides high toughness, durability, and strength to the restoration. In veneering process, the metal is coated with multiple glass-ceramic layers of opaque, dentin, and enamel with different optical properties and compatible CTE with the metal substrate. In the present study, a mixture of kalsilite and LTF is used to form an opaque ceramic layer. Figure 5 shows the opaque layer of kalsilite glass ceramic applied on metal substrate. Opaque ceramic layer is first applied on the metal framework to mask the metal color. An aqueous slurry

Fig. 5. Kalsilite glass-ceramic opaque material applied on metal.

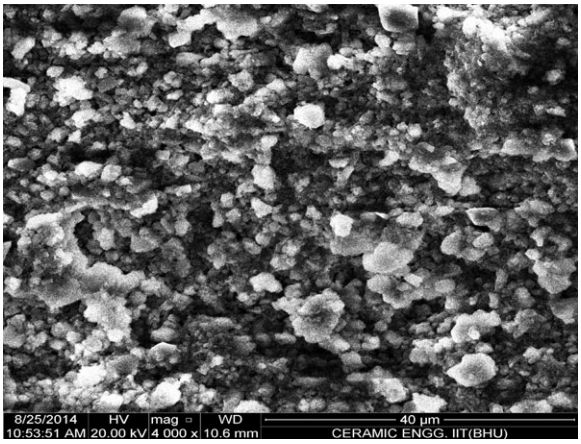

Fig. 6. The microstructures of kalsilite with LTF of $K_{1000\ 45/55}$.

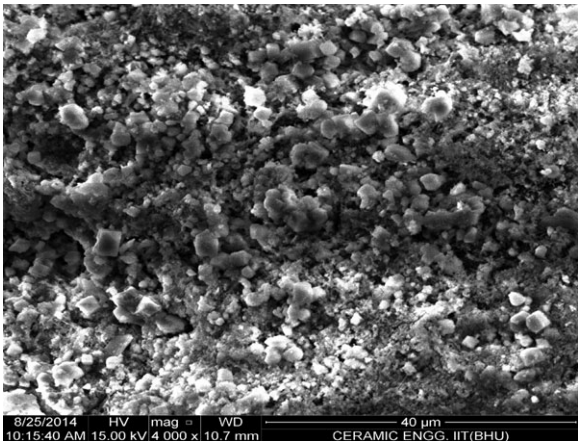

Fig. 7. The microstructures of kalsilite with LTF of $K_{1000\ 50/50}$.

of the opaque ceramic is prepared and applied to the metal substrate (Fig. 5 step 4) and then fired at a temperature between 880 and 950°C for 1 min (Fig. 5 step 5). The fired coated metal substrate is shown in step 6 of Fig. 5. The maturing temperature of the opaque ceramics layer must be kept at least 100°C below the solidus temperature of the metallic framework.

The microstructures of kalsilite with different wt% of LTF are shown in Figs 6 and 7. There is no visible microcrack appearance in the surface of the sample, resulting in higher flexural strength. Hexagonal kalsilite crystals are clearly seen in the micrographs. These fine particles account for the increased flexural strength and the reliability of kalsilite glass ceramic.[21–23]

Figure 8A shows the growth inhibition by kalsilite glass-ceramic materials at constant concentration. Higher concentrations of kalsilite glass-ceramic materials cause moderate levels of growth inhibition against SCC-25 cells, although the cells are tolerant to lower concentration of the compounds. This suggests a broad-spectrum usefulness of the compounds. Figure 8B shows the growth inhibition by kalsilite glass-ceramic materials at constant concentration (100 μg/mL) for different time periods. It is observed that there is a moderate increase in the growth retardation by these materials with increasing period of time.

Figure 8C shows the direct cellular cytotoxicity of kalsilite glass-ceramic materials against SCC-25 cells. The SCC-25 cells are more tolerant to lower concentrations (5 μg/mL) of these materials, and there is an occurrence of significantly less cell lysis at these concentrations than at higher concentrations (500 μg/mL). The present data confirm that this material is well tolerated by buccal epithelial cells and is nontoxic to them.

Growth inhibition by kalsilite glass-ceramic materials at higher concentration raises the question whether it also causes apoptosis of the tumor cells and if so whether it induces cell death. Apoptosis was determined by monitoring changes in the cell size and externalization of phosphatidylserine qualitatively in SCC-25 cells.[24,25] There was a moderate increase in annexin-V-positive cells upon treatment with kalsilite glass-ceramic materials

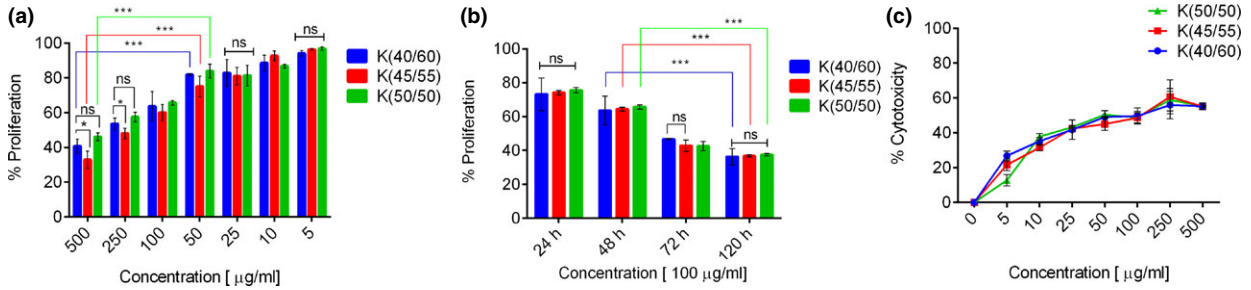

Fig. 8. Higher concentration of kalsilite glass-ceramic materials retards the growth of SCC-25 cells. (A and B) Graphs show concentration–response of kalsilite glass-ceramic materials on tumor cell proliferation and growth. (C) Direct cellular cytotoxicity by kalsilite glass-ceramic materials against SCC-25 cells. Data are presented as mean ± SD, n = 4.

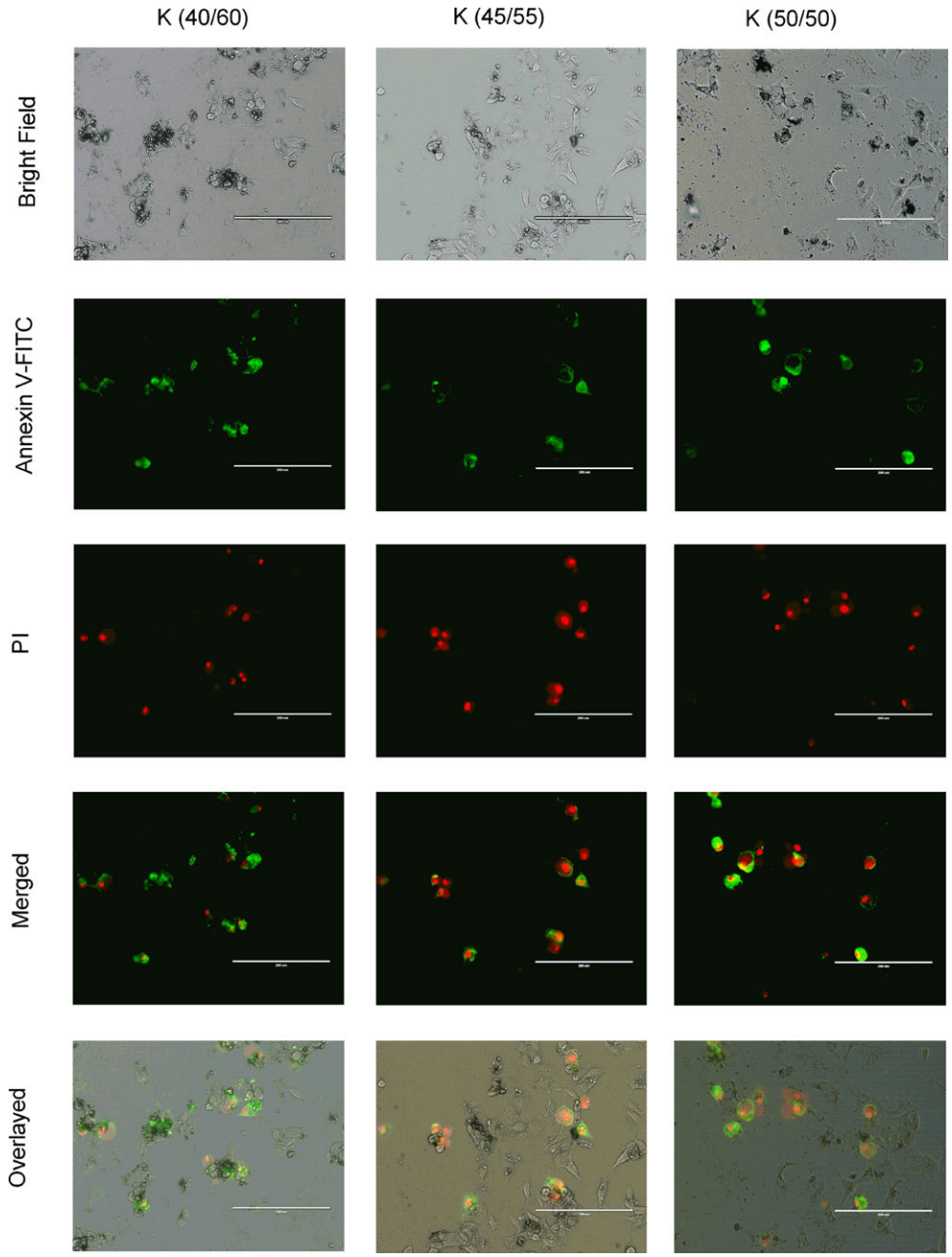

Fig. 9. Microscopic analysis of induction of apoptosis. SCC-25 cells were given indicated treatment with kalsilite glass-ceramic materials at a concentration of 100 μg/mL in complete RPMI 1640 medium for 8 h at 37° C. FITC-conjugated annexin V- and propidium iodide (PI)-stained apoptotic cells were visualized under a fluorescence microscope (Nikon Eclipse 80i; Nikon, Japan) with Plan Fluor, 40X, NA 0.75 objective equipped with green and red filters for FITC and PI, respectively. n = 3.

K40/60 and K45/55 compared to K50/50, which is significantly less toxic (Fig. 9).

A moderate increase in percent lysis was observed in the presence of $K_{40/60}$ and $K_{45/55}$. However, considerably less hemolysis was observed in the case of $K_{50/50}$, and this material may be considered nonhemolytic. Figure 10A and B shows % hemolysis against increasing time period and concentration of kalsilite glass ceramic, respectively. It is observed from these figures that K50/50 does not cause damages to RBC. Microscopic obser-

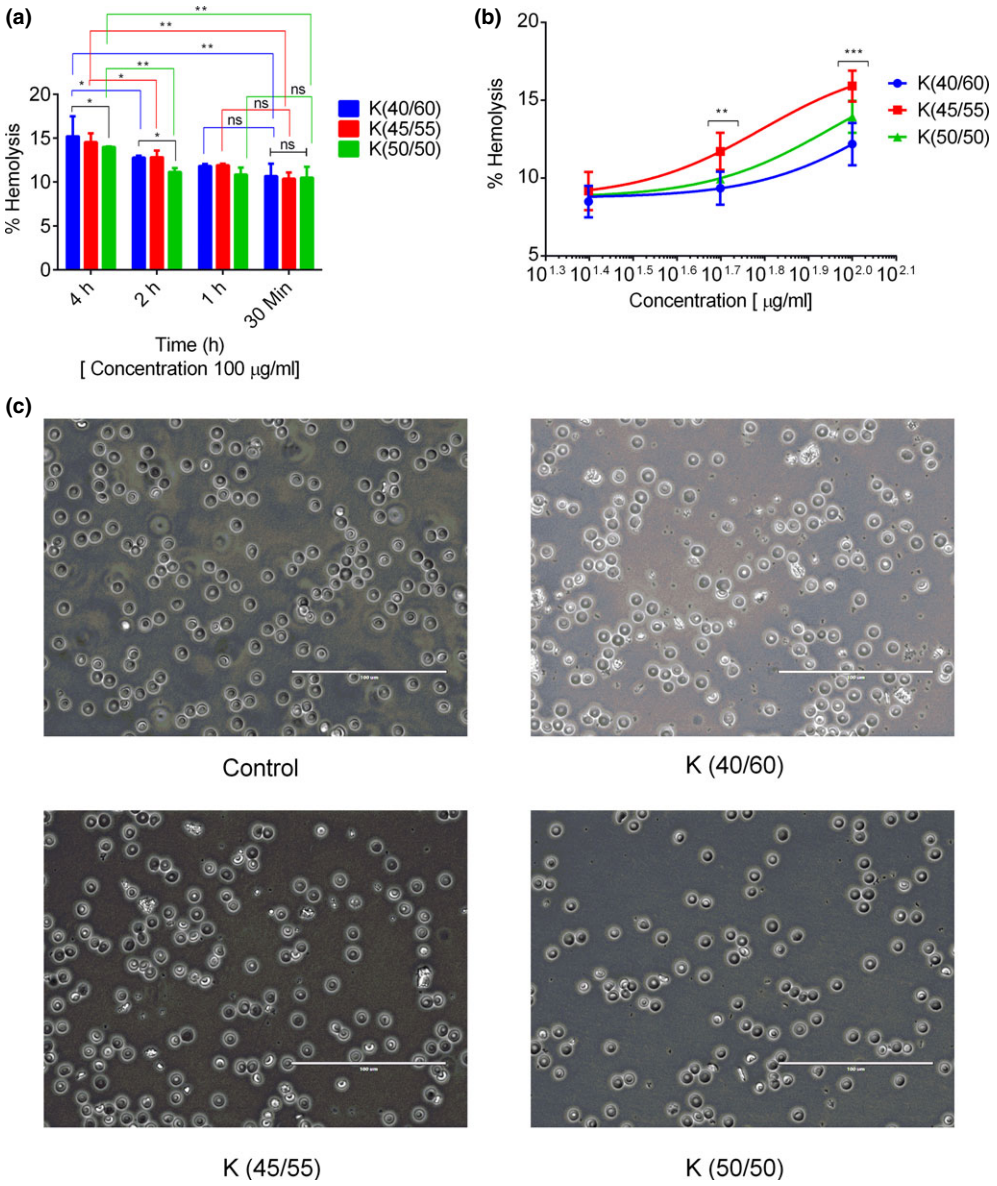

Fig. 10. Hemocompatibility assay. Hemolysis induced by the indicated treatment in whole human blood at a fixed concentration (A) or with increasing concentrations (B), expressed as percent whole blood hemoglobin content. Mean ± SD, n = 3. (C) Photomicrographs demonstrate the absence of detrimental effect of kalsilite glass-ceramic materials on RBC morphology compared to no treatment.

vations shown in Fig. 10C also display no change in morphology of RBC in contact with $K_{50/50}$, whereas a moderate effect is observed in the case of $K_{45/55}$ and $K_{40/60}$. Thus, the major blood component is found to be tolerant to $K_{50/50}$.

Conclusions

Microfine kalsilite has been successfully synthesized using combined sol–gel synthesis method. Kalsilite with different wt% of LTF shows the CTE value of 15.9 to 17.6 × 10^{-6}/°C. This value is close to standard CTE of dental alloys. Samples with 40, 45, and 50 wt% of kalsilite have higher flexural strength due to the presence of microfine kalsilite particles in the matrix. The flexural strength and CTE values of prepared kalsilite were found to be comparable to the values obtained for Vita opaque. This may be potentially porcelain material for the application in porcelain-fused-to-metal. Kalsilite glass-ceramic materials were found to be cytocompatible and were well tolerated by buccal epithelial cells at lower concentrations.

Very high concentration of kalsilite glass-ceramic materials, however, caused a moderate cell death as demonstrated by reduced proliferation and enhanced cytotoxicity of SCC-25 cells. All the materials were relatively tolerated by the SCC-25 cells and caused significantly less apoptosis, suggesting its suitability for the potential clinical application. K50/50 composition was specifically more suitable and appeared to be largely nontoxic to SCC-25 cells. Besides, kalsilite glass-ceramic material K50/50 was also tolerated by RBC, as suggested by hemolysis study.

Acknowledgments

The authors gratefully acknowledge the financial support of DST [TDT Division, Reference No. DST/SSTP/UP/197(G) 2012], Ministry of Science & Technology, New Delhi, India. This work was also supported by grants from the Department of Biotechnology (DBT), New Delhi, India (Nos. BT/PR11490/BRB/10/675/2008 to PPM).

References

1. W. M. Weinstein, L. K. Katz, and S. A. B. Weinstein, Fused porcelain-to-metal teeth, U. S. Patent 3052982, 1962.
2. L. Yin, X. F. Song, S. F. Qu, Y. G. Han, and H. Wang, *J. Biomed. Mater. Res. Part B: Appl. Biomater.*, 79, 365–378 (2006).
3. P. J. Vergano, D. C. Hill, and D. R. Uhlmann, *J. Am. Ceram. Soc.*, 50, 59–60 (1967).
4. J. Perrotta, and J. V. Smith, *Mineral. Mag.*, 35, 588–595 (1965).
5. I. Becerro, and M. Mantovani, *J. Am. Ceram. Soc.*, 92, 2204–2206 (2009).
6. D. Cellai, M. A. Carpenter, and P. J. Heaney, *Eur. J. Mineral.*, 4, 1209–1220 (1992).
7. I. Bogdanovicieni, A. Jankeviciute, J. Pinkas, A. Beganskiene, and A. Kareiva, *Mater. Res. Bull.*, 43, 2998–3007 (2008).
8. P. H. Kumar, A. Srivastava, V. Kumar, N. Jaiswal, P. Kumar, and V. K. Singh, *J. Adv. Ceramics*, 3, 332–338 (2014).
9. Y. Zhang, L. V. Ming, C. Dongdan, and W. Jianqing, *Mater. Lett.*, 61, 2978–2981 (2007).
10. O. C. Kopp, L. A. Harris, and G. W. Clark, *Am. Mineral.*, 46, 719–727 (1961).
11. R. Dimitrijevic, and V. Donduret, *J. Solid State Chem.*, 115, 214–224 (1995).
12. L. H. Kallai, and I. Lapideset, *J. Thermal Anal. Calor.*, 71, 689–698 (2003).
13. D. Green, *An Introduction to the Mechanical Properties of Ceramics*, Cambridge University Press, New York, 1998.
14. T. S. Sheu, W. J. Obrien, S. T. Rasmussen, and T. Y. Tien, *J. Mater. Sci.*, 29, 125–128 (1994).
15. D. A. Duke, J. F. MacDowell, and B. R. Karstetter, *J. Am. Ceram. Soc.*, 50, 67–74 (1967).
16. M. J. Cattell, R. L. Clarke, and E. J. Lynch, *J. Dent.*, 25 409–414 (1997).
17. E. E. Meliegy, and R. V. Noort, Glasses and Glass Ceramics for Medical Applications, Springer science & business media, Chapter-10 Leucite Glass-Ceramics, LLC 2012.
18. M. J. Cattell, J. C. Knowles, R. L. Clarke, and E. Lynch, *J. Dent.*, 27, 183–196 (1999).
19. P. H. Kumar, *et al.*, *Adv. Appl. Ceram.*, 114, 107–113 (2015).
20. A. I. Becerro, A. Escudero, and M. Mantovani, *Am. Mineral.*, 94, 1672–1678 (2009).
21. M. J. Cattell, T. C. Chadwick, J. C. Knowles, R. L. Clarke, and E. Lynch, *Dent. Mater.*, 17, 21–33 (2001).
22. H. Fischer, W. Rentzsch, and R. Marx, *Eng. Fract. Mech.*, 69, 781–791 (2002).
23. A. S. Al-Hiyasat, W. P. Saunders, G. Mc. R. Smith, and W. H. Gilmour, *J. Dent.*, 21, 487–495 (1998).
24. S. K. Hira, A. K. Mishra, B. Ray, and P. P. Manna, *PLoS ONE*, 9, e94309 (2014).
25. P. P. Manna, S. K Hira, A. A. Das, S. Bandyopadhyay, and K. K. Gupta, *Cytokine*, 61, 118–126 (2013).

Available online at www.sciencedirect.com

ScienceDirect

Ceramics International 42 (2016) 3591–3597

CERAMICS INTERNATIONAL

www.elsevier.com/locate/ceramint

Effect of Al_2O_3 on leucite based bioactive glass ceramic composite for dental veneering

Pattem Hemanth Kumar[a], Vinay Kumar Singh[a,*], Pradeep Kumar[b], Gaurav Yadav[a], R.K. Chaturvedi[a]

[a]Department of Ceramic Engineering, Indian Institute of Technology (BHU), Varanasi 221005, India
[b]Department of Chemical Engineering and Technology, Indian Institute of Technology (BHU), Varanasi-221005, India.

Received 28 September 2015; received in revised form 28 October 2015; accepted 5 November 2015
Available online 12 November 2015

Abstract

A wide variety of dental ceramic composites have been introduced in the restorative dentistry in order to associate the desired aesthetics and superior mechanical performance. Mechanochemically derived leucite based bioactive glass ceramic composites have been prepared and studied by their thermal, crystal structure, microstructural, mechanical and biological behavior. In the prepared glass-ceramic composites, fine alumina has been added to improve their mechanical properties because it has biocompatibility, high hardness and good mechanical strength. Flexural strength and coefficient of thermal expansion (CTE) have been studied and the results are compared to the commercial dentine. Alumina added glass ceramic composites show high flexural strength than that of the pure leucite based glass ceramic composite. A second phase nepheline has been formed in the alumina added samples. Nepheline has high CTE. This causes a slight increase in the CTE of the whole matrix. Micrographs show the complete attachment and proliferation of the SSC-25 cells on the surface of the samples. This confirms the bioactive behavior of the prepared composites. Therefore, it is concluded that the addition of alumina to the glass ceramic composite is a successful approach to improve its mechanical and biological properties.

Keywords: A. Milling; B. Composites; C. Thermal expansion; D. Glass ceramics; E. Alumina

1. Introduction

Ceramic materials used in restorative dentistry have specific properties such as durability in the oral environment, similarity with natural tooth structure, high wear resistance and mechanical strength [1–3]. Metal ceramic restorations (MCR) are commonly used due to their good fracture resistance [4]. These consist of metal substructure and several layers of dental porcelain [5]. Feldspathic porcelains consists of glassy aluminosilicate and crystalline leucite is mostly used for MCR [6–8]. Leucite is a precious phase in the dental ceramic restorations. It increases the thermal expansion of dental ceramics and results in a good bonding to the metal framework [9]. Problems occur with the patient is associated with the failure of fixed MCR due to secondary carries [10–12]. This resulted in a plaque accumulation in the marginal area between the fixed tooth and restoration. This causes the bacterial attack leading to pulp irritation and the dissolution of the luting cement [13]. A hypothetical tissue attachment on the margins of a restoration would eliminate the marginal gap, cement dissolution and subsequently the secondary caries. Cells no more adhere to the damaged tooth structure after preparation of a tooth for a restoration. The marginal gap is unavoidable in dentistry but it could be decreased or filled by precipitation of hydroxyapatite by using the developed ceramic composites in only marginal areas of restorations. As well as for different purposes in implant custom ceramic abutments at collar or emerging profile regions.

Dental ceramic materials are bio-inert and unable to interact with the surrounding tissues [1,14]. According to L. L. Hench, a bioactive glass prompts a specific biological response at the interface of the hard tissue and the material [15,16].

*Corresponding author.

http://dx.doi.org/10.1016/j.ceramint.2015.11.022
0272-8842/

A hydroxyapatite (HAp) layer is formed which enhances the cell proliferation and the cell attachment, thereby sealing the marginal gap [17–21]. Over the last few years, research has been carried on the development of apatite layer on dental ceramics by adding the bioactive glass. Chatzistavrou et al. has been reported the growth of a hydroxyapatite layer on the surface of a bioactive glass coated dental ceramic substrate [3]. Kontonasaki et al. has been reported that the bioactive dental glass ceramic composite promotes a higher cell proliferation than that of the unmodified porcelain [19]. Chatzistavrou et al. has been studied the sol–gel derived bioactive glass ceramic composite material for dental application [14]. They found that the prepared bioactive glass ceramic composite shows the similar characteristics to that of a commercial dental ceramic [14]. They also observed the cell attachment and proliferation of the periodontal ligament and gingival fibroblasts cells on the surface of the developed material [14].

Furthermore, the addition of fine alumina to bioactive glass ceramic composite may increase the mechanical properties. Alumina has the biocompatibility, high hardness and good mechanical properties [22–24]. The glass is toughened and strengthened when a crystalline material such as alumina is added to it. This is because the crack cannot pass through the fine alumina particles as easily as it can pass through the glass matrix [25]. This technique has found the application in dentistry in the development of aluminous porcelain particles in a glassy porcelain matrix for porcelain jacket crowns [25]. Most dental ceramics that have a glassy matrix utilize reinforcement of the glass by a dispersed crystalline substance [24,25].

Furthermore, mechanochemically derived leucite based bioactive glass ceramic composite have been previously synthesized by us. A superior bioactivity and the moderate mechanical properties have been investigated [1]. Subsequently, the aim of present study is to enhance the mechanical properties without affecting the biological and thermal properties of the leucite based dental ceramic composite. The results have also been compared with a commercial product (VITA VMK 95) to validate the feasibility of the prepared composite. The composite material does not cause any significant apoptosis of SCC-25 cells and allow the cells to grow over its surface indicating a high degree of biocompatibility. Further, no work has been reported on the effect of addition of alumina to the mechanochemically synthesized leucite based bioactive glass ceramic composite.

2. Materials and methods

2.1. Preparation of leucite, bioglass and LTF

AR grade potassium carbonate, aluminum oxide and silicon dioxide (Loba Chemie Pvt. Ltd., Mumbai, India) was weighed and mixed in a stoichiometric ratio of leucite. This mixture was ground for 6 h in a Fritsch Pulverisette high-energy ball mill and subsequently fired at 1100 °C as discussed in our previous work [7]. Bioglass® 45S5 was prepared on a lab scale by melting in a platinum crucible at 1400 °C. The molten glass was quenched in water and dried at 110 °C for 3 h subsequently milled to pass a 350 BSS mesh. A similar procedure was used for the preparation of LTF [8].

Table 1
Chemical compositions of the composites.

Sample coding	Leucite	Bioglass	LTF	Alumina
Al-0	40	40	20	0
Al-2	39	39	20	2
Al-4	38	38	20	4
Al-8	36	36	20	8

*LTF: Low temperature frit.

2.2. Formulation of composites

Composites (referred as Al-0, Al-1 and Al-2) were prepared by mixing the different wt. % of mechanochemically derived leucite, bioglass, LTF and fine alumina. Compositions are given in Table 1. The mixture was ground in an agate mortar for 20 minutes to get a homogenous mixing. The milled mixture was pelletized using a uniaxial hydraulic press by applying a load of 200 MPa. The pressed pellets were heat treated at 950 °C using a VITA VACUMAT 40 T furnace. The heating schedule is given in Table 2.

2.3. Characterizations

2.3.1. Phase analysis, microstructure and CTE

X-ray diffraction (XRD) of the composite powders (before and after firing) was carried out to confirm the phase formation using a portable X-ray diffractometer (Rigaku, Japan) with Cu K_α radiation employing Ni filter and operating at 30 mA and 40 kV. Diffraction peaks were analyzed using standard JCPDS file (PDF-2 database 2003). All the sintered specimens were polished using emery papers of grade 400–800 (Sia, Switzerland) followed by polishing on a velvet cloth using diamond paste of grade 1/4-OS-475 (HIFIN). These polished specimens were chemically etched with 2% hydrofluoric acid for 10 s. Finally, they were dried and gold sputtered to make a smooth conducting surface. Micrographs of the coated samples were recorded using scanning electron microscopy (SEM) (INSPECT 50 FEI).

The rectangular bars of dimension $50 \times 10 \times 10\ mm^3$ were made in a similar manner as discussed earlier for CTE measurements. CTE and glass transition temperature (T_g) of the composites were studied using a dilatometer (VB Ceramic Consultants, India).

2.3.2. Flexural strength, apparent porosity and bulk density

Flexural strength measurements were done according to ASTM C78 M using a universal testing machine; Instron 3344 (Germany). The specimens were fractured in three-point crossways fit with the 20 mm span between the two supports (three point bending). The load and the corresponding deflections were recorded. The standard deviation, S of the flexural

Table 2
The firing schedule of composites at 950 °C using a VITA VACUMAT 40T furnace.

Samples	Pre-Drying °C	Min. →	Min. ↗	Min. °C/min ↗	Temp. °C	Min. →	VAC min
Al-0	500	2	5.62	80	950	1	5.62
Al-2	500	2	5.68	80	955	1	5.68
Al-4	500	2	5.68	80	955	1	5.68
Al-8	500	2	5.75	80	960	1	5.75

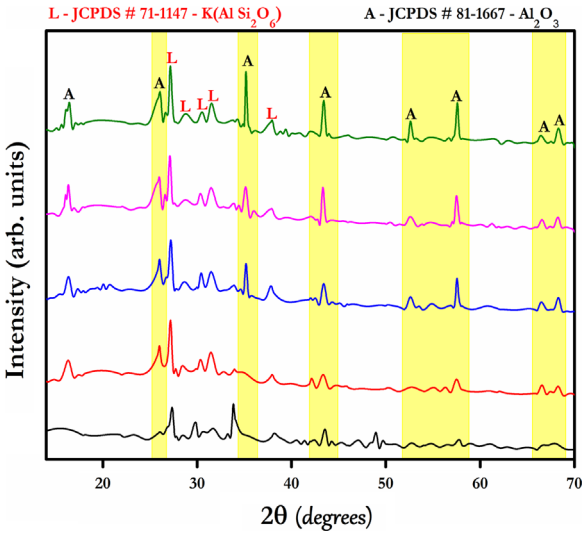

Fig. 1. XRD pattern of the composite before firing.

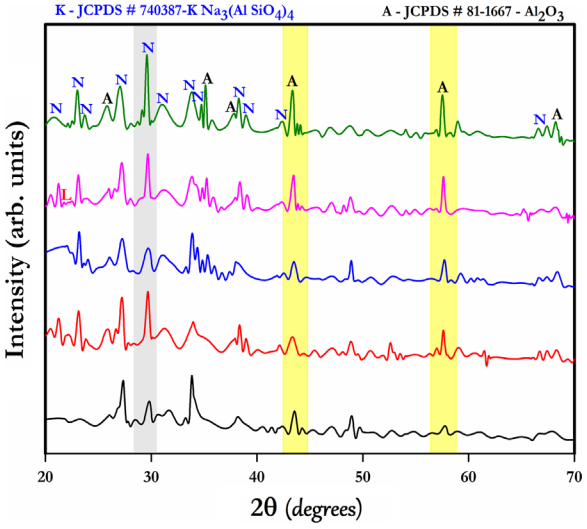

Fig. 2. XRD pattern of the composite after heat treatment up to 960 °C with heating rate 80 °C /min.

strength values was also calculated. Apparent porosity (AP) and bulk density (BD) of all the composite samples were determined according to ASTM C20-00.

2.4. SEM evaluation of cell morphology

Three sintered pellets of each leucite glass–ceramic composites were used to consider cells morphology on their surface at different culture periods. SCC-25 cells were cultured up to 10 days in order to assess the cell's response on the materials surface subsequent increase interaction time. The composite pellets with cells were fixed in 2.5% (v/v) glutaraldehyde in 0.14 M sodium cacodylate buffer (pH 7.3) (both Sigma-Aldrich) at 4 °C, dehydrated in a graded series of alcohols (50%, 70%, 90%, and two changes of 100% ethanol). The pellets were treated with hexamethyldisilazane (Sigma-Aldrich) for 1–2 min and kept in a desiccator to dry overnight. After 24 h, the pellets were attached on aluminum stubs, sputter-coated with gold and record using a scanning electron microscopy (SEM) (INSPECT 50 FEI) at 10 to 12 kV. Representative samples of the surfaces were used for observation and recording of images.

3. Results and discussion

3.1. Phase analysis

Fig. 1 exhibits the XRD pattern of the composites before firing. In the composites, leucite has been found to be a major crystalline phase along with alumina phase. Diffraction peaks are (Fig. 1) well matched to JCPDS Card No. 87–1707 and 81–1667. It is seen that the intensity of the peak corresponding to the Al_2O_3 phase increases with increasing the alumina content in the matrix. Fig. 2 shows the XRD patterns of the composite samples after firing. Diffraction peaks are well matched to JCPDS Card No. 74-0387 and 81-1667. As can be seen from Fig. 2 that a major crystalline phase nepheline has formed after firing (at 950 °C) along with some alumina crystalline phase subsequently decreasing the amorphous phase. A second phase nepheline is formed due to reaction of alumina with the free ions (K^+, Na^+ and Si^{4+}) present in the matrix during heat treatment. Nepheline has the highest coefficient of thermal expansion and good mechanical strength which may further increase the mechanical properties of the prepared composites [26].

3.2. Microstructure

Figs. 3–5 show the surface morphology of Al–0%, Al–4% and Al–8% composites. It is seen that glassy surface reduces slightly with increasing the content of fine alumina in the composites. It is due to the presence of crystalline alumina particles which are distributed homogeneously along the glassy matrix. Micrographs show a very dense morphology with no visible micro-crack on the surface. SEM micrographs along

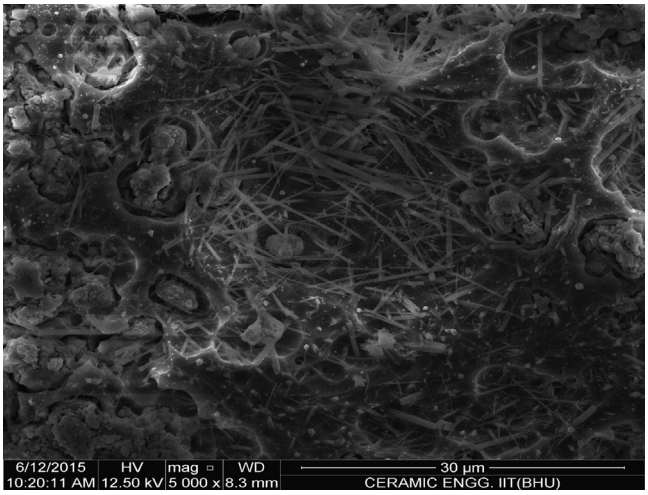

Fig. 3. SEM image showing the surface morphology after heat treatment of Al-0%.

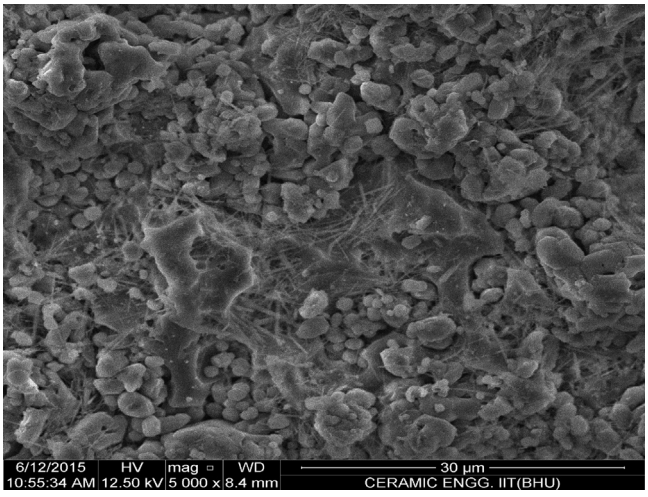

Fig. 4. SEM image showing the surface morphology after heat treatment of Al-4%.

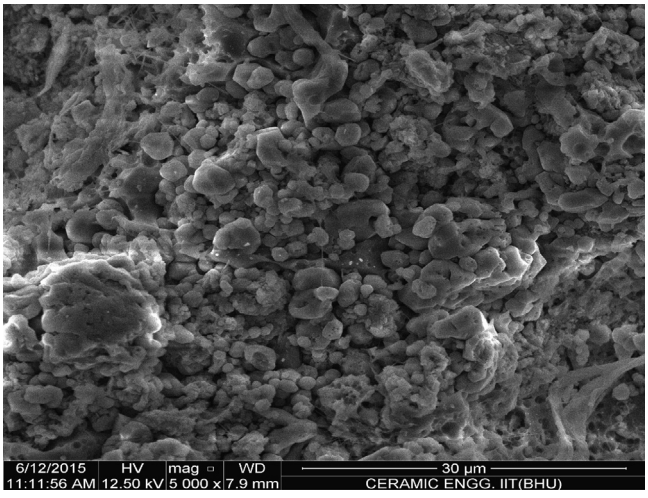

Fig. 5. SEM image showing the surface morphology after heat treatment of Al-8%.

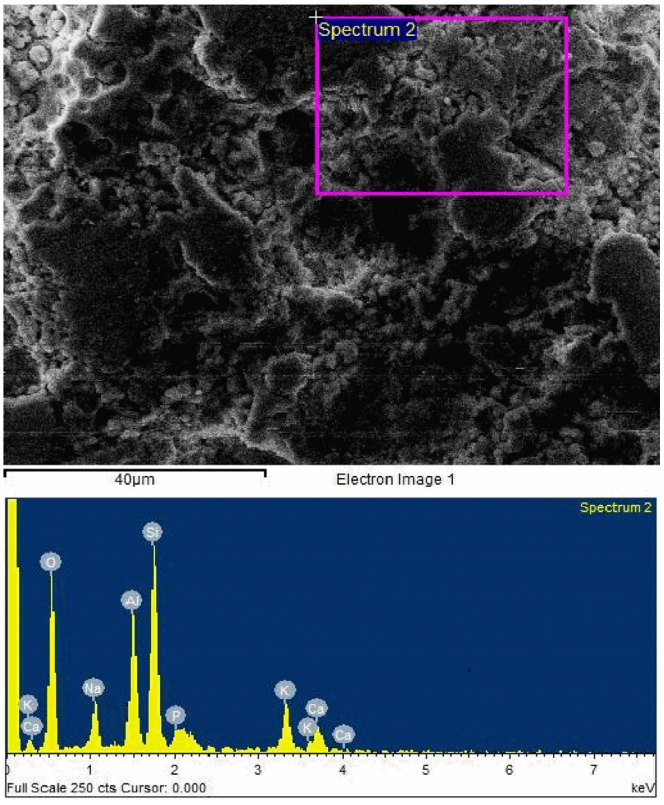

Fig. 6. SEM micrographs and EDS analysis after heat treatment of Al-0%.

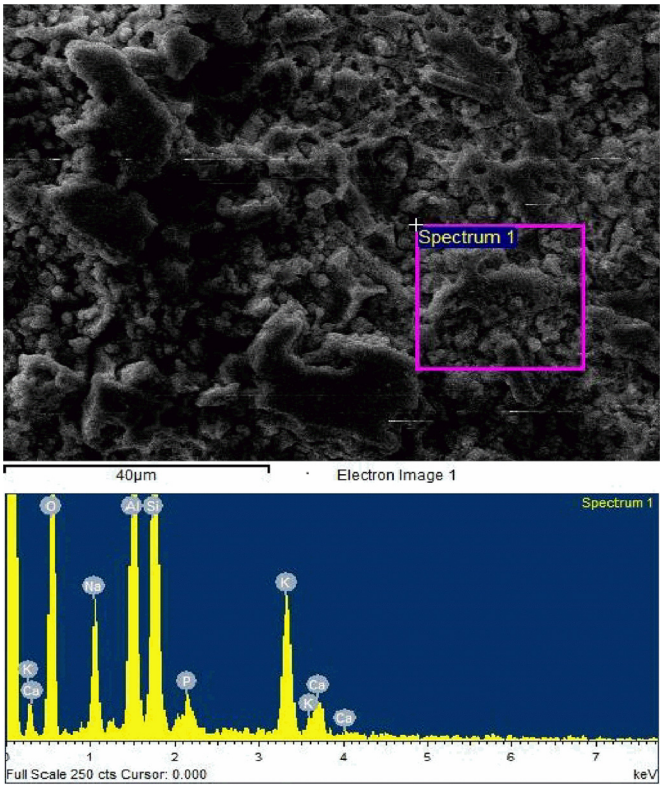

Fig. 7. SEM micrographs and EDS analysis after heat treatment of Al-8%.

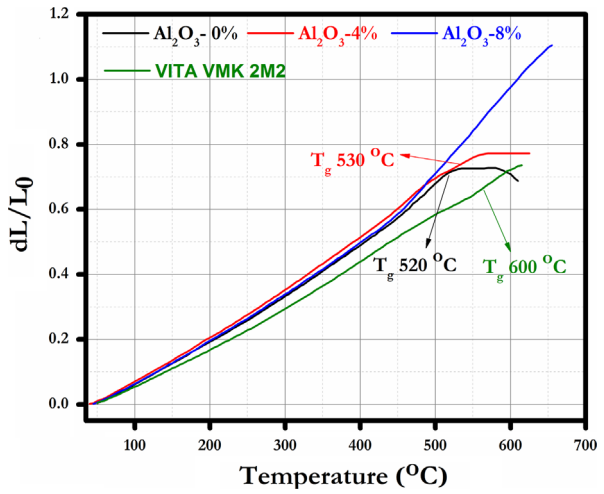

Fig. 8. CTE curves of composites along with commercial dentine (VITA VMK 2 M2).

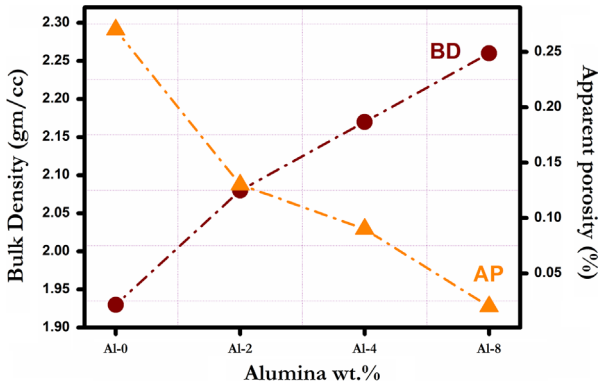

Fig. 9. BD and AP of the bioactive glass ceramic composites with different wt% of alumina.

with the EDX spectra of the compositions, Al–0% and Al–8% are shown in Figs. 6 and 7. EDX spectra confirms the presence of all the constituent elements in an expected concentration.

3.3. Coefficient of thermal expansion (CTE)

Fig. 8 shows the CTE curves of the composites along with the commercial dentine (VITA VMK 2 M2). It has been observed that the compositions, Al–0, Al–4, Al–8% and VITA dentine have a CTE 14.80×10^{-6} /°C, 15.00×10^{-6} /°C, 17.8×10^{-6} /°C and 13.60×10^{-6} /°C respectively. CTE of the composites, Al–0 and Al–4 is very similar to that of commercial dentin. It is seen from Fig. 8 that thermal expansion of the composition Al–8% increase linearly i.e. there is no glass transition. It may be due to high content of alumina present in the matrix. It is found that the addition of fine alumina to the composites increases the CTE values of the final mixture. This is due to the presence of nepheline crystalline phase (as can be seen from XRD patterns in Fig. 2) which has the high CTE in the range $12.1–16.6 \times 10^{-6}$ /K [27]. Khater et al. was also reported that the formation of nepheline in the glass-ceramic increases the CTE of the matrix [28]. These

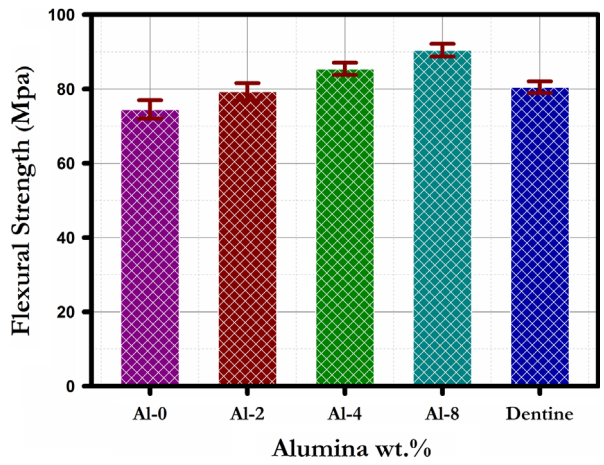

Fig. 10. Flexural strength of composites and commercial dentine.

prepared composite materials are, therefore, suitable for PFM as its CTE values are close to that of nickel–chrome alloy (13.90×10^{-6} /°C).

3.4. Bulk density (BD) and apparent porosity (AP)

Fig. 9 shows the BD and AP of the bioactive glass ceramic composites containing different wt% of alumina. It is seen from Fig. 8 that BD increases (from 1.93 to 2.26 g/cc) with increasing the alumina content followed by a continuous decrease in the AP. Micro fine alumina particles homogeneously dispersed throughout the glassy matrix, improves the packing density of the composites consequently reduces the apparent porosity.

3.5. Flexural strength

Fig. 10 shows the flexural strength of the composite and the commercial dentine VITA VMK 2 M2. Flexural strength increases with increasing the fine alumina in the matrix. Homogenous dispersion of fine alumina particles within the glassy matrix leads to enhance the mechanical strength. This is because a crack cannot pass easily through the crystalline alumina particles whereas in the case of glassy matrix, it passes easily and hence decreases the mechanical strength [24]. This technique has also been used in the dentistry for the development of aluminous porcelains [24,25]. Consequently the synthesized composites show the superior sinterability, low porosity and high flexural strength. The strength of all alumina added composites are nearly similar to that of the commercial dentine. One of the reasons for enhancement in the flexural strength of the alumina added composites is the formation of crystalline nepheline phase. It was also reported in the literature that nepheline increases the mechanical strength of the glass–ceramics [26]. It is, therefore, concluded that fine alumina particles act as ‘crack stoppers’ preventing the propagation of a crack throughout the body of the porcelain.

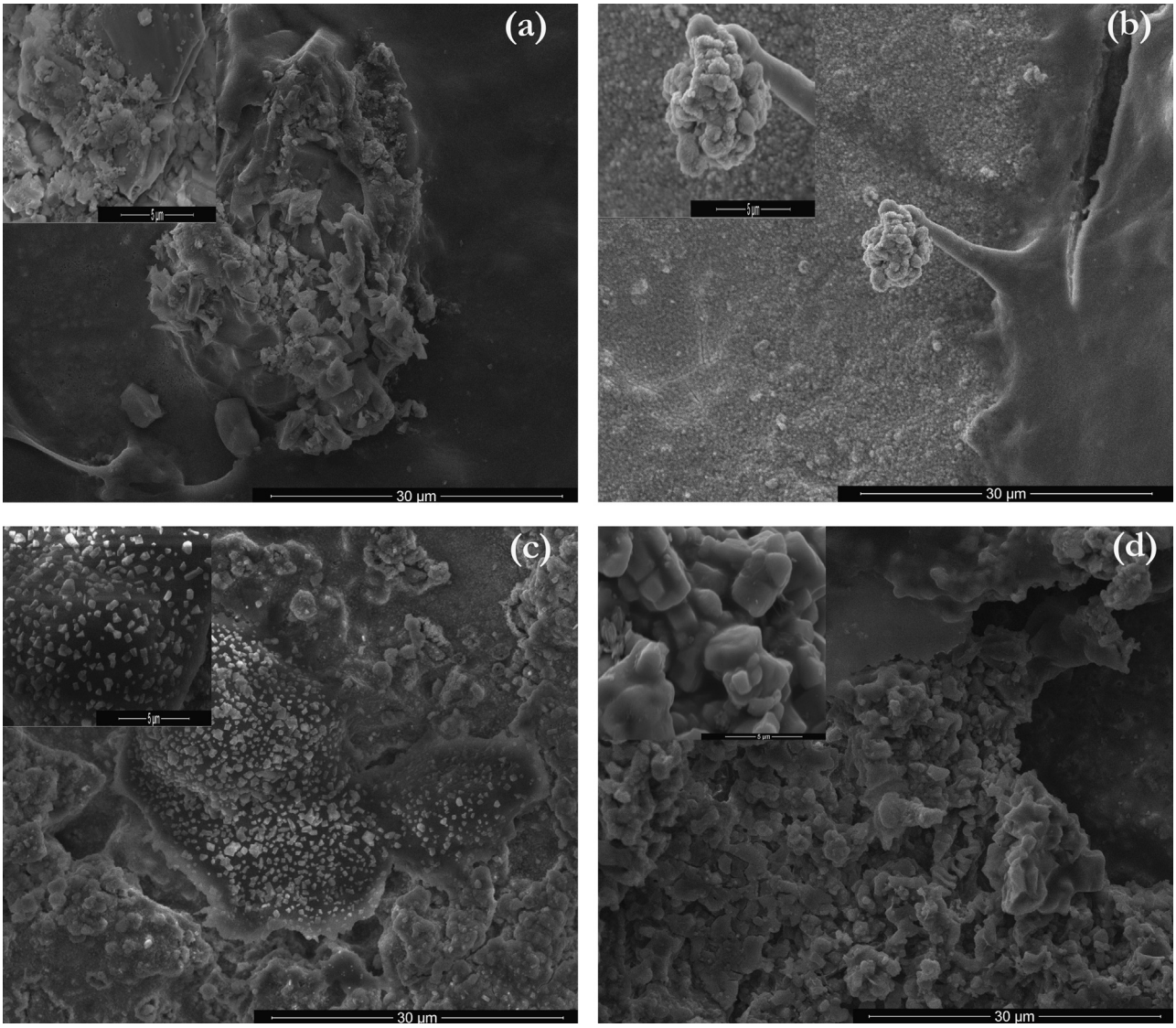

Fig. 11. SEM image of the surface of (a) Al–0%, (b) Al–2%, (c) Al–4%, and (d) Al–8% composites. Showing the proliferation and spreading of SCC-25 cells after 10 days of culture on composites (all images at same magnification and scale bars represent 30 µm (inset).

3.6. Culture of SCC-25 cells on glass–ceramic composites

Fig. 11(a)–(d) show SEM images of the surface of leucite glass–ceramic composite samples. SEM morphology reveals the proliferation of SCC-25 cells after 10 days of culture and it covers the whole surface of the sample. The images also show that the cells adhered to all composites with a flattened and lengthened morphology. Higher numbers of cells are attached on the surface of composites Al-2 and Al-4. This is in consistent with our results as observed with reference to growth inhibition and cytotoxicity [Fig. 11(b) and (c)]. These results also suggest that the prepared composite materials allows the growth of the cells efficiently over its surface (Fig. 11).

4. Conclusions

This study has shown the successful investigation of alumina based leucite glass ceramic composite for possible applications in the dental restorations. The addition of alumina to the glass ceramic composites results in the formation of nepheline crystalline phase. This leads to enhance the CTE and flexural strength of the samples. Alumina added leucite glass ceramic composites show high flexural strength than that of the leucite based glass ceramic composite and commercial dentine. A uniform attachment of SSC-25 cells after 10 days of culture on the surface of the composites has been observed. It confirms that the addition of alumina to the leucite glass ceramic composite is a successful approach to improve its mechanical and biological properties.

Acknowledgement

The authors gratefully acknowledge the financial support of DST [(TDT Division), Reference No. DST/SSTP/UP/197 (G) 2012], Ministry of Science & Technology, New Delhi, India.

References

[1] P.H. Kumar, V.K. Singh, A. Srivastava, S.K. Hira, P.P. Pradeep Kumar, Manna, Mechanochemically synthesized leucite based bioactive glass ceramic composite for dental veneering, Ceram. Int. 41 (2015) 11161–11168.

[2] H. Milly, F. Festy, F.T. Watson, I. Thompson, A. Banerjee, Enamel white spot lesions can remineralise using bio-active glass and polyacrylic acidmodified bio-active glass powders, J. Dent. 42 (2014) 158–166.

[3] X. Chatzistavrou, D. Esteve, E. Hatzistavrou, E. Kontonasaki, K. Paraskevopoulos, A.R. Boccaccini, Sol–gel based fabrication of novel glass-ceramics and composites for dental applications, Mater. Sci. Eng. C 30 (2010) 730–739.

[4] Contemporary Fixed Prosthodontics, in: I.L. Denry, L.W. Laub, S.F. Rosenstiel, M.F. Land, J. Fujimoto (Eds.), Mosby Inc., third ed., St. Louis, 2001, pp. 614–617.

[5] M. Mrazova, A. Klouzkova, Leucite porcelain fused to metals for dental restoration, Ceram. Silik. 53 (2009) 225–230.

[6] J.R. Mackert, M.B. Butts, R. Morena, C.W. Fairhurst, The effect of the leucite transformation on dental porcelain expansion, Dent. Mater. 2 (1986) 32–36.

[7] P.H. Kumar, A. Srivastava, V. Kumar, S. Sharma, H. Singh, P. Kumar, V.K. Singh, Role of CaF_2 on mechanochemically synthesized leucite as dental veneering glass ceramics, Adv. Appl. Ceram. 114 (2015) 107–113.

[8] P.H. Kumar, A. Srivastava, V. Kumar, N. Jaiswal, P. Kumar, V.K. Singh, Role of MgF2 addition on high energy ball milled kalsilite: implementation as dental porcelain with low temperature frit, J. Adv. Ceram. 3 (2014) 332–338.

[9] E.E. Meliegy, R.V. Noort, Glasses and Glass Ceramics for Medical Applications, Springer science & business media, Berlin, Germany, 2012 Chapter-10 Leucite Glass Ceramics, LLC.

[10] R. Ravarian, F. Moztarzadeh, M.S. Hashjin, S.M. Rabiee, P. Khoshakhlagh, M. Tahriri, Synthesis characterization and bioactivity investigation of bioglass hydroxyapatite composite, Ceram. Int. 36 (2010) 291–297.

[11] D. Felton, B. Kanoy, S. Bayne, G. Wirthman, Effect of in vivo crown margin discrepancies on periodontal health, J. Prosthet. Dent. 65 (1991) 357–364.

[12] J.N. Walton, F.M. Gardner, J.R. Agar, A survey of crown and fixed partial denture failures: length of service and reasons for replacement, J. Prosthet. Dent. 56 (1986) 416–421.

[13] J. Waerhaug, Tissue reaction around artificial crowns, J. Periodont. 24 (1953) 172–185.

[14] X. Chatzistavrou, O. Tsigkou, H.D. Amin, K. Paraskevopoulos, V. Salih, A.R. Boccaccini, Sol–gel based fabrication and characterization of new bioactive glass–ceramic composites for dental applications, J. Eur. Ceram. Soc. 32 (2012) 3051–3061.

[15] L.L. Hench, H.A. Paschall, Direct chemical bond of bioactive glass ceramic materials to bone and muscle, J. Biomed. Mater. Res. Symp 4 (1973) 25–42.

[16] O.M. Goudouri, E. Kontonasaki, N. Kantiranis, X. Chatzistavrou, L. Papadopoulou, P. Koidis, K.M. Paraskevopoulos, A bioactive glass/dental porcelain system by the sol gel route: fabrication and characterization, Key Eng. Mater. 396–398 (2009) 95–98.

[17] A.C. Meijering, N.H. Creugers, F.J. Roeters, J. Mulder, Survival of three types of veneer restorations in a clinical trial a 2.5-year interim evaluation, J. Dent. 26 (1998) 563–568.

[18] S. Pitaru, H. Tal, M. Soldinger, A. Grosskop, M. Noff, Partial regeneration of periodontal tissues using collagen barriers. Initial observations in the canine, J. Periodont 59 (1988) 380–386.

[19] E. Kontonasaki, A. Sivropoulou, L. Papadopoulou, P. Garefis, K. Paraskevopoulos, P. Koidis, Attachment and proliferation of human periodontal ligament fibroblasts on bioactive glass modified ceramics, J. Oral Rehabil. 34 (2007) 57–67.

[20] R.G. Craig, R.Z. Legeros, Early events associated with periodontal connective tissue attachment formation on titanium and hydroxyapatite surfaces, J. Biomed. Mater. Res. 47 (1999) 585–594.

[21] A. Noaman, S.C.F. Rawlinson, R.G. Hill, Bioactive glass-stoichiometric wollastonite glass alloys to reduce TEC of bioactive glass coatings for dental implants, Mater. Lett. 94 (2013) 69–71.

[22] F.A.A. Sanabani, A.A. Madfa, N.H. Al-Qudaimi, Alumina ceramic for dental applications: A review article, Am. J. Mater. Res. 1 (2014) 26–34.

[23] Guazzato, M. Albakry, M. Ringer, S.P. Swain, M.V, Strength, fracture toughness and microstructure of a selection of all-ceramic materials. Part I. pressable and alumina glass infiltrated ceramics, Dent. Mater. 20 (2004) 441–448.

[24] J.Anusavice Kenneth, Phillips' science of Dental materials, Dent. Ceram. (2007).

[25] John F. McCabe, Angus W.G. Walls, Applied dental materials, Ceram. Porcelain Fused Metal (PFM) (2008).

[26] E.M.A. Hamzawy, E.A.M. El-Meliegy, Preparation of nepheline glass–ceramics for dental applications, Mater. Chem. Phys. 112 (2008) 432–435.

[27] M.C. Wang, N.C. Wu, M.H. Hon, Preparation of nepheline glass-ceramics dental porcelain, Mater. Chem. Phys. 37 (1994) 370–375.

[28] G.A. Khater, E.M.A. Hamzawy, H.I. Metwally, E. El-Meliegy, Spodumene nepheline- anorthite glass ceramics for dental applications, J. Appl. Sci. Res. 9 (2013) 821–825.

Appl Nanosci
DOI 10.1007/s13204-015-0491-x

ORIGINAL ARTICLE

Mechanochemically synthesized kalsilite based bioactive glass-ceramic composite for dental vaneering

Pattem Hemanth Kumar[1] · Vinay Kumar Singh[1] · Pradeep Kumar[2]

Received: 11 May 2015 / Accepted: 10 August 2015

Abstract Kalsilite glass–ceramic composites have been prepared by a mechanochemical synthesis process for dental veneering application. The aim of the present study is to prepare bioactive kalsilite composite material for application in tissue attachment and sealing of the marginal gap between fixed prosthesis and tooth. Mechanochemical synthesis is used for the preparation of microfine kalsilite glass–ceramic. Low temperature frit and bioglass have been prepared using the traditional quench method. Thermal, microstructural and bioactive properties of the composite material have been examined. The feasibility of the kalsilite to be coated on the base commercial opaque as well as the bioactive behavior of the coated specimen has been confirmed. This study indicates that the prepared kalsilite-based composites show similar structural, morphological and bioactive behavior to that of commercial VITA VMK95 Dentin 1M2.

Keywords Mechanochemical synthesis · Composite · Glass–ceramics · Coating · Simulated body fluid · Dental ceramic

Introduction

Ceramic–metal restorations are a beauty of porcelain and strength of a metal substructure. Metal/ceramic alloys are being challenged by manufacturers of frequent low cost and exhibit superior physical properties (Mclean and Sced 1973; Kumar et al. 2014a, b). However, during the last few years, the technological parameters of dental ceramic alloys have been changed. Dental ceramic materials are bio-inert and unable to interacting with the surrounding tissues. Bioactive dental materials have been developed over the last decades (Chatzistavrou et al. 2010). According to Hench, bioactive glass produces a specific biological response at the interface of the material which results in the formation of a bond between the tissues and the material (Chatzistavrou et al. 2012; Hench and Paschall 1973). Ceramic materials are regularly used in dental restoration, which have specific properties such as similarity with natural tooth structure, wear resistance, high mechanical strength and durability in the oral environment. The main problems that occur with the patients are the secondary caries and cement dissolution, resulting in the marginal gap between existing tooth and restoration (Al-Noaman et al. 2013; Kokoti et al. 2001). This causes a bacterial attack leading to pulp irritation or necrosis and finally remove the prostheses (Kontonasaki et al. 2007). Alteration in this marginal gap leads to increase in the cell attachment and proliferation without affecting the physical–chemical and mechanical properties (Pitaru et al. 1988). It may decrease or eliminate cement dissolution and prevent the bacterial adhesion on the cement surface (Meijering et al. 1998). Chatzistavrou et al. described a successful synthesis of bioactive dental glass–ceramic composite using the sol–gel route. They have also reported the feasibility of developed material to be coated on the surface of dental ceramic substrates (Chatzistavrou et al. 2010). Furthermore, no work has been reported on the synthesis of kalsilite glass–ceramic using mechanochemical route and its formulation with bioglass to form a bioactive composite.

✉ Vinay Kumar Singh
phkumar.rs.cer13@itbhu.ac.in; vinaycer@gmail.com

[1] Department of Ceramic Engineering, Indian Institute of Technology (BHU), Varanasi, India

[2] Department of Chemical Engineering and Technology, Indian Institute of Technology (BHU), Varanasi, India

Published online: 19 August 2015

The present work has been carried out to introduce a successful synthesis of bioactive kalsilite glass–ceramic composite materials with required characteristics for dental applications, especially for porcelain fused to metal system (PFM) used for crown, bridges etc. In this work, bioactive glass and kalsilite-based porcelain were prepared using a traditional melt-quenching method and mechanochemical route, respectively (Kumar et al. 2014). This new composite material is expected to have good thermal, bioactive and mechanical properties.

Materials and methods

Preparation of kalsilite, bioglass and low temperature frit (LTF)

AR grade aluminum oxide, potassium carbonate, and silicon dioxide (Loba Chemie Pvt. Ltd., Mumbai, India) were weighed in a stoichiometric ratio of kalsilite. This mixture was ground for 6 h in a high-energy planetary ball mill and subsequently heat treated at 1000 °C as discussed in our previous work (Kumar et al. 2014). Commercial Bioglass® 45S5 was prepared on a lab scale using traditional melt-quenching in a platinum crucible at 1400 °C. The molten frit was quenched in deionized water, dried at 110 °C for 2 h and subsequently pulverized to pass a 350 BSS mesh. A similar process was adopted for the preparation of LTF (Kumar et al. 2014).

Formulation of kalsilite composite

Composites were prepared by mixing 40 wt% kalsilite, 45 wt% bioglass and 15 wt% LTF. Compositions of the composite 1 (CMP-1) and composite 2 (CMP-2) (given in Table 1) were chosen on the basis of optimizations include glossiness of the surface, thermal expansion and translucency. The batch was ground in a planetary ball mill for 5 min to get a homogenous mixture. The ground mixture was further palletized using a uniaxial hydraulic press by applying a load of 200 MPa. These pellets were heat treated at 960 °C with a heating rate of 80 °C/min using a furnace VITA VACUMAT 40T according to standard dental veneering firing cycle pre-programmed by VITA under vacuum. The vacuum was started at 500 °C and released at 960 °C.

Table 1 Batch composition of composites

Composites	Kalsilite	Kalsilite MgF_2	Bioglass	LTF
CMP-1	40	–	45	15
CMP-2	–	40	45	15

The bonding of CMP-1 and CMP-2 coating materials was analyzed on a substrate made of opaque (from VITA VMK 95 1M2 opaque Product no. B330212, VITA Zahnfabrik, Bad sackingen, Germany). The substrate powder was palletized in a similar manner by heating at 960 °C. Veneer material was prepared by mixing of both the composites (CMP-1 and CMP-2) in a modeling liquid with powder to liquid ratio of 0.3 to make a thick slurry. It is spread manually using a spatula on the substrates. These specimens were fired up to 960 °C using VITA VACUMAT 40T.

Characterizations

Phase identification and microstructural analysis

X-ray diffraction of the composite (before and after heat treatment) was carried out using a portable XRD (Rigaku, Japan) employing Cu Kα radiation with Ni filter operating at 30 mA and 40 kV. Diffraction peaks were analyzed using standard JCPDS file (PDF-2 database 2003). Micrographs of the fractured sample were recorded using scanning electron microscope (SEM) (INSPECT 50 FEI).

Coefficient of thermal expansion (CTE)

Coefficient of thermal expansion and the glass transition temperature (*Tg*) of the composite material were examined using a dilatometer (supplied by VB Ceramic Consultants, India). For CTE measurements, material was compacted into a rectangular bar (50 × 10 × 10 mm) using a uniaxial hydraulic press by applying a load of 200 MPa followed by heat treated up to 950 °C with heating rate 80 °C/min (according to manufacturer's instructions).

Preparation of SBF

Simulated body fluid solution was prepared by dissolving analytical reagent grade NaCl, KCl, $NaHCO_3$, $MgCl_2.6H_2O$, $CaCl_2$ and KH_2PO_4 in double distilled water and buffered at pH 7.25 with tris (hydroxymethyl) aminomethane (TRIS) and 1 N HCl at 35–37 °C (Kokubo and Takadama 2006).

Bioactivity test

The formulated composites have been veneered on the surface of the substrate to study its bioactivity and surface morphology. Furthermore, the formation of hydroxyapatite (HAp) on the interface was also studied. HAp forming ability of the coated specimens was observed through

immersion in simulated body fluid (SBF). For these testing's, three specimens of dimensions 10 mm diameter and 2 mm thickness were prepared and immersed in SBF (40 ml) for 7 and 21 days. At the end of the selected time periods, samples were separated from the SBF solution, rinsed with distilled water and dried in an electrical oven for further analysis. SBF-treated samples were examined by SEM and FTIR to evaluate the possible formation of HAp layer on the material surface as a marker of the bioactive behavior.

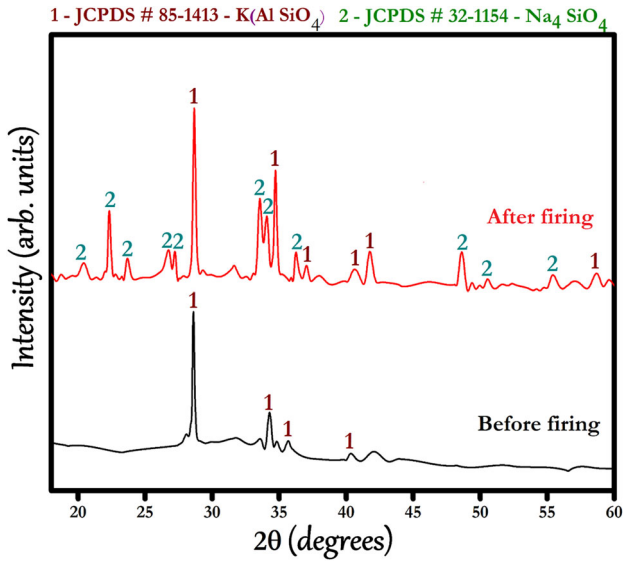

Fig. 1 XRD patterns of kalsilite composite before and after heat treatment

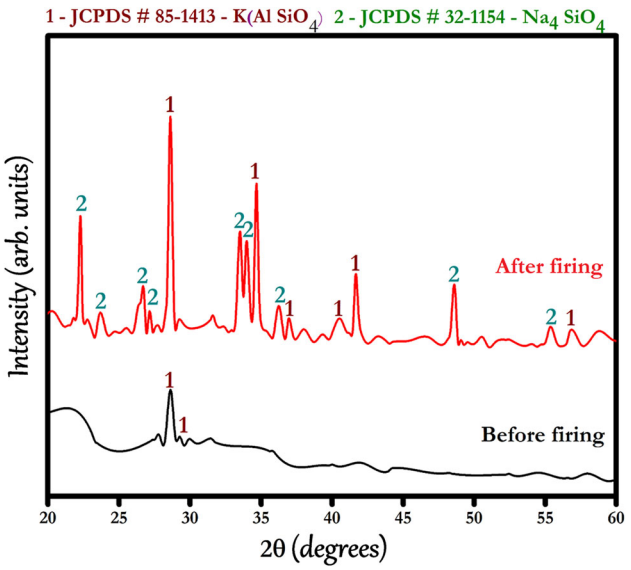

Fig. 2 XRD patterns of kalsilite MgF_2 composite before and after heat treatment

Results and discussion

Phase analysis

Figures 1 and 2 show the XRD patterns of all the kalsilite composites before and after firing. Diffraction peaks are well matched to JCPDS Card No. 32-1154. Before firing, kalsilite has been detected as a crystalline phase along with some amorphous phase in both composites. Furthermore Na_2O. SiO_2 phase has been found as a crystalline phase after firing along with kalsilite as a major phase in both CMP-1 and CMP-2. This may form due to the presence of some free Na_2O and SiO_2 components in the matrix. Figures 1 and 2 show that the peak intensity corresponds to kalsilite phase is higher in CMP-2 as compared to CMP-1. It is therefore concluded that MgF_2 helps in the formation of kalsilite as a major phase (Kumar et al. 2014).

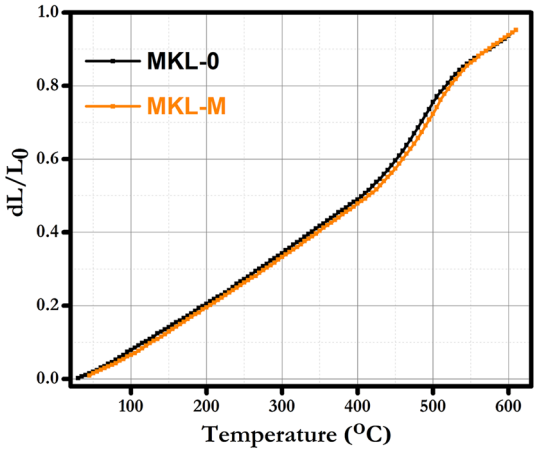

Fig. 3 CTE curves of kalsilite composites MCL-1

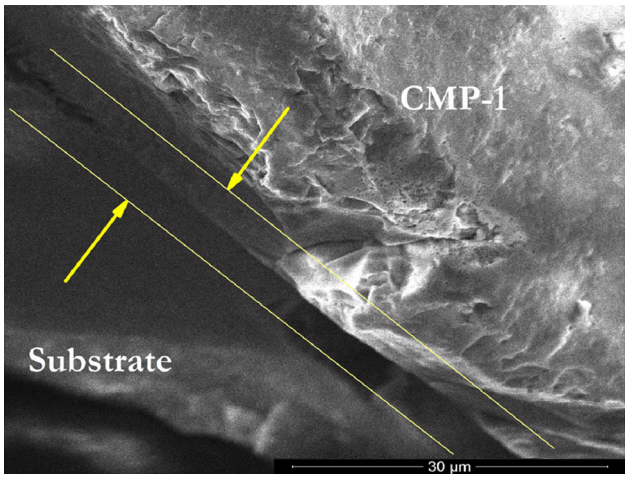

Fig. 4 SEM image of the fracture surface of CMP-1 interface of coated on subtract

Coefficient of thermal expansion (CTE)

Thermal expansion is the important essential for veneering glass–ceramic fused to metal restorations. When a dental ceramic is used on a substrate, then CTE must be exact to confirm good attachment of the dental prosthesis. There is a possibility of formation of the cracks if a mismatch among the CTE of the ceramic coating and the substrate exists. Figure 3 shows the result of CTE curves of kalsilite composites. Values of CTE and glass transition (Tg) of the composites have been found to be 15.9×10^{-6}/°C and 535 °C for CMP-1, 15.6×10^{-6}/°C and 545 °C for CMP-2, respectively. It is nearer to the CTE (14.5×10^{-6}/°C) obtained for dentine (VITA VMK95 Dentin 1M2). CMP-1 has slightly high CTE and low Tg than that of CMP-2. A high CTE of ceramic is to be assured a good bonding with the substrates. The existence of kalsilite phase in composite material causes an increase in the CTE value. Kalsilite has a high CTE which improves the whole CTE of the dental ceramic subsequently thermally compatible with the substrates (Kumar et al. 2014).

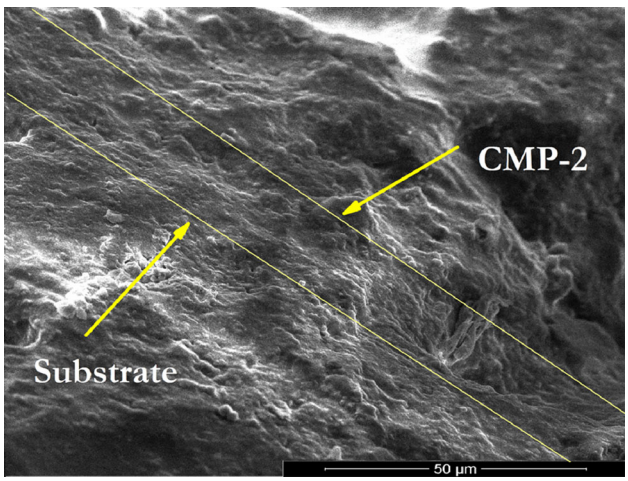

Fig. 5 SEM image of the fracture surface of CMP-2 interface of coated on subtract

Surface morphology

Figures 4 and 5 show the surface morphology of interface layer between the composite and the substrate (composite coated on a commercial vita opaque substrate). This morphology is a confirmation of qualitatively good bonding between the composite and substrate. There are no cracks or peeling off or gap present in the interface region. This confirms that the CTE of composite and substrate is well coordinated (Kumar et al. 2015).

Bioactivity in SBF

Kalsilite composite samples immersed in SBF solution have been analyzed using SEM and FTIR. Immersed in SBF led to the formation of a HAp layer on the surface of the samples. Figures 6 and 7 show the development of HAp layer on the surface of the samples after immersing in SBF solution for 7 days. In FTIR (Figs. 8, 9) spectra, strong peaks appeared in the range of 1150–900 and 650–500 cm^{-1} correspond to the stretching vibrations of PO_4^{-3}. This is indication of the formation of hap layer on the surface of the sample after immersion in SBF for 7 days at 37 °C. The low intense peaks have been observed in the range 1500–1400 cm^{-1} indicate the presence of CO_3^{-2} molecules in the sample. There is also a peak at 450 cm^{-1} allocated to the bending vibration mode of Si–O bond. The results of FTIR are also in conformity with the results of SEM. The formation of HAp layer on the surface of the samples includes few steps reactions (Hench and Paschall 1973). First is exchange between the alkali ions in

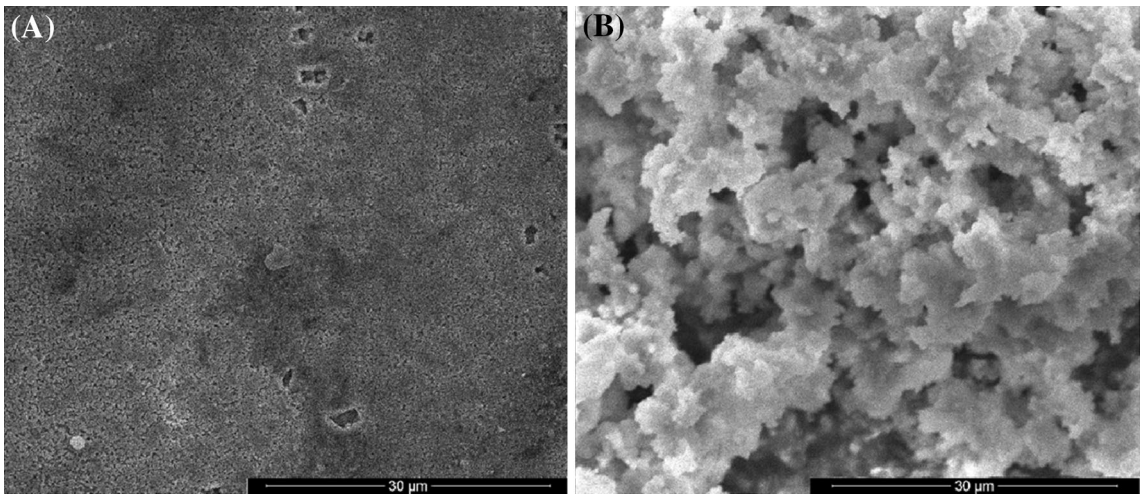

Fig. 6 SEM pictures of the CMP-1 **a** before and **b** after immersion for 7 days in SBF solution, presenting hydroxyapatite formation

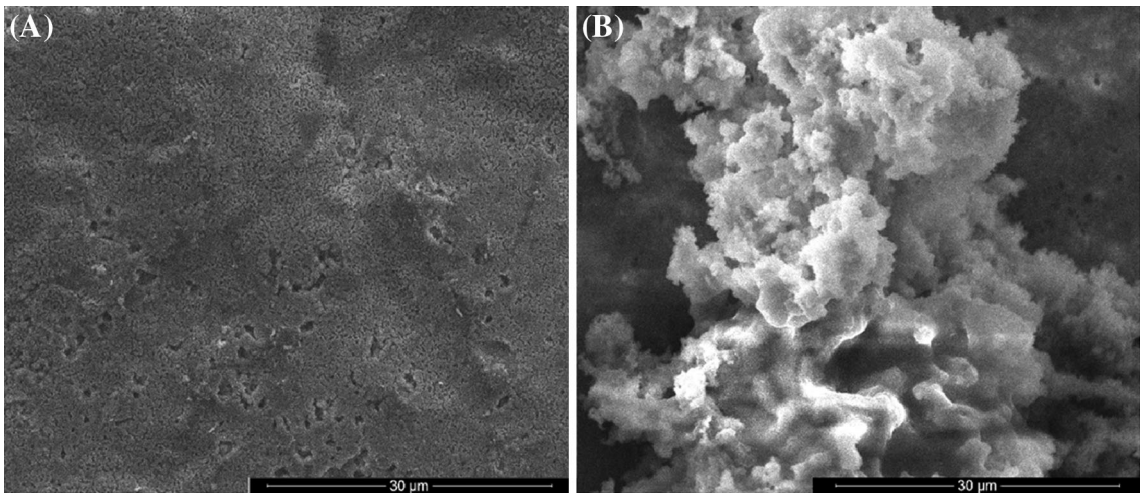

Fig. 7 SEM pictures of the CMP-2 **a** before and **b** after immersion for 7 days in SBF solution, presenting hydroxyapatite formation

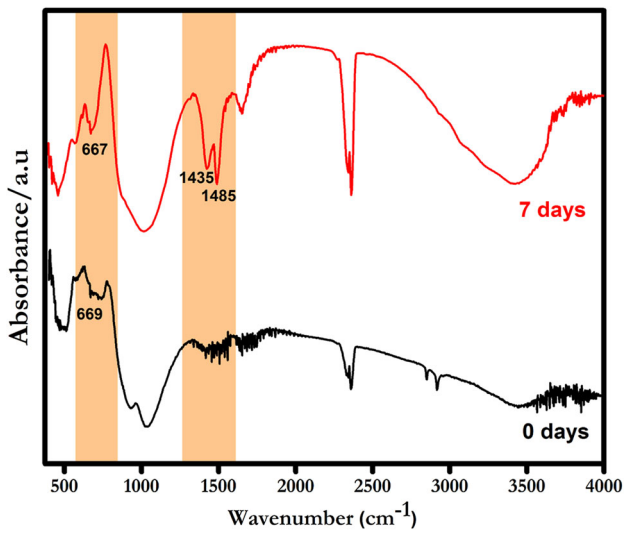

Fig. 8 FTIR absorbance bands of the CMP-1 before and after immersion in SBF solution for 0 and 7 days

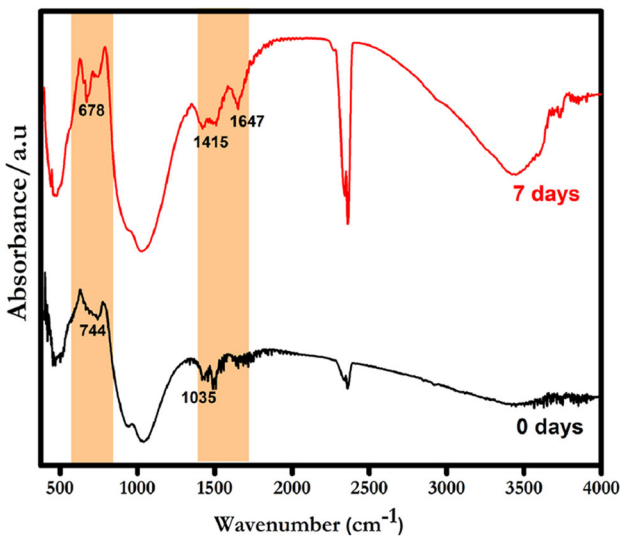

Fig. 9 FTIR absorbance bands of the CMP-2 before and after immersion in SBF solution for 0 and 7 days

the glass and the water. Second is breakdown of the silica network forming silanol bonds that re-polymerize to form a hydrated, high surface area, silica-rich layer. Silica-rich surface enhances the migration of Ca^{2+} and PO_4^{3-} to the surface forming an amorphous CaP layer which further crystallized in HAp layer.

Conclusion

The current work shows the successful mechanochemical synthesis of kalsilite-based composites for potential applications in dental restorations. The strong bonding of CMP-1 and CMP-2 to be applied as a coating on the substrate has been confirmed by SEM. Hydroxyapatite layer formation on the surface of the CMP-1 and CMP-2 has been observed using FTIR and SEM. These composite materials may be used for dental veneering application. These materials will be further characterized by ion leachability test in different acidic agent and wettability test in the future.

Acknowledgments The authors gratefully acknowledge the financial support of DST [(TDT Division), Reference No. DST/SSTP/UP/197(G) 2012], Ministry of Science and Technology, New Delhi, India.

References

Al-Noaman Ahmed, Rawlinson SCF, Hill Robert G (2013) Bioactive glass-stoichiometric wollastonite glass alloys to reduce TEC of bioactive glass coatings for dental implants. Mater Lett 94:69–71

Chatzistavrou X, Esteve D, Hatzistavrou E, Kontonasaki E, Paraskevopoulos K, Boccaccini AR (2010) Sol–gel based fabrication of novel glass-ceramics and composites for dental applications. Mater Sci Eng C 30:730–739

Chatzistavrou X, Tsigkou O, Amin HD, Paraskevopoulos K, Salih V, Boccaccini AR (2012) Sol–gel based fabrication and characterization of new bioactive glass–ceramic composites for dental applications. J Eur Ceram Soc 32:3051–3061

Hench LL, Paschall HA (1973) Direct chemical bond of bioactive glass ceramic materials to bone and muscle. J Biomed Mater Res Symp 4:25–42

Kokoti M, Sivropoulou A, Koidis P, Garefis P (2001) Comparison of cell proliferation on modified dental ceramics. J Oral Rehabil 28:799–804

Kokubo T, Takadama H (2006) How useful is SBF in predicting in vivo bone bioactivity. Biomaterials 27:2907–2915

Kontonasaki E, Sivropoulou A, Papadopoulou L, Garefis P, Paraskevopoulos K, Koidis P (2007) Attachment and proliferation of human periodontal ligament fibroblasts on bioactive glass modified ceramics. J Oral Rehabil 34:57–67

Kumar PH, Srivastava A, Kumar V, Jaiswal N, Kumar P, Singh VK (2014a) Role of MgF_2 addition on high energy ball milled kalsilite: implementation as dental porcelain with low temperature frit. J Adv Ceram 3:332–338

Kumar PH, Srivastava A, Kumar V, Sharma S, Singh H, Kumar P, Singh VK (2014b) Role of CaF_2 on mechanochemically synthesized leucite as dental veneering glass ceramics. Adv Appl Ceram 114:107–113

Kumar Pattem Hemanth, Singh Vinay Kumar, Srivastava Abhinav, Hira Sumit Kumar, Kumar Pradeep, Manna Partha Pratim (2015) Mechanochemically synthesized leucite based bioactive glass ceramic composite for dental veneering. Ceram Int 41:1161–11168

Mclean JW, Sced IR (1973) The gold alloy/porcelain bond. Trans Br Ceram Soc 5:229–238

Meijering AC, Creugers NH, Roeters FJ, Mulder J (1998) Survival of three types of veneer restorations in a clinical trial a 2.5-year interim evaluation. J Dent 26:563–568

Pitaru S, Tal H, Soldinger M, Grosskopf A, Noff M, Periodont J (1988) Partial regeneration of periodontal tissues using collagen barriers. Initial obs Canine 59:380–386

Available online at www.sciencedirect.com

ScienceDirect

Ceramics International 41 (2015) 11161–11168

CERAMICS INTERNATIONAL

www.elsevier.com/locate/ceramint

Mechanochemically synthesized leucite based bioactive glass ceramic composite for dental veneering

Pattem Hemanth Kumar[a], Vinay Kumar Singh[a,*], Abhinav Srivastava[a], Sumit Kumar Hira[b], Pradeep Kumar[c], Partha Pratim Manna[b]

[a]Department of Ceramic Engineering, Indian Institute of Technology (BHU), Varanasi 221005, India
[b]Immunobiology laboratory, Department of Zoology, Banaras Hindu University, Varanasi 221005, India
[c]Department of Chemical Engineering, Indian Institute of Technology (BHU), Varanasi 221005, India

Received 27 February 2015; received in revised form 12 May 2015; accepted 13 May 2015
Available online 21 May 2015

Abstract

The present work was aimed to synthesize leucite based bioactive glass ceramic composite with required characteristics for dental applications. The leucite glass-ceramic was prepared using mechanochemical synthesis. The microstructural, thermal, mechanical and biological properties of the composite coatings and its material–cell interaction were studied. The flexural strength and coefficient of thermal expansion (CTE) of a commercial dentine was also studied comparatively. Results of FTIR indicated the formation of hydroxyapatite layer on the surface of the composite. In-vitro cell proliferation and cytotoxicity assay of MCL composite material demonstrated that it did not inhibit proliferation and cytotoxicity of SCC-25 at low concentration, caused moderate levels of apoptosis at higher concentrations and were also tolerated by human RBC as studied by hemolytic assay. Based on the toxicity and bioactivity observed in this work, it can be concluded that this product may be further processed for potential clinical applications.

Keywords: A. Milling; B. Composites; C. Thermal expansion; D. Glass ceramics; E. Biomedical applications

1. Introduction

Ceramic materials used in restorative dentistry have specific properties such as durability in the oral environment, similarity with natural tooth structure, high wear resistance and mechanical strength [1,2]. Problems which occur with the patient and dental care system is related to the failure of fixed prosthetic due to cement dissolution and secondary caries [3–7]. This results in the marginal gap between the fixed tooth and restoration, which is open to bacterial attack leading to pulp irritation and removal of the prosthesis [8,9]. Dental ceramic materials are bio-inert and incapable of interacting with the surrounding tissues [9]. According to L. L. Hench, bioactive glass elicits a specific biological response at the interface of the material which results in the formation of a bond between the tissues and the material [10]. This formed layer of hydroxyapatite (HAp) enhances cell proliferation and increases cell attachment thereby sealing the marginal gap [11–15]. E. Kontonasaki et al. established that the alteration of dental porcelain with calcium–phosphate based materials brought about significantly higher rates of cell proliferation compared with the unmodified porcelain, thereby increasing the lifespan of dental restoration [16].

Chatzistavrou et al. reported a successful synthesis of bioactive dental glass ceramic composite using sol–gel route. They have also established that developed material can be coated on the surface of dental ceramic substrates resulting in bioactive surface [2]. Further, no work has been reported on the synthesis of leucite glass ceramic using mechanochemical route and its formulation with bioglass to form a bioactive composite.

The present study explores the applicability of mechanochemical process to synthesize leucite glass ceramic for the

*Corresponding author. Tel.: +91 9936182124.
E-mail address: vksingh.cer@itbhu.ac.in (V.K. Singh).

http://dx.doi.org/10.1016/j.ceramint.2015.05.065
0272-8842/

first time. This work also reports preparation of bioglass and low temperature frit (LTF) by traditional melt-quenching method [17,18]. Above three materials were mixed in an optimum ratio to form a composite with desirable properties. The composite prepared was tested for physico-mechanical and thermal properties as well as biocompatibility behavior. It was also compared with a commercial product (VITA VMK 95) to verify the feasibility of the prepared composite.

2. Materials and methods

2.1. Preparation of leucite, bioglass and LTF

AR grade aluminum oxide, potassium carbonate, and silicon dioxide (Loba Chemie Pvt. Ltd., Mumbai, India) were weighed in a stoichiometric ratio of leucite. This mixture was pulverized for 6 h in a high-energy planetary ball mill and subsequently fired at 1100 °C as discussed in our previous work [18]. Commercial Bioglass® 45S5 was prepared on a lab scale using traditional melt-quenching in a platinum crucible at 1400 °C. The molten frit was quenched in deionized water, dried at 110 °C for 2 h and subsequently pulverized to pass a 350 BSS mesh. A similar process was adopted for the preparation of LTF details, which is described elsewhere [17].

2.2. Formulation of composite

Composite (referred as MCL-1 hereafter) was prepared by mixing the 40 wt% leucite glass ceramic, 50 wt% bioglass and 10 wt% LTF powders. Composition of MCL-1 was chosen on the basis of several optimizations, which involve co-efficient of thermal expansion (CTE), the glossiness of the surface and translucency. The batch was ground in a planetary ball mill (V.B. Ceramics, Chennai, India) for 10 min to obtain a homogenous mixture. This ground material was pelletized using a uniaxial hydraulic press by applying a load of 200 MPa. These pellets were heat treated at 960 °C with a heating rate of 80 °C/min using a VITA VACUMAT 40T according to a standard dental veneering firing cycle pre-programmed by VITA under vacuum. A vacuum was introduced at 500 °C and released at 950 °C.

To examine the bonding of MCL-1, pellets made of opaque from VITA VMK 95 opaque 1M2, (Product no. B330212, VITA Zahnfabrik, Bad sackingen, Germany) were used as substrates. The substrate powder was pelletized in a similar manner by heating at 950 °C. Coating material was prepared by mixing MCL-1 in a modeling liquid, using a liquid to powder weight ratio of 0.3 to make a thick paste. It was spread manually using a spatula on the substrates. These specimens were fired up to 960 °C using furnace VITA VACUMAT 40T. To study physical and mechanical properties comparatively, samples from VITA VMK95 Dentin 1M2 (Product no. B333212, VITA Zahnfabrik, Bad Sackingen, Germany) were also prepared in the same manner.

2.3. Characterizations

2.3.1. Phase identification, microstructural analysis and CTE

XRD of the composite (before and after heat treatment) was carried out using a portable XRD machine (Rigaku, Japan) with Cu K_α radiation employing Ni filter operating at 30 mA and 40 kV. Diffraction peaks were analyzed using standard JCPDS file (PDF-2 database 2003). Micrographs of the fractured sample were recorded using scanning electron microscopy (SEM) (INSPECT 50 FEI). CTE and the glass transition temperature (T_g) of the composite material were studied using a dilatometer (VB Ceramic Consultants, India). The material was compacted into a rectangular bar ($50 \times 10 \times 10$ mm) and subsequently fired similar to the composite pellets prepared earlier.

2.3.2. Flexural strength

Flexural strength measurements were done according to ASTM C78 M using a universal testing machine; Instron 3344 (Germany). The specimens were fractured in three-point crossways fit with the 20 mm span between the two supports (three point bending). The load and the corresponding deflections were recorded. The standard deviation, S of the flexural strength values was calculated using the following formula:

$$S = \sqrt{\frac{1}{N-1}\sum_{i=1}^{N}(x_i - \bar{x})^2} \quad (1)$$

where N is the number of samples, x_i is the value of one sample and $\bar{x}$ is the mean value.

2.3.3. Bioactivity

Simulated body fluid (SBF) solution was prepared by dissolving AR grade NaCl, KCl, $NaHCO_3$, $MgCl_2 \cdot 6H_2O$, $CaCl_2$ and KH_2PO_4 (Loba Chemie Pvt. Ltd., Mumbai, India) in distilled water and buffered at pH 7.25 with trishydroxylmethyl aminomethane (TRIS) and 1 N HCl at 35–37 °C. Its composition was maintained equivalent to the ionic concentration of human blood plasma [19].

The hydroxyapatite (HAp) forming ability of the coated specimens was observed through immersion in SBF. For these tests, three specimens of dimensions 10 mm diameter and 2 mm thickness were prepared and immersed in SBF (40 ml) up to 21 days. The SBF solution was replaced every three days since there is a decrease in cation concentration due to the changes in the chemistry of the samples. At the end of each selected time, samples were removed from the SBF solution, rinsed with distilled water, dried and stored in airtight containers for further investigation. SBF treated samples were examined by SEM and FTIR to assess the possible formation of HAp layer on the material surface, as a marker of bioactive behavior.

2.3.4. Cell lines and cell culture

Human buccal epithelial cell line SCC-25 was originally obtained from the American Type Culture Collection (ATCC), Manahass, USA. The cells were maintained in RPMI 1640

(Invitrogen, Carlsbad, CA), supplemented with 10% fetal bovine serum (Hyclone, Logan, UT), 100 U/ml penicillin and 100 mg/ml streptomycin (Invitrogen, Carlsbad, CA), henceforth, called as complete medium. The cell line used in the study was free of mycoplasma.

2.3.5. Cell proliferation assay

The effect of MCL-1 composite material on proliferation of SCC-25 cells was studied by MTT assay [20]. 5×10^3 SCC-25 cells/well were added in a 96-well tissue culture plate, and exposed to serial concentrations of (5, 10, 25, 50, 100, 250 and 500 µg/ml) MCL-1. Plates were incubated at 37 °C, 5% CO_2, for 48 h. The cell proliferation was measured by Cell Titer 96® Nonradioactive Cell Proliferation Assay (MTT) kit from Promega, USA according to the manufacturer's protocol. The plates were incubated for 4 h with the MTT reagent and absorbance was measured at 570 nm using Synergy HT Multi-Mode Microplate Reader BioTek®, USA. The data presented as the percentage of inhibition of tumor cells and was calculated from the following formula:

$$\%\text{Growth Inhibition} = \left[1 - \frac{\text{Experimental OD570}}{\text{Target OD570}}\right] \times 100$$

where experimental OD value is the reading of tumor cells exposed to various concentrations of MCL and Target OD value is the corresponding value of tumor cell cultured in medium only.

2.3.6. In-vitro cytotoxicity assay

The lytic activity of MCL-1 against tumor cells was measured by non-radioactive cytotoxicity assay using the CytoTox 96 Nonradioactive Cytotoxicity assay kit from Promega, USA [21]. Buccal epithelial cells (5×10^3) were added to 96-well tissue culture plates and were exposed to serial concentrations of (5, 10, 25, 50, 100, 250 and 500 µg/ml) MCL and incubated for 18 h at 37 °C, 5% CO_2. Percent-specific lysis was determined using the following formula:

$$\%\text{Cytotoxicity} = \frac{(\text{Experimental} - \text{Effector spontaneous} - \text{Target spontaneous})}{(\text{Target maximum} - \text{Target spontaneous})} \times 100$$

2.3.7. Detection of apoptosis

Apoptotic cell death in SCC-25 cells by MCL-1 composite (100 µg/ml) was assessed by binding of FITC-conjugated Annexin V. After 18 h of incubation, apoptotic cells were analyzed by staining with FITC-conjugated Annexin V and propidium iodide (PI) for 20 min in ice-cold PBS. Cells were washed in Annexin buffer and were mounted on microscope slides with a drop of mounting medium to reduce fluorescence photo bleaching. The FITC-conjugated Annexin V positive cells were visualized under a fluorescence microscope (Nikon Eclipse 80i, Nikon, Japan).

2.3.8. Hemolysis assay

For time dependent kinetics, 100 µg/ml MCL-1 composite was incubated with the blood sample. For concentration dependent kinetics, the blood sample was incubated with varying concentrations (25, 100, and 150 µg/ml) of MCL-1 for 4 h. Hemolysis assay was performed according to the standard protocol [22]. In brief, an aliquot of each blood sample was centrifuged for 5 min. 25 µl plasma aliquot was diluted with 225 µl Drabkin's reagent (Sigma) in a 96-well plate and mixed for 2 min under lateral agitation (300 rpm). After 10 min equilibration at room temperature, optical density was recorded at 540 nm in Synergy HT Multi-Mode Microplate Reader BioTek, USA. Blood hemoglobin was determined by measuring the absorbance of 100 fold dilution of the whole blood in Drabkin's reagent at 540 nm. Saponin (2 mg/ml final blood concentration) and PBS were used as positive and negative control respectively. A sample of plasma without additives was considered as basal conditions. The standard calibration curve was obtained with the solution containing 0.07–3.8 mg/ml bovine hemoglobin (Sigma) treated with a Drabkin's reagent. The results are presented as percent hemolysis indicating the free plasma hemoglobin (mg/ml) and was measured as released hemoglobin divided by the total blood hemoglobin (mg/ml) multiplied by 100. All measurements were performed in triplicate.

3. Results and discussion

3.1. Phase analysis

The XRD pattern of mechanochemically synthesized leucite powder, heat-treated at 1100 °C is portrayed in Fig. 1 whereas Fig. 2 exhibits the XRD pattren of the composite (MCL-1) before and after heat treatment. Leucite was found to be only crystalline phase with some amorphous phase before the heat treatment. Diffraction peaks as shown in Fig. 1, matched well with the JCPDS card no. 81-1147 of tetragonal leucite having unit-cell parameters $a=b=13.09$ and $c=13.75$ Å. After heat treatment, calcium silicate ($2CaO \cdot SiO_2$) and wollastonite ($CaO \cdot SiO_2$)

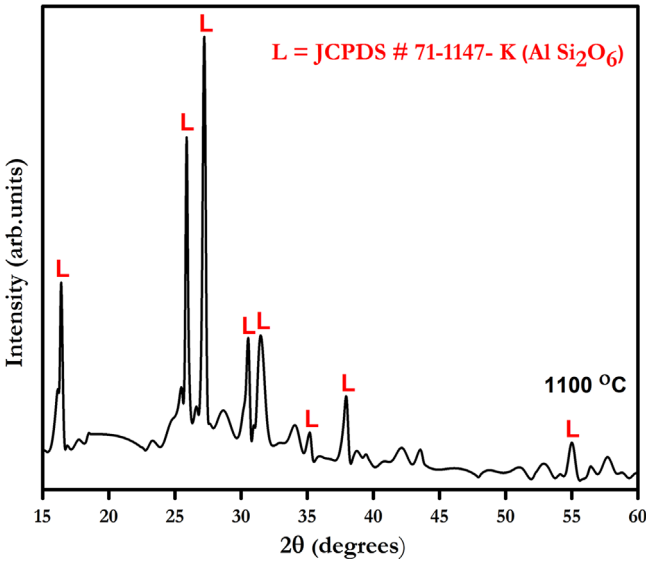

Fig. 1. XRD pattern of milled leucite powder heat-treated at 1100 °C.

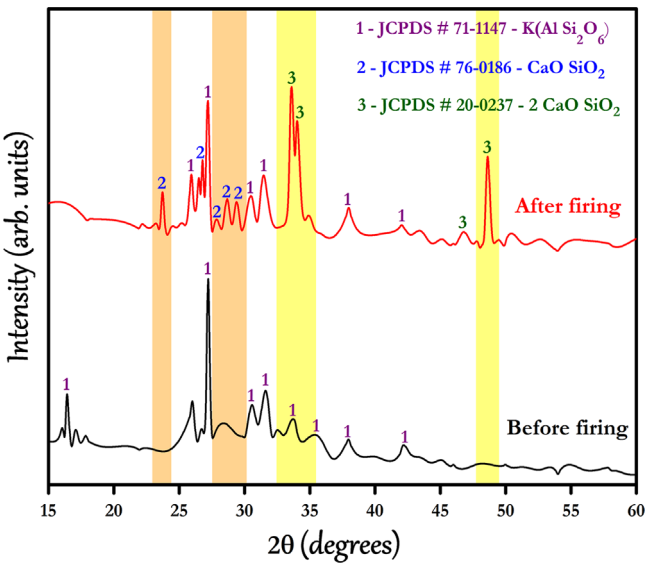

Fig. 2. XRD pattern of the composite before and after heat treatment up to 960 °C with heating rate 85 °C/min.

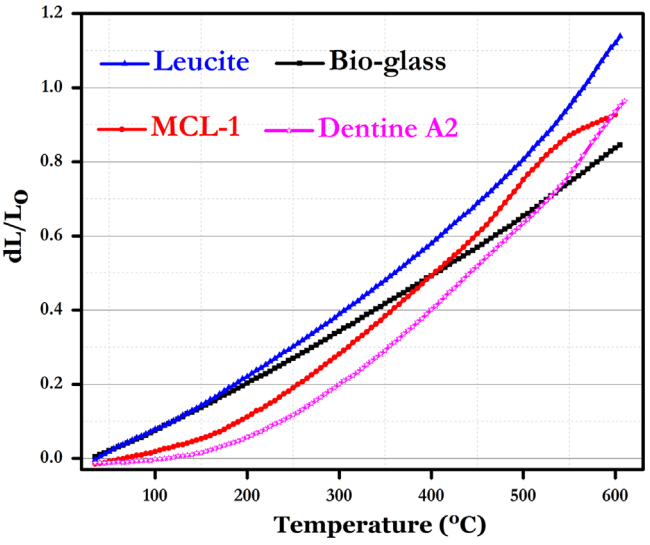

Fig. 3. CTE curves of leucite, bioglass and composite (MCL-1) along with commercial dentine.

crystalline phases were formed along with leucite. The leucite phase intensity was reduced after heat treatment, due to formation of two additional phase viz., calcium silicate and wollastonite; accordingly amorphous phase also decreases.

3.2. Thermal expansion

Fig. 3 shows CTE curves of leucite, bioglass and composite (MCL-1) along with commercial Dentine A2. It was found that the mechanochemically prepared leucite has a CTE 25.50×10^{-6}/°C, which is very close to the theoretical value of pure leucite [23,24]. CTE of Bioglass® 45S5 was 13.4×10^{-6}/°C. Values of CTE and glass transition (T_g) of the composite (MCL-1) have been found to be 15.8×10^{-6}/°C and 480 °C respectively, which is comparable to CTE value obtained for dentine (VITA VMK95 Dentin 1M2) as 14.5×10^{-6}/°C. There was no visual crack or defect after heat treatment of the composite coated on the substrate. This displays a suitable bonding and is only possible due to well matched CTE values of the composite and the substrate. The deviation between CTE of the composite and commercial dentine was very low ~8.22%. The presence of the leucite phase in the composite influenced the CTE value. Inclusion of leucite which has a high CTE value, improved the CTE of composite.

3.3. Mechanical behavior and microstructure

Fig. 4 shows the flexural strength of the composite and commercial dentine VITA VMK95 Dentin 1M2. The prepared composite sample presented the flexural strength comparable with that of commercial dentine. This may be due to the formation of crystalline calcium silicate and wollastonite after heat treatment. The mean and standard deviation values are given in Table 1. Fig. 5 shows the surface morphology of interface layer between the composite and the substrate (composite coated substrate). This microstructure is a confirmation of qualitatively good bonding between the substrate and the composite. The interface area was crack and gap free. This also confirmed that the CTE of composite and substrate

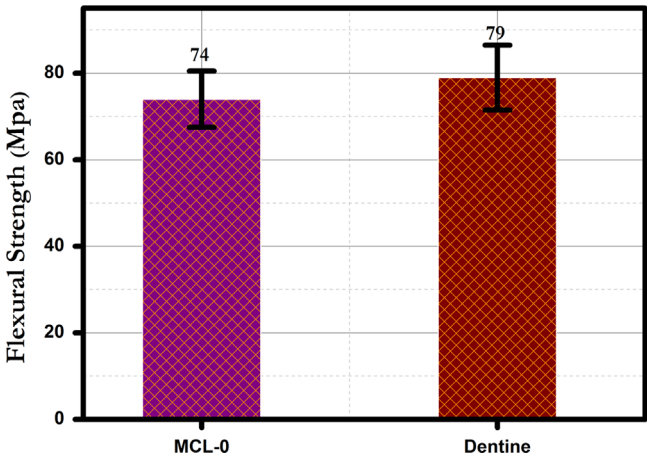

Fig. 4. Flexural strength of composite and commercial dentine.

Table 1
Flexural strength and CTE values of composite and dentine.

Sample coding	Firing temperature (°C)	CTE(/°C) (50–600° C)	Mean (MPa)	SD (MPa)
Leucite	1100	25.50×10^{-6}	–	–
Bioglass	960	13.40×10^{-6}	–	–
MCl-1	960	15.80×10^{-6}	74	9.26
Dentine (VITA VMK95)	960	14.50×10^{-6}	79	7.96

*CTE—coefficient of thermal expansion; SD—standard deviation.

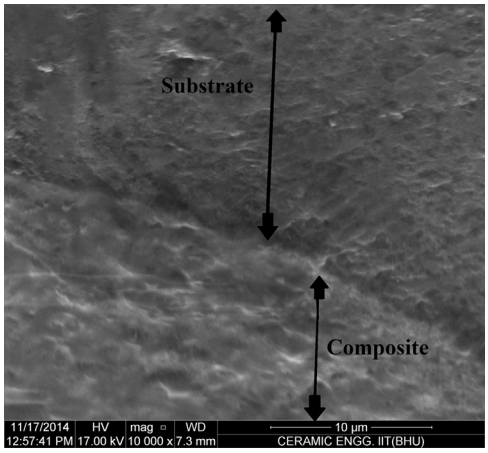

Fig. 5. SEM image showing the surface morphology of interface layer between the composite and the substrate.

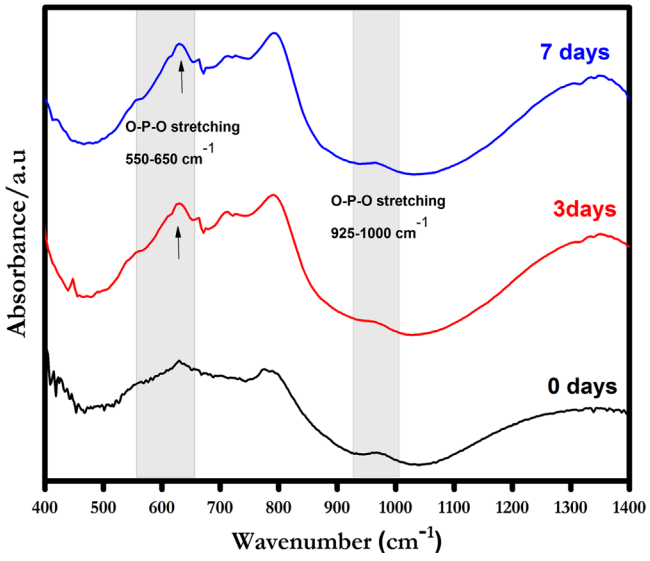

Fig. 6. FTIR absorbance bands of the composite before and after immersion in SBF for 0, 3 and 7 days.

were well matched. Composite coating on a substrate and application of heat, did not lead to any crack or peeling-off due to matching CTE.

3.4. Bioactivity in SBF

Composite samples soaked in SBF were analyzed by FTIR and SEM. Soaking in SBF led to the formation of a HAp layer on the surface of the samples. Fig. 6 shows the FTIR transmittance bands of the composite before and after immersion in SBF for 0, 3 and 7 days. Intense peaks appeared in the range of 650–550 cm^{-1} due to the stretching vibrations of phosphate groups (PO_4^3) have been formed after soaking in SBF for 7 days at 37 °C. Few low intensity peaks appeared in the range 1500–1400 cm^{-1} which indicates the presence of CO_3^{-2} molecules in the sample. Surface micrographs (Fig. 7(a) and (b) demonstrate the formation of an apatite layer on the surface of the samples after immersing in SBF solution for 3 days. The results of SEM are also in conformity with the results of FTIR. It is noticed that after 7 days in SBF the HAp layer forms covering the entire surface of the sample. Furthermore, the thickness of forming HAp layer increases with time. The period of immersion did not have an effect on any volumetric increase or failure of the coating.

3.5. Biocompatibility

3.5.1. Cellular growth inhibition by MCL-1 glass ceramic materials

High concentration of MCL-1 glass ceramic materials caused moderate levels of growth inhibition against SCC-25 cells, although lower concentrations of the compounds are tolerant to the cells. This proposes a broad spectrum usefulness of the compounds (Fig. 8A). Growth inhibition with MCL-1 glass ceramic materials (100 μg/ml) for longer periods (120 h) of time causes a moderate retardation of cell growth compared to treatment for 48 h (Fig. 8B).

Moreover, cellular proliferation, we have also performed the direct cellular cytotoxicity by MCL glass ceramic materials against SCC-25 cells (Fig. 8C). Compared to higher concentration (500 μg/ml), the lower concentrations of MCL-1 glass ceramic materials are tolerant to SCC-25 cells and causes significantly less cell lysis (Fig. 8C). The present data shows that MCL-1 glass ceramic materials work well tolerated and relatively nontoxic to buccal epithelial cells.

3.5.2. Apoptosis study

Growth inhibition by MCL-1 glass ceramic materials at higher concentration raised the question whether it also caused apoptosis of the tumor cells and if so whether it induced cell death. Apoptosis was determined by monitoring changes in the cell size and externalization of phosphatidylserine qualitatively in SCC-25 cells. There was a very low level of increase in Annexin V positive cells upon treatment with MCL-1 glass ceramic materials. This indicate that MCL-1 was significantly less toxic to buccual epithelial cells (Fig. 9).

3.5.3. RBC integrity and size distribution and hemocompatibility

MCL-1 glass ceramic materials did not affect RBC and PBMC (peripheral blood mononuclear cell) significantly with respect to hemolysis and viability Fig. 10A and B. As a confirmation to RBC counting, hemolysis rate was determined in the presence of the formulations MCL which shows a moderate increase in percent lysis and exhibits significantly less hemolysis and may be considered as non-hemolytic Fig. 10B. Microscopic observations also demonstrate no change in morphology in RBC following contact with the MCL-1 as shown Fig. 10C.

4. Conclusions

The present work illustrates a successful mechanochemical synthesis of leucite glass ceramic and its implementation in the formulation of a bioactive dental veneering composite. The strong bonding and feasibility of the composite material as coating

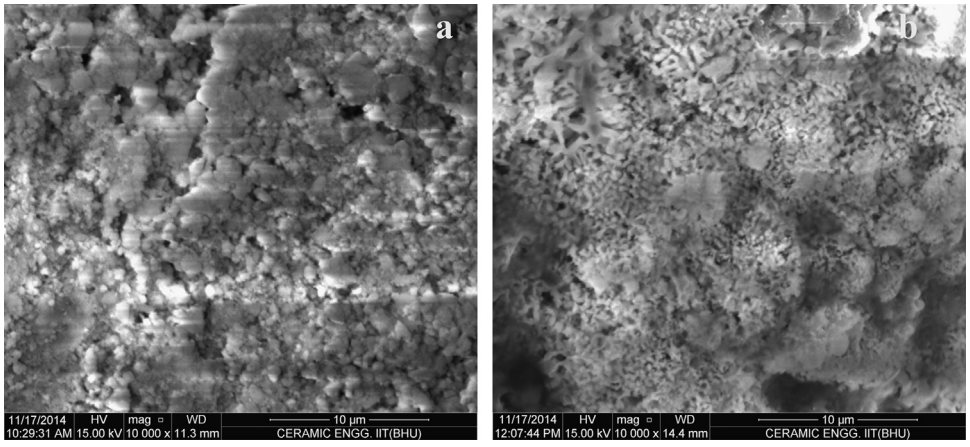

Fig. 7. SEM images of the coated specimens (a) before and (b) after immersion for 7 days in SBF showing HAp formation.

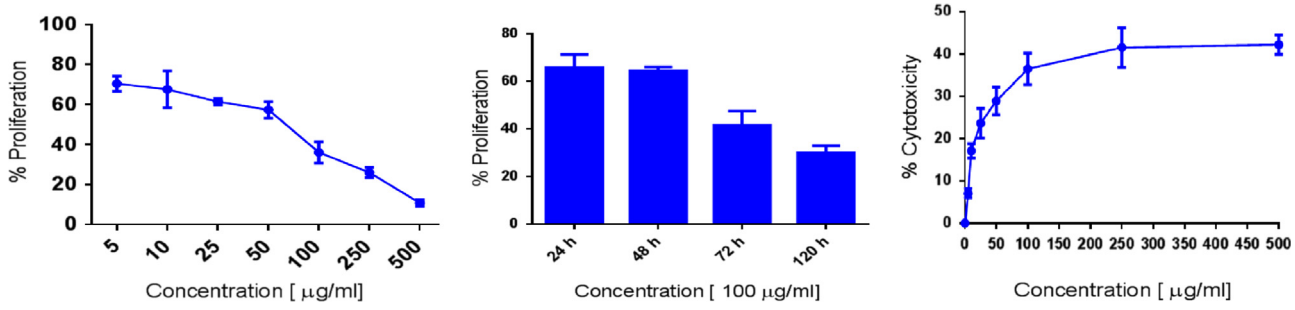

Fig. 8. Higher concentration of MCL-1 composite retards growth of SCC-25 cells. (A and B) Graphs show concentration response of MCL-1 on tumor cell proliferation and growth. (C) Direct cellular cytotoxicity by MCL-1 against SCC-25 cells.

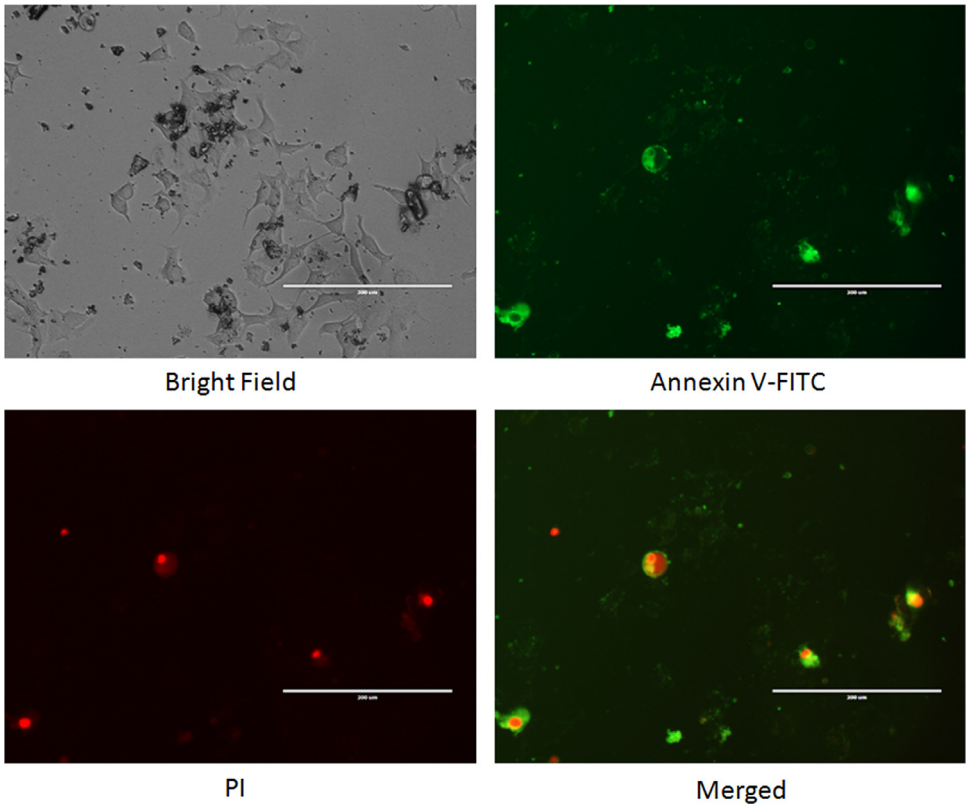

Fig. 9. Microscopic analysis of induction of apoptosis. SCC-25 cells were given indicated treatment with MCL-1 at a concentration of 100 μg/ml in complete RPMI 1640 medium for 8 h at 37 °C. FITC-conjugated Annexin V and Propidium iodide (PI) stained apoptotic cells were visualized under a fluorescence microscope (Nikon Eclipse 80i, Nikon, Japan) with Plan Fluor, 40X, NA 0.75 objective equipped with green and red filters for FITC and PI, respectively. $n=3$.

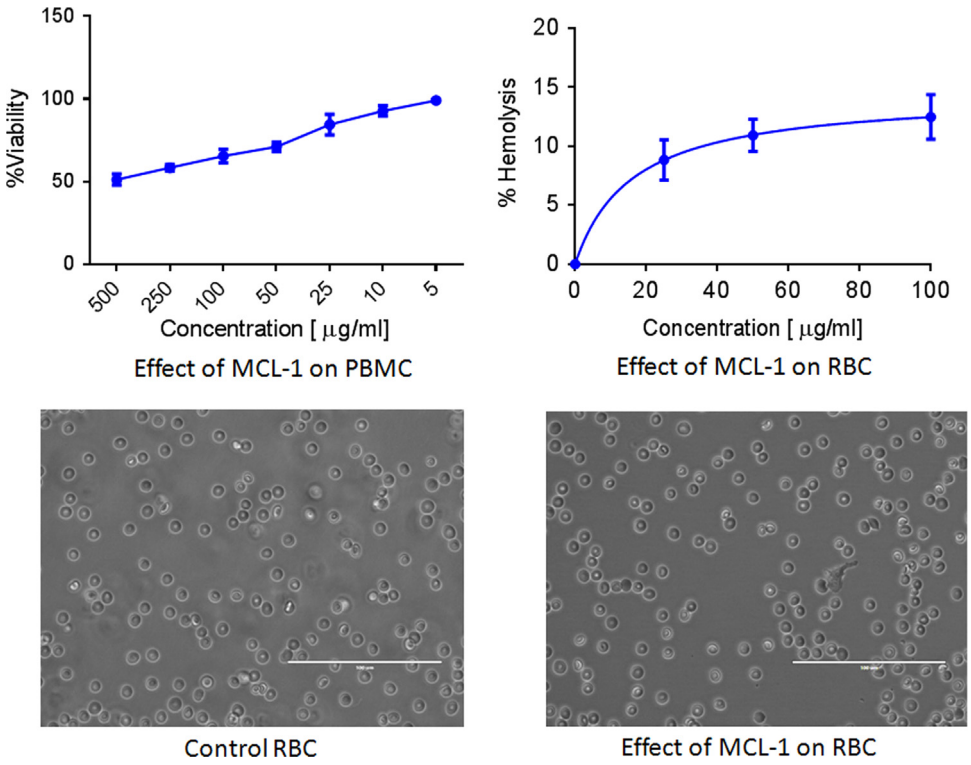

Fig. 10. Hemocompatibility assay. Hemolysis induced by indicated treatment in whole human blood at a fixed concentration (A) or with increasing concentrations (B), and is expressed as percent whole blood hemoglobin content. Photomicrographs demonstrate the absence of detrimental effect of MCL-1 on RBC morphology compared to no treatment.

material on the substrate has been confirmed by SEM. The flexural strength and CTE values observed for composite was close to that of dentine of Vita International. The bioactivity of the composite was satisfactory owing to the growth of HAp layer after 3 days immersion in SBF solution. HAp layer formation on the surface of composite was confirmed by FTIR and SEM. This material was well tolerated by buccal epithelial cells at lower concentrations. Very high concentration of MCL-1 glass ceramic materials, however, causes a moderate cell death as demonstrated by reduced proliferation and enhanced cytotoxicity of SCC-25 cells. The formulated composite though, were tolerated by the SCC-25 cells and caused significantly less apoptosis, suggesting its suitability for potential clinical application. This material may also be used in implant supported all-ceramic and metal-ceramic restorations around emerging profile regions.

Acknowledgments

1. The authors gratefully acknowledge the financial support of DST [(TDT Division), Reference No. DST/SSTP/UP/197 (G) 2012], Ministry of Science & Technology, New Delhi, India.
2. The authors gratefully acknowledge to Dr. Atul Bhatnagar, Professor, Faculty of Dental Sciences, Institute of Medical Sciences, BHU.
3. The present work was partially supported by a grant from the Department of Biotechnology (DBT), New Delhi, India, No. BT/PR11490/BRB/10/675/2008 (PPM)

References

[1] H. Milly, F. Festy, F.T. Watson, I. Thompson, A. Banerjee, Enamel white spot lesions can remineralise using bio-active glass and polyacrylic acid-modified bio-active glass powders, J. Dent. 42 (2014) 158–166.
[2] X. Chatzistavrou, D. Esteve, E. Hatzistavrou, E. Kontonasaki, K. Paraskevopoulos, A.R. Boccaccini, Sol–gel based fabrication of novel glass-ceramics and composites for dental applications, Mater. Sci. Eng. C 30 (2010) 730–739.
[3] R. Ravarian, F. Moztarzadeh, M.S. Hashjin, S.M. Rabiee, P. Khoshakhlagh, M. Tahriri, Synthesis characterization and bioactivity investigation of bioglass hydroxyapatite composite, Ceram. Int. 36 (2010) 291–297.
[4] V. Decock, K. De Nayer, J.A. De Boever, 18-Year longitudinal study of cantilevered fixed restorations, Int. J. Prosthodont. 9 (1996) 331.
[5] D. Felton, B. Kanoy, S. Bayne, G. Wirthman, Effect of in vivo crown margin discrepancies on periodontal health, J. Prosthet. Dent. 65 (1991) 357–364.
[6] J.L. Wickens, Tooth surface loss: dealing with failures, Br. Dent. J. 186 (1999) 443–446.
[7] M. Kokoti, A. Sivropoulou, P. Koidis, P. Garefis, Comparison of cell proliferation on modified dental ceramics, J. Oral Rehabil. 28 (2001) 880–887.
[8] M. Ghaffari, F. Moztarzadeh, A. Sepahvandi, M. Mozafari, S. Faghihi, How bone marrow-derived human mesenchymal stem cells respond to poorly crystalline apatite coated orthopedic and dental titanium implants, Ceram. Int. 39 (2013) 7793–7802.
[9] X. Chatzistavrou, O. Tsigkou, H.D. Amin, K. Paraskevopoulos, V. Salih, A.R. Boccaccini, Sol–gel based fabrication and characterization of new bioactive glass–ceramic composites for dental applications, J. Eur. Ceram. Soc. 32 (2012) 3051–3061.
[10] L.L. Hench, H.A. Paschall, Direct chemical bond of bioactive glass ceramic materials to bone and muscle, J. Biomed. Mater. Res. Symp. 4 (1973) 25–42.

[11] A.C. Meijering, N.H. Creugers, F.J. Roeters, J. Mulder, Survival of three types of veneer restorations in a clinical trial a 2.5-year interim evaluation, J. Dent. 26 (1998) 563–568.
[12] S. Pitaru, H. Tal, M. Soldinger, A. Grosskop, M. Noff, Partial regeneration of periodontal tissues using collagen barriers. Initial observations in the canine, J. Periodont. 59 (1988) 380–386.
[13] E. Kontonasaki, A. Sivropoulou, L. Papadopoulou, P. Garefis, K. Paraskevopoulos, P. Koidis, Attachment and proliferation of human periodontal ligament fibroblasts on bioactive glass modified ceramics, J. Oral Rehabil. 34 (2007) 57–67.
[14] R.G. Craig, R.Z. Legeros, Early events associated with periodontal connective tissue attachment formation on titanium and hydroxyapatite surfaces, J. Biomed. Mater. Res. 47 (1999) 585–594.
[15] A. Noaman, S.C.F. Rawlinson, R.G. Hill, Bioactive glass-stoichiometric wollastonite glass alloys to reduce TEC of bioactive glass coatings for dental implants, Mater. Lett. 94 (2013) 69–71.
[16] E. Kontonasaki, A. Sivropoulou, L. Papadopoulou, P. Garefis, K. Paraskevopoulos, P. Koidis, Attachment and proliferation of human periodontal ligament fibroblasts on bioactive glass modified ceramics, J. Oral Rehabil. 34 (2007) 57–67.
[17] P.H. Kumar, A. Srivastava, V. Kumar, N. Jaiswal, P. Kumar, V.K. Singh, Role of MgF_2 addition on high energy ball milled kalsilite: implementation as dental porcelain with low temperature frit, J. Adv. Ceram. 3 (2014) 332–338.
[18] P.H. Kumar, A. Srivastava, V. Kumar, S. Sharma, H. Singh, P. Kumar, V.K. Singh, Role of CaF_2 on mechanochemically synthesized leucite as dental veneering glass ceramics, Adv. Appl. Ceram. 114 (2015) 107–113.
[19] T. Kokubo, H. Takadama, How useful is SBF in predicting in vivo bone bioactivity, Biomaterials 27 (2006) 2907–2915.
[20] S.K. Hira, A.K. Mishra, B. Ray, P.P. Manna, Targeted delivery of doxorubicin-loaded poly (epsilon-caprolactone)-b-poly (N-vinylpyrrolidone) micelles enhances antitumor effect in lymphoma, PloS One 9 (2014) 9430–9439.
[21] P.P. Manna, S.K. Hira, A.A. Das, S. Bandyopadhyay, K.K. Gupta, IL-15 activated human peripheral blood dendritic cell kill allogeneic and xenogeneic endothelial cells via apoptosis, Cytokine 61 (2013) 118–126.
[22] N.R. Kuznetsova, C. Sevrin, D. Lespineux, N.V. Bovin, E.L. Vodovozova, T. Mészáros, J. Szebeni, C. Grandfils, Hemocompatibility of liposomes loaded with lipophilic prodrugs of methotrexate and melphalan in the lipid bilayer, J. Control. Release 160 (2012) 394–400.
[23] S. Hashimoto, A. Yamaguchi, K. Fukuda, S. Zhang, Low temperature synthesis of leucite crystals using kaolin, Mater. Res. Bull. 40 (2005) 1577–1583.
[24] P. Cesar, H. Yoshimura, J.W. Miranda, C. Okada, Correlation between fracture toughness and leucite content in dental porcelains, J. Dent. 33 (2005) 721–729.

PERSONAL PROFILE

Pattem Hemanth Kumar

Research Scholar,

Department of Ceramic Engineering

Indian Institute of Technology (B.H.U),

Varanasi-221005 (U.P.) – INDIA.

Contact No.: 09450921541

E-mail Id: phemanth111@gmail.com

Pattem Hemanth Kumar was born on July 22, 1986 in Guntur (Andhra Pradesh), INDIA. He completed his Diploma in Ceramic Engineering from GICT Gudur in 2005, B.Tech in Ceramic Engineering from IIC Kolkata in 2008 and M.Tech in Ceramic Engineering at Indian Institute of Technology (B.H.U.). He successfully completed his M.Tech. from Department of Ceramic Engineering with a CGPA of 8.48 in 2011. In July 2013 he got registered as a Ph.D. research scholar in the Ceramic Department under the supervision of Prof. Vinay Kumar Singh and co-supervision of Dr. Pradeep Kumar (Department of Chemical Engineering, I.I.T. (B.H.U.)).

His area of research includes Synthesis & Characterization of Bioactive Glass Ceramic Composites for Dental Veneering. He has published 9 research papers in international journals having good impact factor and has 2 research papers in international and national conferences. He has a good citation of his research papers.

(Pattem Hemanth Kumar)